

POLYTECHNIC UNIVERSITY OF TURIN

Department of Mechanical and Aerospace Engineering

Master's degree in Biomedical Engineering

Master's Degree Thesis

***Finite element modelling of periprosthetic
hip fracture at third distal femur level treated
with internal plate fixator***



Supervisor

prof. Cristina Bignardi

Co-supervisor

Dott.ssa Mara Terzini

Candidate

Stefania Nurisso

Academic year 2018/2019

Summary

Introduction	1
1. Periprosthetic femoral fractures related with hip implants	3
1.1 Incidence, risk factors and aetiology.....	3
1.2 Classification methods	3
1.3 Treatment strategies	5
1.4 Mortality and failure rates	6
2. Clinical data collection about the O’Nil distal femoral plate in the treatment of periprosthetic femoral fractures related with hip implants	7
2.1 Clinical evaluation planning.....	7
2.1.1 Device description	7
2.1.2 Equivalent device selection.....	9
2.1.3 Competitor devices	11
2.2 Clinical data collection	15
2.2.1 Literature search protocol.....	15
2.3 Clinical data evaluation	17
2.3.1 Evaluation plan	17
2.3.2 Weight of the data sets.....	19
2.3.3 Discursive relevance.....	23
2.4 Introduction to data processing	25
2.5 Introduction to CER compilation	25
2.6 Conclusions	26
2.6.1 Plate features.....	26
2.6.2 Treated medical condition	26
3. Simulation of a real case of periprosthetic femur fracture treated with the O’Nil plate..	27
3.1 Problem description	27
3.2 Geometric model creation.....	30
3.2.1 Femoral model scaling	30
3.2.2 Fracture reproduction	33
3.2.3 Femur geometry refinement.....	35
3.2.4 Prosthesis modification and positioning.....	36
3.2.5 Screws and bushings modification.....	38
3.2.6 Femoral plate features.....	39
3.2.7 Geometry assembly.....	40
3.3 Preprocessing phase.....	42
3.3.1 Mesh creation	42
3.3.2 Material properties assignment	45
3.3.3 Boundary conditions assignment	49
3.3 Results analysis	57
2.3.1 Walking - A configuration	59
2.3.2 Walking - B configuration	69
2.3.3 Stumbling.....	71
2.3.4 Falling.....	77
2.3.5 Sensitivity analysis.....	83
3.4 Conclusions	85

4. Analysis on a generic oblique periprosthetic fracture	87
4.1 Models creation.....	87
4.2 Results	88
4.2.1 Walking - A configuration	88
4.2.2 Walking - B configuration	94
4.2.3 Stumbling.....	96
4.2.4 Falling.....	98
4.3 Conclusions	103
Bibliography	104

Introduction

The incidence of periprosthetic fractures has rapidly increased in the last two decades and has been the cause of a large number of surgical interventions and permanent physical discomforts for many people, as well as a significant socioeconomic burden for many nations. The present thesis deals the periprosthetic fractures of the distal femur following total hip arthroplasty, focusing on one of the most widespread internal fixation methods for its treatment, the plating. The work is composed by three sections.

Initially, an analysis of the current state of the art on bone reduction through plating was conducted, in order to collect a sufficient amount of clinical data useful for the update of the clinical evaluation report of the "O'Nil Serie 5" implant, produced by the Intrauma company located in Rivoli (TO).

Subsequently, the finite element modelling of a real femur case, treated with plating, was conducted. The femur in question suffered a periprosthetic hip fracture at the level of the third distal femur, treated with an internal plate fixator, on which a subsequent rupture of the same occurred. The support in question is the "O'nil Serie 5" model for distal femur, produced by the "Intrauma" company. Some load situations acting on it during daily and incidental activities, were simulated, in order to validate the correct functioning of the plate, according to the use conditions recommended by the manufacturer. The analysis demonstrates that the plate failure occurs in situations of unconventional loading and with a predominant vertical component, such as that caused by stumbling, and in presence of poor bone reduction. The softwares used in the simulation preprocessing and postprocessing phases are Hypermesh and Hyperview, part of the Hyperworks package (Altair Engineering, Troy, Michigan, US). The chosen processor is Abaqus (v13, Simulia, Dassault Systèmes, Providence, RI).

The last section deals the analysis of a generic case of oblique periprosthetic fracture treated with the O'Nil plate, subject to the load configurations previously applied. The influence of the fracture inclination and healing level on the stress generated into the plate was evaluated, through the implementation of a further finite element model. The maximum values of stress in the plate, depending on the inclination of the fracture, assume different trends depending on the load situation considered. Furthermore, these values increase significantly with the reduction of the level of consolidation of the bone callus.

1. Periprosthetic femoral fractures related with hip implants

Periprosthetic fractures (PF) are bone accidents associated with an orthopaedic implant, whether a replacement or internal fixation device. With the increase in the average age of the last twenty years, the population has experienced a growth in the percentage of elderly, implanted hip prostheses, and consequently of the rate of total hip arthroplasty revisions. The most common postoperative PF localisation is the femur, with a higher incidence associated with total hip arthroplasty (THA) respect those related to total knee arthroplasty (TKA) [1, 2]. The periprosthetic femoral fractures (PFF) can range from minor injuries, with a minimal effect on the patient's outcome to being catastrophic and drastically reduce the patient's quality of life. Furthermore, the increase of the PF related to THA during the last two decades, has been a worldwide considerable economic burden for the national economies. A reference is given in a study conducted by R.F. Lyons et al. that analyses the mean cost of the treatment per patient, ranging from 14600 € to 27000 € [3].

1.1 Incidence, risk factors and aetiology

The PF can be intraoperative or postoperative. The first ones are effect of the surgical procedure while the others are caused by different reasons. Intraoperative PFF occur during the course of the surgery, postoperative ones occur averagely in the first decade from the intervention and are more frequent in patients with prior total knee or revision total hip replacements. The incidence of postoperative PFF, according to the actual available literature, range from 0.1% to 18% of the primary total hip arthroplasty interventions and from 4% to 11% of the hip replacement ones [1, 2].

The risk factors influencing the occurrence of PFF can be related to patient condition, surgical intervention type and quality and to implant features. The PFF are often determined by the mechanical properties adjustment of the implant-surrounding bone stock and the preoperatively mechanical quality of the bone structure itself. For this reason patient's advanced age, osteoporosis, rheumatoid arthritis and every other condition with pathologic bone, implant loosening, implantation technique and type of implant are significant risks factors for tardive PF. Sex and body mass index, according to the current state of the art, do not affect the probability of PFF. Approximately, in the 75% of the cases, these fractures occur because of a low energy trauma, such as a low energy fall from sitting or standing [4, 5].

1.2 Classification methods

Many PFF classification systems has been proposed that generally provide information about fracture location, fracture pattern, implant stability and potential for loosening. Of all the proposed classification techniques the Vancouver one, developed by Duncan and Masri, is the most widely applied. It includes information about fracture location, pattern and implant stability. It is reliable, simple and reproducible and permit to identify a treatment strategy basing on easily identifiable fracture features [1, 6]. It classify the PFF associated with total hip replacement in three types (Fig. 1.1).

Type *A* fractures occur around trochanteric region. The subclasses *Ag* and *Al* are assigned depending on whether the area considered is the greater or the lesser trochanter (Fig. 1.2). Type *B* fractures involve the bed supporting or adjacent to the implant and represent approximately 80% of the cases. These are subclassified considering implant stability and quality of the surrounding bone. Type *B1* fractures occur

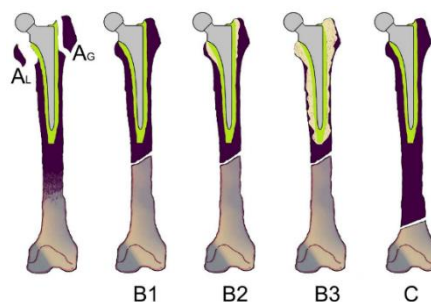


Figure 1.1: Vancouver classification of periprosthetic femoral fractures. Figure taken from [5].

around a well-fixed component, in type *B2* ones the implant is loose but the quality of the surrounding bone stock is acceptable and in type *B3* fractures the component is loose with substantial osteolysis and bone loss (Fig. 1.3). Type *C* fractures involve the diaphyseal area distal respect to the bed of the implant (Fig. 1.4).

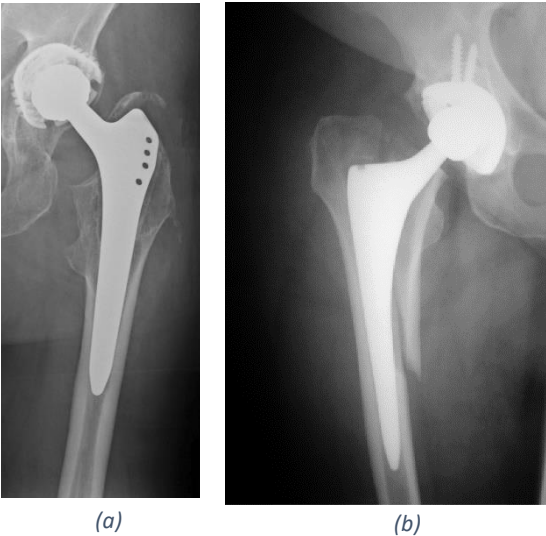


Figure 1.2: X-rays of A1 (a) and A2 (b) Vancouver type periprosthetic femur fractures. Figures taken from [1, 4].

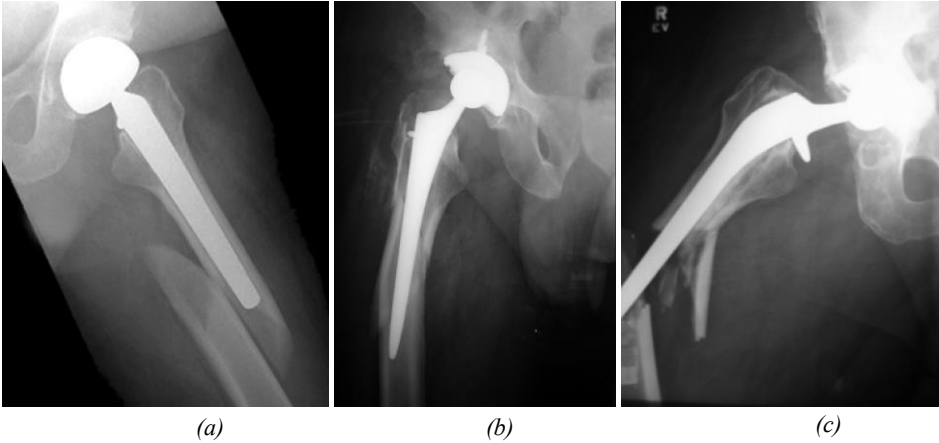


Figure 1.3: X-rays of B1 (a), B2 (b) and B3 (c) Vancouver types periprosthetic femur fractures. Figures taken from [1].



Figure 1.4: X-rays of a C Vancouver type periprosthetic femur fracture. Figure taken from [1].

1.3 Treatment strategies

The Vancouver classification includes some general indications about the recommended treatment for each fracture class. Despite this, many treatment options have been described in the literature, and no single treatment has been shown to be the gold standard.

Type *A1* fractures usually require non-operative treatment. In the case where the lesion is extended the treatment can include cerclage wires and revision if the implant is unstable [1].

Type *A_g* fractures are generally stable and treated non operatively with protected weight bearing and avoidance of hip abduction until the complete reduction is obtained. In rare cases the surrounding bone can be displaced and require fixation with a cerclage construct or a hook cable plate. Sometime this fracture is caused by osteolysis and should be treated with the add of bone grafting [1].

Type *B1* fractures are currently treated with the open reduction and internal fixation (ORIF) techniques, with the eventual add of cortical strut allograft depending on the bone stock's quality. The ORIF strategy involves the treatment with an external plate fixed upstream and downstream to the fracture with screws, cables or other strategies, in order to promote bone reduction. Different systems have been produced such as the Ogden plate, which is linked to the proximal fragment cerclage bands and to the distal one by screws. The Mennen plate works as an internal splint that embraces the diaphysis along all its length and is fixed through the closing of the hooked arms. In the Dall Miles plate, holes for screws and for cerclages are alternated along all the length. The locking plate involves the fixation to the bone in multiple points through its locking screws system. For the treatment of comminuted proximal B1 fractures, the locking attachment plate construct offer a good alternative. It is based on the addition to a traditional locking plate of a construct which lateral screws embrace the implant stem [6]. Many modification of the same treatment modality conducted to different available strategies in the actual plating systems. Every plate type can be used in combination with external cerclages or the augmentation with cortical strut grafts [1, 8]. Alternatively, one or more strut grafts can be used as the only means for the stabilisation. These have the advantage to be osteoconductive and to reduce the stress shielding due to similar modulus of elasticity as the native bone. On the other hand, the soft tissue stripping required for its application may delay the bone reduction and cause infections and immune reactions [9]. An alternative involves the fixation of the fracture with cerclage bands alone, but this technique has demonstrate to produce a high rate of failures. Concluding, the preferred treatment for B1 PFF, according to the actual literature opinion, is the use of a plate with distal bicortical and proximal unicortical screws fixation method, with the add of cortical struts or cerclage bands [10]. If the bone quality is very poor is preferable to choose a locking compression plate [11, 12].

Type *B2* fractures need stabilisation of the fracture and revising the femoral component. Such fractures are treated with revision arthroplasty with a longer stem due to the implant loosening or with eventual cable wires, plates or strut grafts for fracture reduction. Many parameters need to be controlled during the revision treatment such as length and fixation technique of the new stem. Where the bone quality around the stem area is not sufficient, a distally fixed porous-coated stem is required to obtain the fixation [1]. Spina et al. conducted a comparative study on the use of stem revision versus internal fixation with plate for the treatment of B2 periprosthetic fractures. They concluded that the stem revision is the better choice and guaranteeing minor failure rates and better outcomes, despite in some cases the internal fixation with a plating system can be a solution [13].

Type *B3* fractures are generally treated with revision arthroplasty using a longer stem. Because of the worst bone stock quality, with respect to the B2 case, the new implant can be an allograft prosthesis composite or a tumour prosthesis. Alternatively, the new stem can fixed through cement, bone grafting or a porous coating [1]. Was demonstrated by Griffiths et al. that long fluted tapered stems allow to reach a good quality of the new stem fixation [14].

Type *C* fractures are treated with the same ORIF approaches indicated for the B1 ones. These consist in locking or non-locking plates, screw and cable plates. In some situations can be useful the implant of intramedullary devices. In case of a bad quality bone stock, strut allografts can be added [1].

1.4 Mortality and failure rates

The total surgical revision rate after PFF treatment is around 16.5% and, in almost all cases, failure occurs in the first year after surgery. Generally, failure reasons are plate loosening or breaking and infection for fracture treated with ORIF and stem subsidence, hip dislocation and infection for fracture treated with revision surgery. The mortality rate during the firsts 30 days after surgery is around 1.6 % and the one-year mortality rate is around 13.2%. After one year usually this value decrease with the time. The highest mortality failure rate is associated with Vancouver type B3 fractures [15].

2. Clinical data collection about the O'Nil distal femoral plate in the treatment of periprosthetic femoral fractures related with hip implants

The first section of this thesis aims to collect information necessary for conducting the clinical evaluation concerning the O'Nil distal femoral plate model, produced by the Intrauma company located in Rivoli (TO). In order to update the current version of the report, a literature research was conducted, regarding the plating treatment of periprosthetic fractures of the femoral shaft following total hip arthroplasty. A research protocol was followed, the methods of which comply with 7.3.7 of the UNI CEI EN ISO 13485: 2016, the Annex X of DIRECTIVE 93/42 / EEC and with the MEDDEV 2.7 / 1 guideline rev.4 " *Clinical Evaluation: a guide for Manufacturers and Notified Bodies under Directives 93/42 / EEC and 90/385 / EEC* ". During the composition of the clinical evaluation, it is necessary to acquire and analyse a sufficient amount of data regarding the medical device and to evaluate if there is sufficient clinical evidence to confirm compliance with the essential performance and safety requirements, when it is used according to the manufacturers' instructions. Clinical data can be obtained from clinical investigations related to the considered device or to an equivalent one, from information obtained through post marketing surveillance and from scientific literature. The relevant scientific studies concern the devices whose equivalence to the device in question can be demonstrated. The purpose of clinical evaluation is to identify the risks and benefits of the device, its nature, probability, degree, duration and frequency. It is therefore necessary to determine the benefits / risks profile and to demonstrate the acceptability of this profile based on the current knowledge / state of the art in the medical field concerned. Data obtained from experimental tests, clinical trials and post marketing surveillance (PMS) are not available as confidential information of the producer. The process leading to data collection, based on the available information, is defined below. In this thesis, clinical data from scientific literature were identified. The following research protocol defines four discrete phases in the execution of the clinical evaluation, of which the first three lead to the collection of useful information for the subsequent evaluation of the benefits and risks profile. Simultaneously, the available data are also analysed with respect to another model of femoral plate produced by the Intrauma company, not yet on the market, in order to contribute to the first production of the relative CER.

2.1 Clinical evaluation planning

The stage 0 (in relation to the MEDDEV 2.7/1 rev.4 document) includes the definition of the purpose and the planning of the clinical evaluation. It is necessary to define the scope of the work and collect the available information. These ones must concern the features of the device, its intended use, the principle with which it acts, the expected performances and the countries in which it is commercialized. It is then necessary to identify alternative medical solutions and equivalent devices justifying their choice. The information material provided by the manufacturer must also be collected. The obtainable information, in the context of this thesis, can be obtained from the product brochure, available online on the company's website.¹

2.1.1 Device description

The device in question is the O'Nil distal femoral plate model, currently produced by the Intrauma company (Fig. 2.1) [16]. It is on the market in various European and American countries, as well as in some areas in South America and South Asia. It is available in four different lengths from 139 mm to 327 mm. The anatomically pre-shaped geometry allows a good adaptation to the bone profile. The screws are located in holes, of which seven in the distal zone and a variable number based on the size in the diaphyseal area. The side profile has been designed to guarantee the reinforcement of the areas surrounding the holes. The coupling of the screws to the plate takes place through a series of bushings, which allow to maintain fixed angular stability positions. The screws in the femoral condyles may be

¹ www.intrauma.com

arranged in a convergent polyaxial configuration that guarantees the plate grip even in osteoporotic or comminuted bone volumes.

The screws are coupled to the bone through a conical shape. The locking system provides the possibility to obtain bicortical fixation, according to the surgeon choice. The screws are available in different lengths from 12 mm to 110 mm. In the distal area there are 3 additional holes for temporary stabilization with Kirschner wires. The plate is made of AISI 316 LVM - ISO 5832-1 steel, screws and bushings are made of titanium grade 5 Ti6Al4V - ISO 5832-3. The first one is an austenitic stainless steel quite ductile. The HRC hardness coefficient is equal to 30.5, so it has a quite large range of plastic behaviour. The Ti6Al4V alloy has high mechanical resistance, corrosion resistance and good biocompatibility. The O'Nil device is designed for bone reduction in intraarticular, extraarticular and periprosthetic distal femoral fractures. The use is aimed to every adult and elderly person in presence of the previous cited conditions. It is compatible with other devices such as hip or knee prosthesis and intramedullary nails. It can be used in combination with other bone reduction methods such as cerclages, lag screws and bone grafts.

The device is designed to be inserted through the use of conventional open reduction and internal fixation (ORIF) technique.

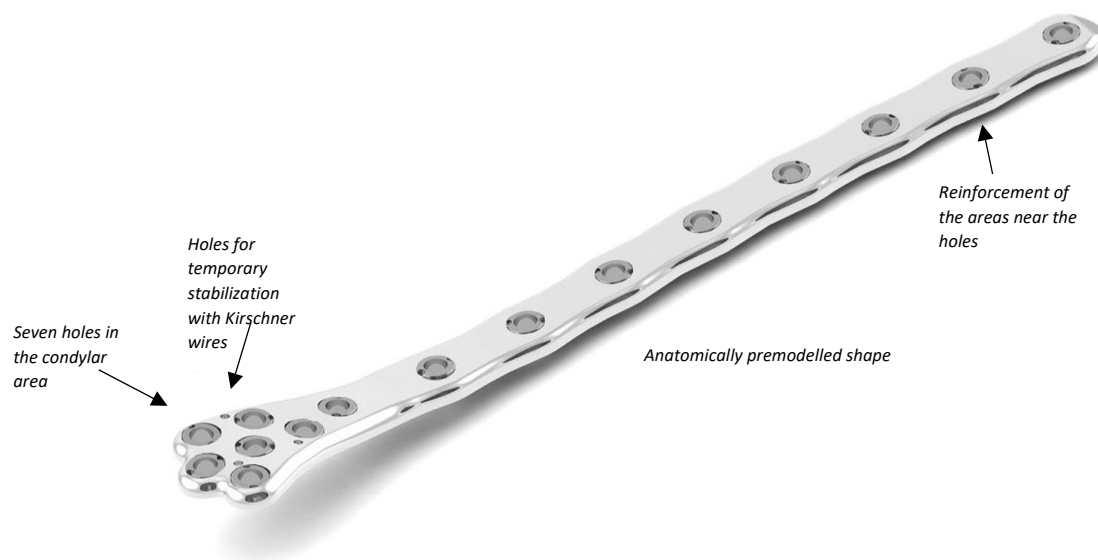


Figure 2.1: O'Nil distal femoral plate features. The image was taken from the device relative brochure [16].

Plate implant surgical techniques

Two are the main implantation techniques for distal femoral plating: conventional open reduction and internal fixation (ORIF) and minimally invasive plate osteosynthesis (MIPO). The conventional ORIF technique involves the lateral skin incision along the femur longitudinal direction to obtain the exposition of the entire fracture. The plate is inserted between the lateral vastus muscle and the periosteum and then temporarily fixed through the introduction of some k-wires at both ends of the plate. Using a drill guide some reference points are identified on the bone surface and some holes are made into the bone. Through a depth gauge the appropriate screw lengths are determined. Some screws are inserted in the made holes. Afterwards the osteosynthesis is completed by introducing additional screws where needed [16, 17].

The MIPO technique involves the lateral skin incision of the iliotibial area, of generally 80 mm of length. If there is an intraarticular fracture is necessary to fix and stabilize it before the introduction of the plate. The space between the lateral vastus muscle, situated on the femoral crest, and the periosteum is opened

and the plate is inserted through it, using the less invasive stabilisation system (LISS) (Fig. 2.2). The plate is then positioned and fixed distally through the insertion of a trocar, whose location is verified using real time x-rays images [17, 18].

The LISS system is finally removed. B.W. Min et al. conducted a study comparing the performance of the treatment of B1 Vancouver periprosthetic femoral fractures, fixed with locking compression plates through the MIPO and the ORIF techniques. The outcomes showed that the performances of the two



Figure 2.2: Less invasive stabilisation system applied to the Non contact bridging Zimmer distal femoral plate. The image was taken from the relative brochure of the device [17].

systems are comparable with respect to the patient reduction outcomes, with the only difference that the minimally invasive technique guarantee some intraoperative advantages such as shorter operating time and less blood loss [19].

2.1.2 Equivalent device selection

The identification of the equivalent device is based on some criteria. The characteristics must be similar in such a way that they do not produce clinically significant differences in the performance and safety respect to the device under evaluation.

The non-contact bridging distal femur system (NCB-DF), produced by the Zimmer company (Warsaw, Indiana, US), was identified as equivalent device (Fig. 2.2). This plate is available in different lengths from 167 to 324 millimeters. It has six screw holes in the condylar zone and a series of locking caps that allow the screws positioning with angular stability. The screws can then be positioned at any desired angle within a 30° cone of angulation, allowing different polyaxial configurations. The device is anatomically pre-shaped in order to be adapted to the bone profile and allows the bicortical screws fixation. Is possible, alternatively, to fix the plate to the bone through cables and associated cable buttons. The screws are self-locking because the stable screw-bone interface due to the conical locking system. The plate has three small holes in the diaphyseal area for the possible housing of Kirschner wires. Plate, screws and cable buttons are made of titanium grade 5 Ti6Al4V - ISO 5832-3, bushings are in Ti6Al7Nb alloy - ISO 5832-11 and cerclages are in a CoCr alloy. The device can be implanted using both the ORIF and the MIPO surgical techniques, according to the surgeon choice.

The demonstration of equivalence was effectuated in accordance with the indications provided by the *MEDDEV 2.7/1 revision 4*.

Clinical equivalence

The equivalent device must provide the same indications of use in terms of clinical condition treated, purpose, interested part of the body, target population and expected performances with respect to the device under study. The NCB plate is used for the treatment periprosthetic, comminuted, intra and extra articular and distal femur fractures. It is indicated for temporary internal fixations and stabilization of fractures and osteotomies. The use is recommended for adult and elderly patients.

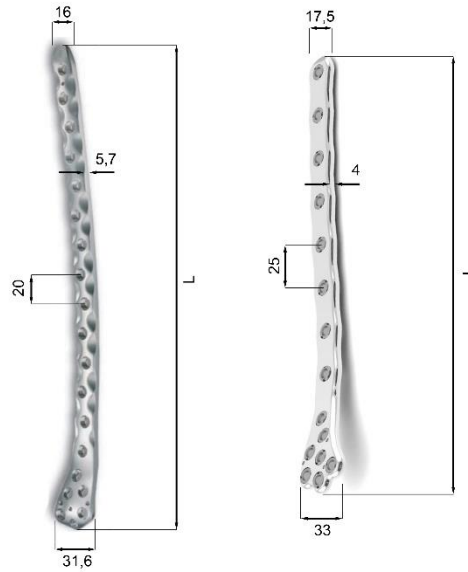


Figure 2.3: Geometric features of the NCB and O'Nil distal femoral plates compared [16, 17].

	NCB	O'Nil
Holes numbers	5, 9, 13	11, 12, 15, 18
Available lengths	167, 246, 324	139, 179, 254, 327

Table 2.1: Comparison between the available lengths and holes numbers of the NCB and the O'Nil distal femoral plates.

Technical equivalence

The equivalent device must have similar designs, specifications, physicochemical properties, installation methods, operating principles and fundamental performance requirements, with respect to the O'Nil device. The NCB plate is similar, but not identical, to the O'Nil considered one, in terms of dimension, frontal profile and anatomically pre-formed shape. Schmidt et al carried out a biomechanical experiment on synthetic fractured femurs treated with plating, to evaluate the stiffness conferred on it by different implant geometries. They demonstrated that applying on the femur loads comparable to those acting during the walk, the axial and torsional stiffness imparted to the bone by the fixation device does not vary beyond 10% of the medium value, even for significant design differences [20]. For this reason the influence of the small variation in the O'Nil implant geometry with respect to the NCB one, on the loads transferred between bone and plate, is considered negligible.

In both devices the bicortical and polyaxial configuration of the screws positioned in the condylar area is foreseen and the bone anchoring system is self-locking due to the conical shape of the screws thread. In both cases is possible to insert Kirshner wires through the small holes situated in the condylar zone. The NCB plate gives to the surgeon the possibility to implant it with the conventional ORIF surgical method. Some reference dimensions were compared, in order to demonstrate the similarity of design between the two devices (Fig. 2.3, Table 2.1). The screws of both implants are constructed of Ti6Al4V titanium alloy. The body of the NCB plate is made of titanium alloy, unlike the reference device made of AISI 316 LVM steel. Schmidt et al. demonstrated that by applying on the femur loads comparable to those acting during the walk, the axial and torsional rigidity conferred to the bone by a steel plate is greater than those obtained by one in titanium [20]. The deduction is consistent with the expectations as the average elastic modulus of the steel (equal to 210 GPa) exceeds by about 90% the one of the titanium alloys commonly used in the production of plate implants (equal to 110 GPa). The main mechanical features of the materials constituting the O'Nil and the NCB plates were individuated (Table 2.2). It is assumed that the difference in materials identified does not lead to neglect biomechanical problems.

Biological equivalence

The equivalent device must place the same materials in contact with the same human tissues or body fluids, for similar contact type and duration, respect to the studied device. As mentioned previously, the screws of both systems are made of the same material. The NCB plate has Ti6Al7Nb titanium alloy self-tapping. The body of the NCB plate is made of titanium alloy, unlike that of the reference device made of AISI 316 LVM steel. However, by demonstrating the compatibility of the Ti6Al7Nb alloy and the steel in question, with the biological tissues in contact, the difference is not influential on the sustained declaration of biological equivalence. Ni Putu Mira Sumarta et. al conducted a study showing the difference in cytotoxicity between plates made of 316L stainless steel and commercially pure Titanium, in body hamster kidney fibroblast cultures. They concluded that both plates showed non-toxic behaviours in contact with fibroblasts, although the stainless steel plate showed lower cytotoxicity level compared to titanium [21]. A literature revision conducted by Qizhi Chen and George A. Thouas affirm that the biocompatibility level of 316L stainless steel is good, although less satisfactory than the titanium alloys one. However, the use of austenitic stainless steel has to be confined to temporary devices, due to his poor corrosion resistance in body fluids as longer-term implant, from which harmful ions like nickel and chromium can be released. Some cases of metallosis and corrosion of the surface layer of stainless steel devices have been observed between 9 and 21 years after the implant. The device is applied in almost all cases to elderly patients. Therefore, the plate is usually in contact with the body tissues for a time minor than the minimum period of possible occurrence of the aforementioned complications. It is however necessary to take this aspect into consideration during the analysis of the clinical data concerning the NCB plate, in fact the titanium alloy cause almost no toxic metal ions release [22].

	<i>Steel AISI 316 LVM</i>	<i>Alloy Ti6Al4V</i>	<i>Alloy Ti6Al7Nb</i>
<i>Elastic modulus [Mpa]</i>	210000	110000	105000
<i>Tensile strength [Mpa]</i>	1014	850	921
<i>Yield Strength (0.2%) [Mpa]</i>	859	960	1024

Table 2.2: Comparison between the mechanical features of the material present on the NCB and the O'Nil distal femoral plates [23].

2.1.3 Competitor devices

In order to better understand the subsequent clinical literature analysis, a research regarding the currently much commercialized plating systems for the reduction of periprosthetic diaphyseal femoral fractures, was carried out. These plates have not been identified as equivalent devices, but provide complete information about the characteristics of the data collected in the subsequent phases.

Depuy Synthes Locking compression plate

The most diffused locking compression plate (LCP) model is produced by the DePuy and Synthes companies (Raynham, Massachusetts, US). The particular aspect of the LCP is the combination of two completely different anchorage technologies in one implant (Fig. 2.4). Hybrid holes, in fact, gives to the surgeon the opportunity to combine principles of internal fixation and dynamic compression, depending on the fracture site. The device has a regular shape but can be bended to better adapt to the bone anatomy and to obtain a polyaxial screws placing. In the dynamic compression version, the screws are used to apply a compressive preload at the interface between plate and bone. This means that accurate shaping of the plate is essential. Instead, when the LCP is used as an internal fixator, exact adaptation of the implant to the bone surface is not necessary. The screws can be used in bicortical configuration. The two distal holes in the thinned area of the plate, which are angled at 11° towards the centre of the plate, may allow an application of the locking screws in the epiphyseal area. In the distal area there is a little hole for temporary stabilization with Kirschner wires. This device is available in different lengths from 59 mm to 293 mm and in stainless steel or in commercially pure

titanium (TiCP). The screws are made of a titanium Ti6Al7Nb alloy. The device is implanted using the MIPO surgical technique [24].

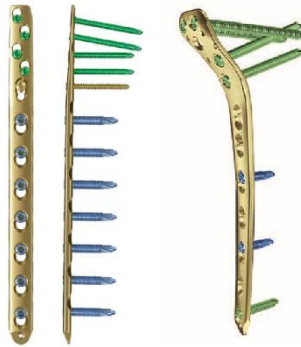


Figure 2.4: LCP (DePuy-Synthes) before and after bending [24].

Zimmer Periarticular Distal Femoral Locking Plate

The Periarticular Distal Femoral Locking Plate (PDF-LP) is produced by the Zimmer company (Warsaw, Indiana, US). The Periarticular Locking Plates can accommodate standard screws, as well as locking screws with threaded heads (Fig. 2.5). All plate configurations contain locking screw holes in the plate head, and alternating locking and compression screw slots in the shaft. By combining locking screw holes with compression screw slots in the shaft, the plate can be used as both a locking device and a fracture compression device. The screws are placed in polyaxial configuration. The plate is anatomically precontoured in order to create a fit that requires little or no additional bending. In the distal area there is a little hole for temporary stabilization with Kirschner wires. It is also available in different length from 159 mm to 368 mm. The plate is made of titanium grade 4 Ti6Al4V - ISO 5832-3 and the screws can be chosen in the the same material or in stainless steel. The device is implanted using the MIPO surgical technique [25].



Figure 2.5: PDF-LP (Zimmer) [25].

DePuy Polyax distal femoral locked plating system

The Polyax distal femoral Locking Plate is produced by the DePuy company (Warsaw, Indiana, US). The plate can accommodate fixed-angle locking, variable-angle locking and no locking screws (Fig. 2.6). Its technology allows for freedom of screw position at any desired angle within a 30° cone of angulation. The used condylar screws are usually self-locking due to the buttress thread form. This guarantee a conic arrangement in the bone. Screw locking is accomplished either by threading a screw directly into the plate (fixed-angle construct) or into a patented polyaxial bushing contained within the plate. It is anatomically shaped to fit the condylar profile of the distal femur. In the distal and proximal areas there are three little holes for temporary stabilization with Kirschner wires. It is furthermore available in different lengths from 179,4 mm to 395,8 mm. Plate and screws are both made of the titanium alloy Ti6Al4V [26]. The device is implanted using the MIPO surgical technique.



Figure 2.6: Polyax distal femoral Locking Plate (Depuy) [26].

DePuy locking attachment plate

The most diffused locking attachment plate (LAP) model is produced by the DePuy and Synthes companies (Warsaw, Indiana, US). The LAP is a component added on the surface of a proximal locking compression plate in order to improve its ability in the treatment of periprosthetic diaphyseal fractures with implanted femoral stem (Fig. 2.7). The particularity of the device is given by the arms on each side of it, that allows to avoid the prosthesis stem. Two or more screws results disposed on the sides of the prosthetic stem crossing the bone for 3.5 mm. The plate is anatomically contoured to fit the femoral shaft and the arms can be bent if necessary. The LAP and the associated screws are available in



Figure 2.7: LAP (Depuy-Synthes) [27].

Stainless steel and in Ti4Al6Nb alloy, with four or eight lateral holes. The implant is expected with the conventional ORIF technique, supposing the combined LCP already fixed on the femoral shaft [27].

Zimmer NCB periprosthetic femur plate system

The NCB periprosthetic femur plate system (NCB-PPS) is produced by the Zimmer company (Warsaw, Indiana, US). It has a better plate contouring across solid cross-sections, away from holes and is shaped to fit the proximal femoral zone on which is positioned (Fig. 2.8). It allows polyaxial screw placement (30° cone) with screws locking achieved through the use of locking caps that are threaded into the plate holes. In the locked mode, the plate acts as an internal fixator without contact between the plate and the bone surface. This NCB model is similar to the other previously described. The main difference is the possibility to use bicortical fixation around the stem of the implanted prosthesis, through its diagonal three holes pattern that allows lateral screws disposition. The centrale holes can eventually accommodate unicortical screws. Moreover, fixation using cables and cable buttons is also possible. Plate, screws and cable buttons are made of titanium grade 4 Ti6Al4V - ISO 5832-3, bushings are in Ti6Al7Nb alloy - ISO 5832-11 and cerclages are in a CoCr alloy. The device is available in different lengths from 115 mm to 401 mm and the recommended surgical technique is the conventional one [28].

Zimmer Cable-Ready

The Cable Ready bone plate system is produced by the Zimmer company (Warsaw, Indiana, US). This device cover the femoral diaphysis and is designed to incorporate cerclages into the plate without the use of cable buttons (Fig. 2.9). The cerclages pass through some lateral holes and is fixed to the plate. Some bone non-locking screws can be added. The plate is available in different lengths from 187 mm to 305 mm. The plate is made of titanium grade 4 Ti6Al4V - ISO 5832-3 and the cable is in stainless steel. The recommended surgical technique is the conventional one paying attention to insert a cable on each end of the plate prior to applying the plate to the bone [29].



Figure 2.82: NCB-PPS (Zimmer) [28].



Figure 2.91: Cable Ready system (Zimmer) [29].

2.2 Clinical data collection

The stage 1 provide the identification of useful data for the composition of the clinical evaluation. These include data owned by the manufacturer or obtainable from literature. The first category includes information obtained from pre-marketing investigation, PMS and direct tests on the device. The data obtained from the literature concern information on the device in question, on an equivalent device or on the current state of the art regarding the medical field concerned. It is therefore data related to the medical condition treated, to reference devices and other devices working in this field, and to existing medical alternatives. The data obtained from literature are intended to describe the past and current clinical background regarding the pathological condition treated, identify potential risks caused by similar devices on the market or justify the criteria used for the demonstration of equivalence.

It is necessary to establish a literature search protocol that establishes the scope and objective of the research, specifying the research questions and the methods for selecting, collecting and evaluating relevant publications. The search strategy and the inclusion / exclusion criteria, used in the selection of the found documents, are then defined.

2.2.1 Literature search protocol

The considered articles include clinical analyses performed on equivalent devices and on the selected medical condition, and articles comparing the device under analysis with others predisposed for the same purpose. The literature considered deals with the equivalent O'Nil devices, previously identified, of similar plaque type devices, or of available medical alternatives such as intramedullary nails and prosthetic revision treatments. The relevant articles for clinical evaluation are based on studies performed on patients. Studies on mechanical stress agents and finite element simulations are not taken into account. The "case reports", ie the studies concerning extraordinary clinical conditions, are discarded as they do not provide adequate statistical data to assess risks / benefits due to the device under examination.

Literature sources

The research of relevant scientific articles was carried out through the scientific literature databases MEDLINE and PubMed, and the SpringerLink and Science journals. Information on harmonized standards and devices brochures has been found through internet searches and on the manufacturers websites. The portal "*online libraries*" made available by the "*Polytechnic of Turin*" allowed free access to many useful resources.

Keywords

To conduct of the research, it was necessary to identify the keywords related to the topic in question. The research focuses on the treatment of periprosthetic distal femoral fractures with plating. Subsequently, further keywords were identified regarding the treatment fields of the device and its features.

The research was accomplished through the following:

- Periprosthetic femoral fractures
- Vancouver
- Total hip arthroplasty
- No contact bridging plate
- Polyaxial locking plate

PICO protocol

Before conducting the research, it is necessary to identify the basic characteristics that make an article relevant to the field in question. Initially the articles are identified according to the relevance of the title to the topic. Subsequently, reading of the abstracts, a first selection is made based on the topics covered in the studies. The PICO protocol defines four parameters that allow to identify well-defined research questions, useful for the initial evaluation of the studies.

The *P* factor (patient / population) indicates the group of treated patients united by at least one common statistical element (age, sex, illness, etc.). The posed question is therefore "On which group of patients

are data sought?". In this case we are looking for studies concerning adult individuals of every sex and gender, with periprosthetic fractures of distal femoral diaphysis.

The *I* factor (intervention) indicates the condition, pathology or event that affects the population. The question asked is therefore "What kind of intervention or treatment is carried out?". The considered treatment is bone reduction using the distal femoral plate osteosynthesis device.

The *C* factor (comparison / control) indicates the term used to compare the factor *I* able to relate to the outcome *O*. To evaluate the effectiveness of the intervention within the study, it is necessary that each article establishes a term of comparison. It is a question of comparing the performance, benefits and risks of the plate, with others having different characteristics or with devices or treatments useful for achieving femoral diaphyseal bone reduction.

The *O* factor (outcome) is the result of the research. It is necessary to identify the results obtained and the deductions drawn at the end of the study.

The PICO model has been updated to EPICOT +, adding the two factors of evidence and publication date to the previous ones. It was decided to use the PICO protocol, as the factors added in the EPICOT+ standard will be taken into account later [30, 31].

Inclusion criterias

The topics related to the articles were identified by reading the abstracts. Subsequently, the main aspects of each one were collected, to consider only the studies with sufficient quality for the demonstration of the clinical performance and safety of the device. Studies are excluded according to the following aspects:

a) Omission of fundamental information such as:

- Methods used for treatment and selected surgical techniques
- Types of devices used (e.g. plaques, intramedullary nails)
- Number of treated patients
- Clinical results obtained
- Undesirable effects, complications, failures observed
- Calculation of the statistical significance to demonstrate the validity of the results

b) Number of patients minor than 9, too low to guarantee statistical significance.

c) Improper statistical methods:

- Results obtained by tests applied to subgroups in which no correction has been applied for multiple comparisons
- Calculations and tests based on data distributions not consistent with the type of data acquired

d) Lack of adequate controls such as:

- Results based only on subjective evaluations of the patient
- Patients in which the assessed symptoms are subject to natural fluctuations
- Influence of external factors on the study
- When there are significant differences between the results of existing publications, with reference to variable and badly controlled influence factors.

e) Inadequate collection of mortality and data on serious adverse events. Sometimes the occurrence of serious outcomes limits a patient's ability to be available for follow-up contacts. In this type of study:

- The consequences of missing data on the results should be analysed
- In the mortality studies procedures for investigating the serious outcomes of the patients, the number of subjects lost to follow-up, the reasons why the subjects leave the study and the results of the analysis of sensitiveness should be disclosed

f) Wrong interpretation by the authors in which conclusions are not in line with the report or publication results section

g) Illegal activities. Includes clinical investigations not conducted in accordance with the EN ISO 14155, local regulations and the Helsinki Declaration.

2.3 Clinical data evaluation

The stage 2 includes the assessment, of previously identified documents, in terms of quantity and quality of data. It is necessary to identify more accurately the information contained in each document and then evaluate the methodological quality of the work done by the authors, the scientific validity of the data and the relevance of these regarding the device. For these reasons, an evaluation plan was created by assigning some weight values to the data sets.

2.3.1 Evaluation plan

The evaluation plan describes the used procedure to evaluate the data collected. It includes the criteria for determining methodological quality, scientific validity and relevance to the device.

Scientific validity

The scientific validity of an article is represented by the Origin index (OI), quantifying the authors expertise, the publishing company fame and the publishing date. Minor weights were assigned to articles published before the year 2005. The great growth of periprosthetic fractures following THA of the early 2000s, taken into account, was caused to the increase in the number of orthopaedic implants during the 1990-2000 decade. Many studies of current literature analyse the incidence and diffusion of this type of fractures, starting from the year 2005 [32].

A weight has been assigned to each article as follows:

- 10 = Publication by an international scientific company, published after the 31/12/2004
- 9 = Publication by an international scientific company, published before the 31/12/2004
- 7 = Publication by a national scientific company, published after the 31/12/2004
- 6 = Publication by a national scientific company, published before the 31/12/2004
- 3 = Publication by a scientific or clinical publisher
- 2 = Publication by authors already included in the documentation previously analysed
- 1 = Publication by a generic publisher

Publications on generic newspapers and magazines have not been considered. Since the documentation related to the production of the previous report was not available, the penultimate indication was not considered.

Relevance of the data

The collected data can be pivotal data or not. The first ones show directly the clinical performance and safety of the device. The others are evaluated and weighted according to the given contribution to the interested field. The relevance of a document is related to the type of patients analysed and to the objective of the research. The data should be representative of the device concerning its performance, safety, complaints, risks, estimation and management of risks, criteria for acceptability of undesirable effects, equivalence to another device. Furthermore, the data can be relevant regarding the development of the device or a specific size, model, medical indication, age and gender of the patients, treated medical condition, time range.

The relevance of the clinical contained in an article is represented by the Pivotal index (PI). A weight has been assigned to each article as follows:

- 3 = the article contains clinical cases that use the device recognized as equivalent. Specifically, it must treat the implant of distal femoral plate models that are equivalent to O'Nil for technical, mechanical and chemical features, target patients, surgical technique used and medical condition treated for bone reduction. This category includes studies that contain cases of treatment with the NCB-DF plate (Zimmer, Warsaw, Indiana, US), whose implant was performed using the ORIF conventional surgical technique).
- 2 = the article contains clinical cases that use a distal femoral plate device suitable for diaphyseal bone reduction, whose design is not substantially different from the one of the O'Nil (reference is made to the above mentioned competitors). Cases treated with Mennen plates, blade plates and proximal femur plates whose characteristics differ considerably from those of the O'Nil plate are excluded. The implant must be performed according to the ORIF surgical technique. Alternatively, the article can contain cases that use the equivalent device implanted with the minimally invasive surgery technique. This category contains the articles whose relevant information about the type of device or the surgical technique can be retrieved.

- 1 = the article does not contain any clinical case that use a plate whose characteristics fully or partially reflect the ones of the O'Nil device. This category includes studies that describe plates whose design is not representative of the study object or alternative treatments to the treated medical condition. Alternatively, the article contains a device similar to the O'Nil one, whose implant was performed using exclusively the minimally invasive surgical technique.

Methodological quality

The methodological quality indicates to what extent the observed effects are caused by the considered device or by external factors. A score representing the scientific reliability of each article is assigned to the quality index (QI). Ideally, a well-conducted study should be compliant with the Good Clinical Practice (GCP). The GCP are an international standard of ethics and quality necessary for the design, conduction and registration of clinical trials involving human subjects. The criteria used to verify that a study complies with the GCP are summarized here:

- The study is derived from a controlled clinical research. The results must be evaluated on the basis of comparison with a control situation different from the considered one.
- The study is designed in an adequate manner. This category includes studies whose the methods used to quantify symptoms and results are adequate, that the choice of the included subjects has been carried out according to suitable criteria and that these are sufficiently randomized. The study results have to be analysed using appropriate statistical methods. The number of patients should be greater than 20 to guarantee a good level of statistical significance of the study. The follow-up should be frequent and conducted for long enough to detect temporary complications. During the analysis of the articles, an average healing time between 3 and 6 months was identified, after which the risk of complications of mechanical and biological nature related to the implant is considered to be limited. A limit of average duration of follow-up of 12 months and of minimum duration of 3 months is established as sufficient. In order to quantify the design quality of each study, is useful to consider the number of citations received, as indicator of the opinion of clinician experts. The value assumed by the citation index of each article is considered. This value is calculated as the number of citations received divided by the number of passed years since the publication date. For the articles published less than one year ago, the citation index was not taken into account. Summarizing, a study treating more than twenty clinical cases, with a mean follow-up time major than 12 months and a citation index greater than 5 is considered correctly designated.
- The study must be performed by physicians or researchers with good experience in the clinical field considered. To evaluate this factor the Hirsch index is used. This value quantifies the prolificity and scientific impact of an author, based both on the number of publications and of citations received. A scientist has an index “*n*” if at least “*n*” works among those he published were cited at least *n* times each. A study conducted by some clinicians with an H index major than 20 respects this requirement.
- The study include well-documented clinical cases. Adverse events and deficiencies of used devices should be reported, as well as pharmacological treatments and concomitant patient interventions during follow-up. The information retrieval procedures must be complete and the causes of any missing data must be specified. A well-documented study, in case of loss of some subjects during the follow-up, performs a sensitivity analysis to determine if the missing information affects the conclusions. The results should be evaluated according to appropriate and well presented criteria, and the conclusions drawn should be relevant to them. A study is well documented if the listed aspects are treated.

Each of the 4 points listed is considered satisfied if almost all the indications given are respected.

The score assigned to the quality index is the following:

- 5 = the article completely fulfils GCP requirements or equivalent;
- 4 = the article fulfils 3/4 GCP requirements or equivalent;
- 3 = the article fulfils 2/4 GCP requirements or equivalent;
- 2 = the article fulfils 1/4 GCP requirements or equivalent;
- 1 = the article does not fulfil any of GCP requirements or equivalent.

2.3.2 Weight of the data sets

After the weight assessment, the resulting index (RI) is calculated and assigned to each article included in the literature investigation. Its value is obtained as the product of the three above mentioned indices:

$$RI = OI * PI * QI \quad (2.1)$$

and its value can vary in the range 1-150.

A priority level is assigned to each article depending on the final score obtained. Articles with a score between 135 and 150 are classified with primary priority. These studies are the most reliable and contain the pivotal data, from which is possible to directly extract information on efficacy, risks and benefits of the device in question. Articles with a secondary priority have a score of between 80 and 130 and contain data on the analysed device that can be obtained indirectly. Articles with IR value minor than 50 were excluded, these, in fact, contain data that are not representative of the device regarding its use and/or its operative condition.

To make the work clear, a table has been created containing the list of the selected articles. Each article was accompanied by the motivation for which it was considered relevant, the assigned weights, the clinical, technical and biological correspondence evaluation between the O'Nil device and the one in the study and eventual notes. A part of the table has been shown (Table 2.3).

The columns indicating the clinical, technical and biological equivalence between the device described by the article and the O'Nil plaque were inserted to quickly identify which features of this one are represented in the studies.

The three clinical equivalence fields indicate, in this order, the following factors:

- The study describes periprosthetic diaphyseal femoral fractures, treated in order to obtain bone reduction. The article represents the clinical condition treated by the device.
- The subjects considered are adults, with a normally developed femoral anatomy, in the presence of the condition explained above. The article represents the target population for which the use of the device is expected.
- The study describes a device implanted in the distal femoral zone. The article concerns the implant in the body area treated by the device.

The four technical equivalence fields indicate, in this order, the following factors.

- The study describes plates for the reduction of distal femur fractures. The article represents the function assumed by the device.
- The study describes devices with specifications and technical properties similar to those of the O'Nil plaque. If the plate in the study is made of 316L steel and the screws are of titanium alloy Ti6Al4V, the technical properties (e.g. viscosity, tensile strength and surface characteristics) are represented.
- The study describes devices whose designs are similar to that of the O'Nil plate. The characteristics of anatomical shape, length, conical locking and arrangement of the screws, possibility of bicortical implantation and angular stability configuration are identified.
- The study includes cases using traditional implantation surgical technique (ORIF). The article therefore represents the operating technique recommended by the manufacturer of the O'Nil plate.

The biological equivalence field indicates studies that describe devices whose implant causes the contact of the materials 316L steel and Ti6Al4V titanium alloy with the subcutaneous, muscular, nervous and bone tissues present in the thigh area. These articles are representative of the biological effects that the device causes in contact with the body.

The article "*Minimally invasive plate osteosynthesis with locking compression plate in patients with Vancouver type B1 periprosthetic femoral fractures*" compares two surgical methods of distal femoral plate implantation, in order to identify the merits and defects of each [33]. It was considered important as regards the treatment of periprosthetic diaphyseal femoral fractures that occurred after total hip arthroplasty (THA), with plating. In the first analysis was recognised that the article does not omit

fundamental information such as surgical techniques used, number of patients, type of patients. It is based on 40 well randomized subjects. Includes patients with Vancouver B1 periprosthetic fractures, treated at the Keimyung University hospital (Daegu, Korea) with the MIPO technique and the LCP plate (DePuy Synthes, Solothurn, Switzerland) between 2011 and 2017, and the subjects, in the same condition, treated with the ORIF technique and the LCP plate between 2006 and 2011. In addition, cases whose minimum follow-up was minor than 12 months were excluded. The benefits obtained using the plate are assessed objectively through number and severity of the complications and radiological deduction of effective bone reduction. The results are quantified and presented in an appropriate manner. Any treatment other than the study object is not specified.

AUTHORS	INCLUSION		WEIGHT			EQUIVALENCE							NOTES	
			IO	IP	IQ	CLINICAL			TECHNICAL					BIOLOGICAL
TITLE	Y/N	REASON	IR = IOxIPxIQ			1	2	3	1	2	3	4	1	
<u>Byung-Woo Min, Chul-Hyun Cho, Eun-Suck Son, Kyung-Jae Lee, Si-Wook Lee, Kyung-Keun Min</u>	YES	Intended use of the plate and operative conditions similar to our medical device	10	2	5									
<i>Minimally invasive plate osteosynthesis with locking compression plate in patients with Vancouver type B1 periprosthetic femoral fractures</i>			100			x	x	x	x				x	
INJURY (2018)														
<u>J. B. Erhardt, K. Grob, G. Roderer, A. HoVmann, T. N. Forster, M. S. Kuster</u>	YES	Intended use of the plate and operative conditions similar to our medical device	10	3	5									
<i>Treatment of periprosthetic femur fractures with the non-contact bridging plate: a new angular stable implant</i>			150			x	x	x	x		x	x		
TRAUMA SURGERY (2007)														
<u>Steffen Ruchholtz, Bilal el Zavati, Dimitri Kreslo, Benjamin Bucking, Ulrike Lewan, Antonio Kruger, Ralph Zetti</u>	YES	Intended use of the plate similar to our medical device	10	2	5									
<i>Less invasive polyaxial locking plate fixation in periprosthetic and peri-implant fractures of the femur: a prospective study of 41 patients</i>			100			x	x	x	x		x			
INJURY (2013)														

Table 2.3: Part of the clinical data evaluation conducted. It comprise motivation of the inclusion, assigned weight and clinical, technical and biological correspondence evaluation, for each article.

The origin index is 10 because the article was published by the world-renowned international magazine "Injury", in 2018.

The pivotal index is 2 because the article concerns the locking compression plate (LCP) for distal femur device, treated with ORIF and MIPO techniques.

The quality index (IQ) is 5 because all the criteria defining the GCP are respected:

- The study aims to provide information regarding the performance of implanted plaque with minimally invasive surgery, comparing the results with the control sample treated with traditional surgery.
- Radiographic and clinical analyses are performed to quantify the benefits brought by the plate. The fracture is considered to be reduced when the callus is observed radiographically in at least 3 of 4 cortices. The clinical evaluation of the results includes the analysis of the modified Harris hip score regarding the patient's mobility level. Other factors that have been taken into account are operative time, blood loss during the operation, time of union and complications. The number of patients is major than 20. The average duration of the follow-up is equal to 33.8

months and the minimum duration is 12 months. The results were analysed with statistical methods consistent with the type of study, depending on whether the variable considered is categorical (Cross table, Chi-squared, Fisher's exact tests) or quantitative (Student's t-test and Meann-Whitney U test). The article was published less than one year ago, for this reason the citation index has not been taken into account. The study is considered appropriately designated.

- Some authors of the study have H index greater than 20, for this reason the study is conducted by experienced clinicians.
- No deficiencies of the used device or the presence of medications taken by patients during follow-up are specified. No subjects were lost during the follow-up. The results are evaluated appropriately and presented clearly. The type, number and causes of the complications are specified, as well as the deductions made. The conclusions drawn are consistent with the results and well specified. The study presents well-documented clinical cases.

The resulting index is 100. To the article was assigned the secondary level of priority.

By comparing the LCP plaque device (DePuy Synthes, Solothurn, Switzerland) with the O'Nil (Intrauma, Rivoli, Italy) one and identifying the features in common, the parameters of clinical, technical and biological equivalence are established. The study describes the treatment of adult patients who have undergone periprosthetic fractures of distal femur of Vancouver type 1, in which the prosthetic hip stem is anchored to the bone. The purpose of treatment is bone healing. The LCP is available in 316L steel and titanium grade 2 TiCP and the screws are available in 316L steel and in TAN alloy. The materials used in the study are not specified. The LCP is not pre-shaped in anatomical form, the screws adhere to the bone through a conical system and are, in the areas where possible, of bicortical type. The plate has holes with a hybrid locking system and runs along the entire diaphyseal length. Both the ORIF and MIPO implant techniques are used in the study.

The article " *Treatment of periprosthetic femur fractures with the non-contact bridging plate: a new angular stable implant* " analyses the performance the of non-contact bridging distal femur (NCB-DF) plating system (Zimmer, Warsaw, USA) in the bone reduction treatment of periprosthetic fractures of distal femur [34]. It was considered important as regards the treatment of periprosthetic diaphyseal femoral fractures that occurred after total hip arthroplasty (THA), with plating.

It does not omit fundamental information such as surgical techniques used, number of patients, type of patients. It is based on 24 adequately randomized subjects. The included cases were the distal femoral fractures treated at the cantonal hospital of St. Gallen (Switzerland) and at the university hospital in Ulm (Germany), with the NCB-DF plate, between 2003 and 2005.

The benefits obtained using the plate are assessed through clinical and radiographic analysis. The results are quantified and presented in an appropriate manner. Any treatment other than the study object is not specified.

The origin index is 10 because the article was published by the international journal in the field of orthopaedics "Trauma surgery", in 2008.

The pivotal index is 3 because the NCB-DF device is represented and treated with the ORIF surgical technique.

The quality index is 5 because all the criteria defining the GCP are respected:

- The study aims to provide data on the benefits and risks obtained as a result of the treatment of periprosthetic distal femoral fractures with the NCB-DF plate. It is controlled because the results evaluation terms have been compared with information found in the literature concerning different plaques, in order to objectively deduce the advantages of the NCB.
- To quantify the benefits brought by the plate, movement range and pain, number and severity of complications, unions, malunions and not radiological unions were evaluated. The number of patients is major than 20. The average duration of follow-up is 12 months and the minimum duration is 3 months, a low factor compared to similar studies. The citation index of the article is 9,73 times and for this reason the methodological quality is supposed to be good.
- The H-index of some authors in greater than 20. For this reason the study in conducted by experienced clinicians.

- No deficiencies of the used device or the presence of medications taken by patients during follow-up are specified. A detailed description of the follow-up of the patients has been made. Some subjects, not being present personally, were interrogated through telephone questionnaires while others died during the follow-up. Despite this, the results are evaluated in an adequate manner and presented clearly. The type, number and causes of complications are specified, as well as the deductions made in this regard. The conclusions drawn are consistent with the results and well specified. The study presents well-documented clinical cases.

The resulting index is 150. To the article was assigned the first level of priority.

The study describes the treatment of adult patients who have undergone periprosthetic distal femoral fractures following THA and TKA. The purpose of treatment is bone healing. Therefore the three parameters of clinical equivalence are respected. The NCB-DF plate and the associated screws are made of titanium alloy Ti6Al4V, therefore the biological compatibility parameter is not respected. As explained, the specifications and technical characteristics of the NCB are representative of the O'Nil plate. The ORIF surgical technique is used in the study.

The article "*Less invasive polyaxial locking plate fixation in periprosthetic and peri-implant fractures of the femur: a prospective study of 41 patients*" analyses the performance of two NCB femoral plating systems (Zimmer, Warsaw, USA) in the treatment of bone reduction of periprosthetic fractures with fixed implant, that occurred after THA and TKA [35]. It was considered important as regards the treatment of periprosthetic diaphyseal femoral fractures that occurred after total hip arthroplasty (THA), with plating.

The article does not omit fundamental information such as surgical techniques used, number of patients, type of patients. It is based on 41 adequately randomized subjects.

Cases of periprosthetic and peri-implantal femoral fractures treated at the Marburg university hospital in Baldingestrasse (Marburg, Germany), with NCB distal femur system and NCB periprosthetic femur plate system (Zimmer, Warsaw, USA), between 2008 and 2011, were included. Cases with dissection of the hip or knee prosthesis and pathological fractures were excluded. The benefits apported by the plate systems are assessed through clinical and radiographic analysis. The results are quantified and presented in an appropriate manner. Any treatment other than the study object is not specified.

The index of origin (IO) is 10 because the article was published by the world-renowned international magazine "Injury", in 2013.

The pivotal index (IP) is 2 because the article contains information about the NCB-DF device, treated with the MIPO surgical technique.

The quality index (IQ) is equal to 5 because all the criteria defining the GCPs are respected:

- The study aims to provide data on the benefits and risks obtained as a result of the treatment of distal femoral fractures with NCB plates. The study is controlled because the terms of performance evaluation have been compared with an analysis of the available literature regarding the treatment of periprosthetic fractures with locking plates.
- To quantify the benefits brought by the plate, rate of postoperative complications, rate of surgical changes required following implantation, number of unions, malunions and non-radiological unions and subjective evaluations expressed by patients regarding the perception of pain and the level of mobility were evaluated. The number of patients was major than 20. The duration of follow-up was 12 months for patients that could be evaluated. The citation index is 6,83. The results were analysed using statistical methods consistent with the type of study. The design of the study is considered of sufficient quality.
- The H-index of some authors in greater than 20. For this reason the study in conducted by experienced clinicians.
- No deficiencies of the device in use or any medications taken by patients are specified. During the follow-up, 20% of the patients were lost and the evaluation of the results was made by reducing the sample to the remaining 32 subjects. The results are evaluated appropriately and presented clearly. The type, number and causes of the complications are specified, as well as

the deductions made. The conclusions drawn are consistent with the results and well specified.

The study presents well-documented clinical cases.

The resulting index is 100. To the article was assigned the second level of priority.

The study describes the treatment of adult patients who have undergone periprosthetic distal femoral fractures and peri-implantation, and the aim of treatment is bone healing. The three parameters of clinical equivalence are respected. The NCB plates and the associated screws are made of titanium alloy Ti6Al4V, therefore the biological compatibility is not present. The characteristics of the NCB-DF are representative of the O'Nil plate and, even if only a part of the plaques used is of this model, we consider the data useful to such an extent to assume clinical equivalence in terms of design. The MIPO surgical technique is used in the study.

2.3.3 Discursive relevance

After sorting the articles according to validity, quality and the relevance to the subject, the most important information contained in them was identified and classified in order to confirm the correct allocation of the assigned weights. Some conclusions were drawn about effectiveness, benefits and risks of the O'Nil plate. The data retrieved from the previous presented articles has been shown (Table 2.4).

The field "*What kind of device provides useful data?*" identify which is the relation between the O'Nil plate and the device described in the study. This is useful in order to understand to what extent the data are representative of the device under evaluation. The study can concern one or more of the following fields: the O'Nil plate, the equivalent device, a benchmark device "plate for distal femoral fractures", other medical alternatives and the medical condition treated.

The field "*What aspects are covered?*" identify which kind of data are contained in the article. It can contain data regarding one or more of the following: pivotal performance data, pivotal safety data, claims, caused hazards, management of risks, information about the state of the art, determination and justification of criteria for the evaluation of the risk/benefit relationship, determination and justification of criteria for the evaluation of acceptability of undesirable side-effects, determination of equivalence, justification of surrogate endpoints.

The field "*How much are the provided data representative?*" identify if the data are representative of the entire condition of use of the device. The article can represent the intended purpose of the device with all the patient populations and all the claims foreseen, concerning all the models/sizes/settings or, alternatively, can only represent some of these aspects. In the latter case model, size and setting of the device, user group, given medical indications, age group of users, gender of users, type of medical condition and duration of the treatment and of the follow-up were specified.

AUTHORS	What kind of device provides useful data?	What type of data is provided?	How much is the provided data representative?	Is the data representative of a specific conditions regarding:			
				size of the device	user group	medical application	age group
				gender	type and severity of medical condition		range of time
<u>Bvung-Woo Min, Chul-Hyun Cho, Eun-Suck Son, Kyung-Jae Lee, Si-Wook Lee, Kyung-Keun Min</u>	benchmark device	performance (healing rate, mean healing time) identification of hazards (non-union, plate break)	represents specific aspects of the device and of the purpose				
-				specialists surgeons	periprosthetic femoral fractures	old age	
-				B1 fractures according to the Vancouver classification		follow up: 33,8 months	
<i>Minimally invasive plate osteosynthesis with locking compression plate in patients with Vancouver type B1 periprosthetic femoral fractures</i>							
INJURY (2018)							
<u>J. B. Erhardt, K. Grob, G. Roderer, A. HoVmann, T. N. Forster, M. S. Kuster</u>	equivalent device	performance (healing rate, mean healing time) identification of hazards (non-union, plate break, infection)	represents specific aspects of the device and of the purpose				
-				specialists surgeons	periprosthetic femoral fractures	old age	
female						follow up: 12 months	
<i>Treatment of periprosthetic femur fractures with the non-contact bridging plate: a new angular stable implant</i>							
TRAUMA SURGERY (2007)							
<u>Steffen Ruchholtz, Bilal el Zavati, Dimitri Kreslo, Benjamin Bucking, Ulrike Lewan, Antonio Kruger, Ralph Zettl</u>	equivalent device	performance (healing rate, mean healing time) identification of hazards (non-union, plate break)	represents specific aspects of the device and of the purpose				
long				specialists surgeons	distal femoral periprosthetic and simple intraarticular fractures	old age	
-				B1, B2 and B3 according to the Vancouver classification 33 according to the AO/OTA classification		follow-up: 36,5 months	
<i>Less invasive polyaxial locking plate fixation in periprosthetic and peri-implant fractures of the femur: a prospective study of 41 patients.</i>							
INJURY (2013)							

Table 2.4: Part of the clinical data retrieved from the previous presented articles.

2.4 Introduction to data processing

This phase involves the re-elaboration of the collected data, in order to define if these are sufficient for the demonstration of the relevance of the device to the essential requirements of performance and clinical safety [MDD 93/42], when used according to the manufacturer's instructions.

Through the data obtained previously from the literature and from clinical investigations, the information regarding the performance of the device and the associated risks is identified. The essential requirements to be considered and the methods for verification are described below.

- ER1: *“The devices must be designed and manufactured in such a way that, when used under the conditions and for the purposes intended, they will not compromise the clinical condition or the safety of patients, or the safety and health of users or, where applicable, other persons, provided that any risks which may be associated with their intended use constitute acceptable risks when weighed against the benefits to the patient and are compatible with a high level of protection of health and safety”.*²

This requirement states that the devices shall be ‘designed and manufactured in such a way’ that safety of patients and users shall not be compromised. The data must provide sufficient evidence that the risks associated with the use of the device are compatible with an high level of safety, which are minimal and acceptable compared to the benefits brought to the patient. It is therefore necessary to quantify, using pre-established criteria, the benefits provided by the device, the possible risks including the severity and consequences, and their probabilities. An assessment of the acceptability of the benefit / risk relationship is constructed, taking into consideration the clinical data collected from literature and obtained from the PMS.

- ER3: *“The devices must achieve the performances intended by the manufacturer and be designed, manufactured and packaged in such a way that they are suitable for one or more of the functions referred to in Article 1, as specified by the manufacturer”.*²

Information on the direct and indirect beneficial effects of the device to the patient is identified, taking into consideration the clinical data collected from literature and obtained from the PMS.

- ER6: *“Any undesirable side-effect must constitute an acceptable risk when weighed against the performances intended”.*²

Data on nature, frequency and severity of the side effects caused by the device is identified. The manufacturer assesses whether these are acceptable using information regarding state of the art and detailed knowledge of the technical characteristics of the device.

2.5 Introduction to CER compilation

The clinical evaluation report is the document that summarizes the procedure of the conduction the Clinical Evaluation, allowing to identify the level of quality of it and the consistency of the conclusions drawn. The report is compiled in a schematic way and explains in temporal order, following the steps of the evaluation, how the data were acquired and analysed. Finally, the conclusions drawn regarding the adequacy of the device to obtain, or reconfirm, the CE mark, the identified risks, the conditions of PMS and the indication of missing information within the material provided by the manufacturer, are drawn up.

Alternative device from the Intrauma company

As previously mentioned, data collection was also conducted regarding to another plate device, designed by the Intrauma company and not yet in the market. This one is similar to the O’Nil model, but provides the addition of a series of cables incorporated to the devices without the use of cable buttons. Moreover, unlike the O’Nil, this system is designed in titanium grade 5 Ti6Al4V.

² MDD 93/42/CEE annex1, MDR annex1

2.6 Conclusions

Following the reading of the articles some conclusions are drawn about the O'nil plate features and the treated medical condition. A small part of the conclusions drawn by the analysed articles is reported here.

2.6.1 Plate features

It is confirmed that the titan alloys have greater biocompatibility than steel. The treatment of periprosthetic steel fractures is more likely to develop non-unions. The bone callus formed by fractures treated with a titanium plate, in fact, is greater [36].

The MIPO surgical technique was not shown to be statistically superior than the ORIF one, however, it showed several intraoperative advantages. It guarantee a shorter operation time and healing time, and a lower blood loss rate, compared with the ORIF one. With the MIPO technique, fracture healing without complications is higher than with the ORIF one [33].

The screws polyaxial locking mechanism allows for the positioning of the plate near the prosthesis area, with bicortical configuration. These polyaxial screws trajectories can account for differences in femoral anatomy, fracture patterns or variations in plate positioning. [35, 37]. Usually there are no failures of the polyaxial screw–plate interface and screw angle did not reduce the overall strength of these constructs, hence lending support to the biomechanical effectiveness of polyaxial plate designs under axial loading. According to a study conducted by J. B. Erhardt et al., that polyaxial plating systems demonstrate a high rate of union (90%) and a low rate of mal-union (5%)[34].

Fractures that fail to heal usually maintain alignment and form less callus, suggesting callus inhibition rather than hardware failure is the primary problem. Compared with external fixators, locking plate constructs can be considerably more stiff, given the proximity of the plate to the bone, and they may act like extremely rigid internal fixators preventing callus from forming. The high stiffness of the locking plates can cause also healing difficulties, including nonunion, delayed union [36].

Has been demonstrated that the combination of plaque and cerclage is often useful in order to reduce the loss of fixation probability.

Is necessary to carefully choose the operating parameters during the plating operation. The main ones are the screw density, the proximal screw mode, the number of screw cortices, the screw fixation technique, the working length and the total length of the plate. The type of proximal screw fixation technique did affect union rate, a bicortical fixation gives in fact better outcomes. The number of proximal screws, the number of screw cortices and the proximal screw density were not associated with a significant difference in total union. All proximal screw constructs were more likely to develop non-union with respect to the hybrid and non-locking ones. As previously specified, in fact, in some instances locking plate constructs may be too stiff. [38]. Constructs with a higher total length and working length have a better healing rate than constructs with a lower one [36, 37].

2.6.2 Treated medical condition

The factors that influence the plating treatment failure are many. Obesity, open fractures, cemented implants, highly comminuted fractures and presence of revision implants are associated with an high risk of nonunion. Also the time between the fracture and the plating surgery is influent. Gender and age the patient, and osteoporosis are not correlated with the treatment failure [15, 36, 39].

The complications that occur most frequently after the plating treatment are infection, plate failure, bone fracture, loosening, non union and delayed union [37, 40, 41].

It is sometime difficult to differentiate between Vancouver type B1 and B2 fractures because there in no way to evaluate the stem stability directly without the dislocation of the prosthetic hip joint during the surgery. Is important to effectuate a prior planning surgical treatment to consider the preoperative stability of the femoral stem [8]. The main reason for the failure of the treatment of B1 periprosthetic fractures is, in fact, the misinterpretation by the surgeon of the stability of the femoral stem and the classification of a type B2 fracture as a type B1, that is then treated incorrectly [40].

3. Simulation of a real case of periprosthetic femur fracture treated with the O'Nil plate

3.1 Problem description

This thesis aims to analyse the possible causes of a real case of femoral plate break, implanted following a periprosthetic fracture. The patient was initially subjected to total hip arthroplasty (THA) of the right femur, the cause of which is unknown. Subsequently, a type C, according to the Vancouver classification, periprosthetic fracture occurred (Fig. 3.1). It was, therefore, a distal femur fracture with respect to the prosthetic implant, which maintained a good stability within the bone. According to the more general classification AO/OTA, however, it was a of type 32 A1 fracture, because it was located in the distal femur, the shape was spiroidal and the bone stock was of good quality. A month later, an O'Nil distal femoral plate model, was implanted. The surgeon chose to use a cerclage to secure to the bone the higher part of the plate. An interfragmentary screw, crossing the fracture surface, was inserted. The x-rays of the femur after the operation and after one and two months are showed (Fig. 3.2 - 3.5). After three months the plate suffered of catastrophic break in the area where the healing bone was present, accompanied by a further femoral fracture with the same profile as the previous one (Fig. 3.6). The context and reason of the break are unknown.

Problem characteristics

The patient in question is a 73-years-old woman with no history of bone disease at the time of the accident, whose weight is unknown. The aforementioned fracture was treated with an O'Nil external plate fixator, of extra-long size (code 152.30006 of the relative documentation), whose design and technical features have been previously explained. All the screws are fixed in a bicortical way, except the three proximal ones that are unicortical in order to avoid the contact with the prosthesis stem. The used plate screws diameters and lengths known. The materials constituting the cerclage and the interfragmentary screw, as well as the model of the implanted prosthesis, are unknown.



Figure 3.1: Anteroposterior (a) and right-left (b) X-ray views of the periprosthetic fracture. Is highlighted the fact that the thickness of the lower femur is reduced compared to the upper one.



Figure 3.2: Anteroposterior (a) and right-left (b) X-ray views of the periprosthetic fracture after the plate implant



Figure 3.3: Anteroposterior X-ray views of the periprosthetic fracture after one month from the plate implant

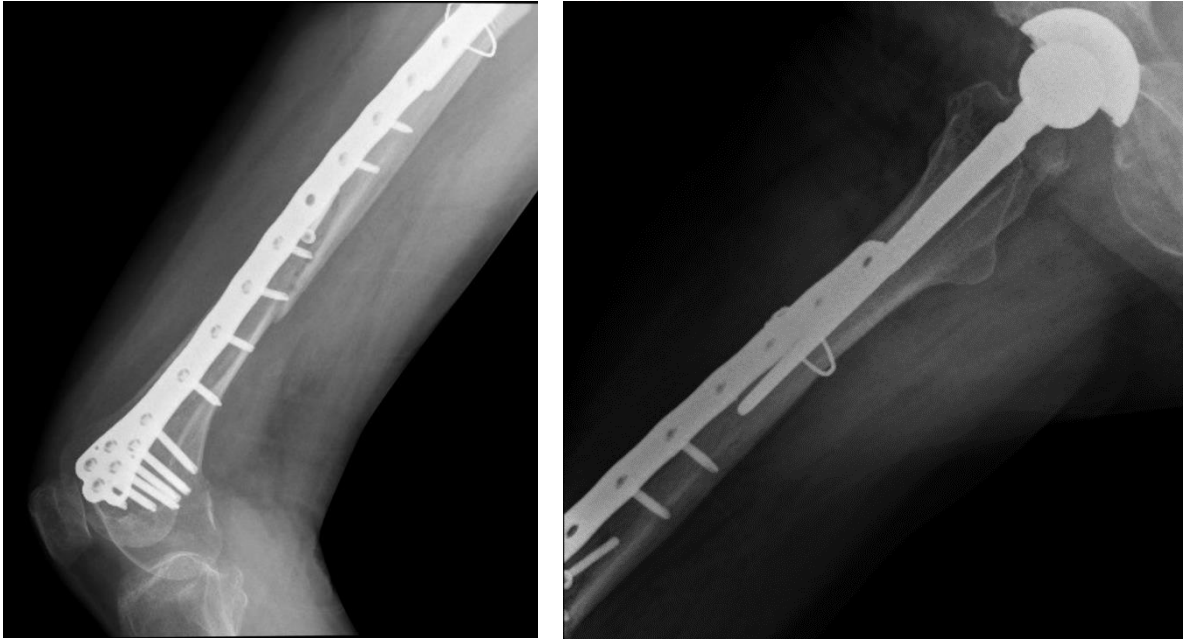


Figure 3.4: Right-left X-ray views of the periprosthetic fracture one month after the plate implant

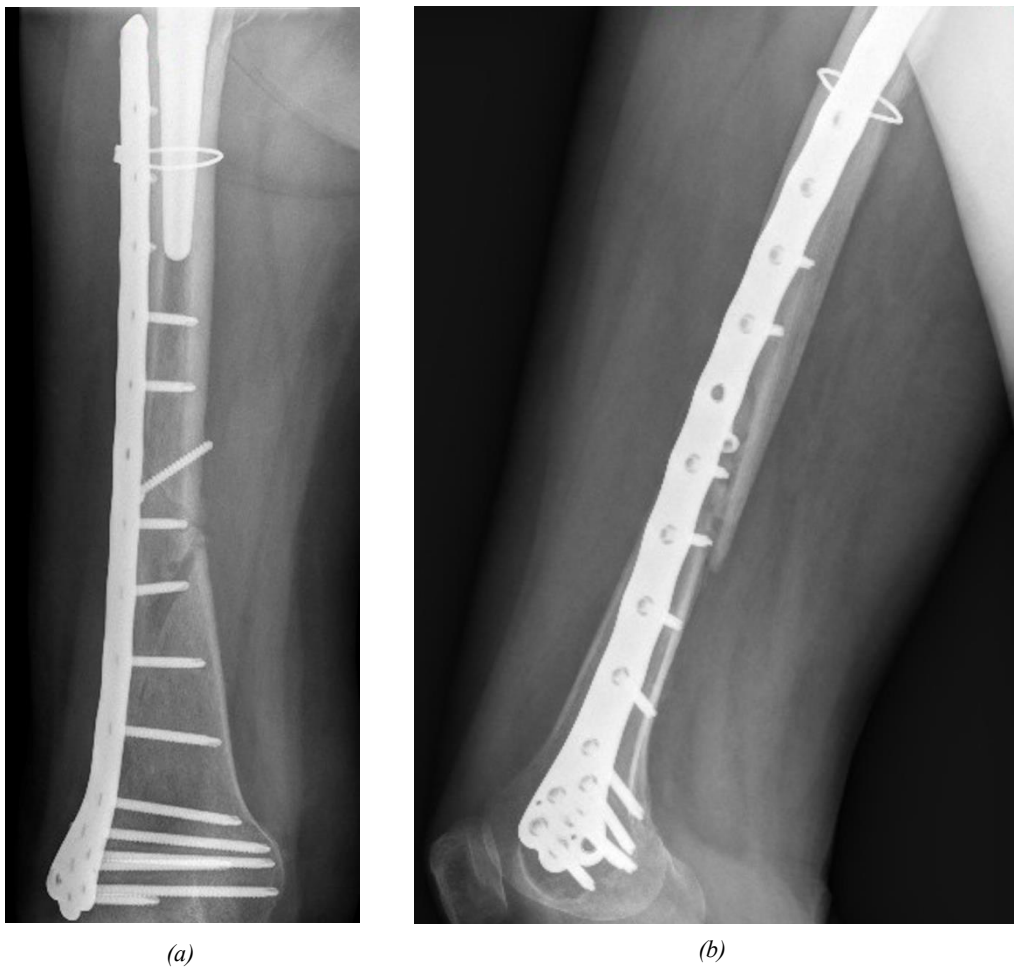


Figure 3.5: Anteroposterior (a) and right-left (b) X-ray views of the periprosthetic fracture two months after the plate implant



Figure 3.6: Anteroposterior (a) and right-left (b) X-ray views of the plate break

3.2 Geometric model creation

In order to validate the correct functioning of the plate during the use and identify the possible cause of its break, the creation of a finite element model that simulates the described situation is fundamental. By analysing stress and strain peaks inside the fixator, under common and accidental load conditions, it is possible to identify the situations which can overstress the plate beyond the breaking limit.

3.2.1 Femoral model scaling

In order to simulate the situation described, a standard geometric model of an adult woman's right femoral bone has been used. The available model contains only the cortical region geometry and neglects the trabecular one. However, according to Papini et. al, the removal of the region containing cancellous bone should not affect femoral axial and torsional stiffness more than 1% [42]. This is clearly due to the wide difference between the Young's modules. The cancellous bone one is more than one order of magnitude smaller than that of cortical bone. Moreover, according to the available geometry, the epiphyses are filled with cortical bone, and not with trabecular one as usually occurs. These assumptions have negligible influence on the stresses on the plate, the main object of the present study.

The femur and the plate cad models were imported into Solidworks (Dassault Systèmes, Providence, RI). Some reference measurements were obtained from the CAD models via Solidworks and from X-ray images using ImageJ (National Institutes of health, US). The plate dimensions provided by brochure correspond to those measured from the cad model, but not to those measured from the radiographies (Fig. 3.7, 3.8). Comparing the sets of plate measures, the Scale factor (SF) between the radiography and the reality has been calculated. Its value is 1.12 (Table 3.1). Since the available model is a generalization of the femoral shape and size of the average subject, is not exactly similar (according to the definition of similarity) to the patient's bone. The CAD femur model is reduced of a factor of about 1.02 along the longitudinal direction of the femur (Longitudinal factor: LF) with respect to the x-ray image (Fig. 3.9,

3.10). Along the antero-posterior and right-left directions, however, the reduction factor is dependent on the area considered. The diaphyseal section is the same in the model and in the radiographies, while for the proximal and distal areas a scale factor cannot be calculated.

The values of the characteristic bone measurements are approximate to the millimeter, considering the clarity level of the radiographs that reduce the sensitivity of the measurement method.

Since it is possible to resize the CAD according to a uniform value along all the directions, it is necessary to choose a scale factor according to which the model is as similar as possible to the femur with radiographic dimensions. The femur was dilated according to a factor equal to the LF, as the longitudinal dimension was considered of greater importance in the study. In fact, it is necessary that the plate extremities are positioned at the right height respect to the femoral longitudinal axis. Through this operation the femoral model was brought in the same scale observed in radiography. To adapt it to the real case it was necessary to make a reduction in the size of a factor equal to the SF. In this way the obtained femoral CAD model has the real dimensions and is proportionate to the plate model.

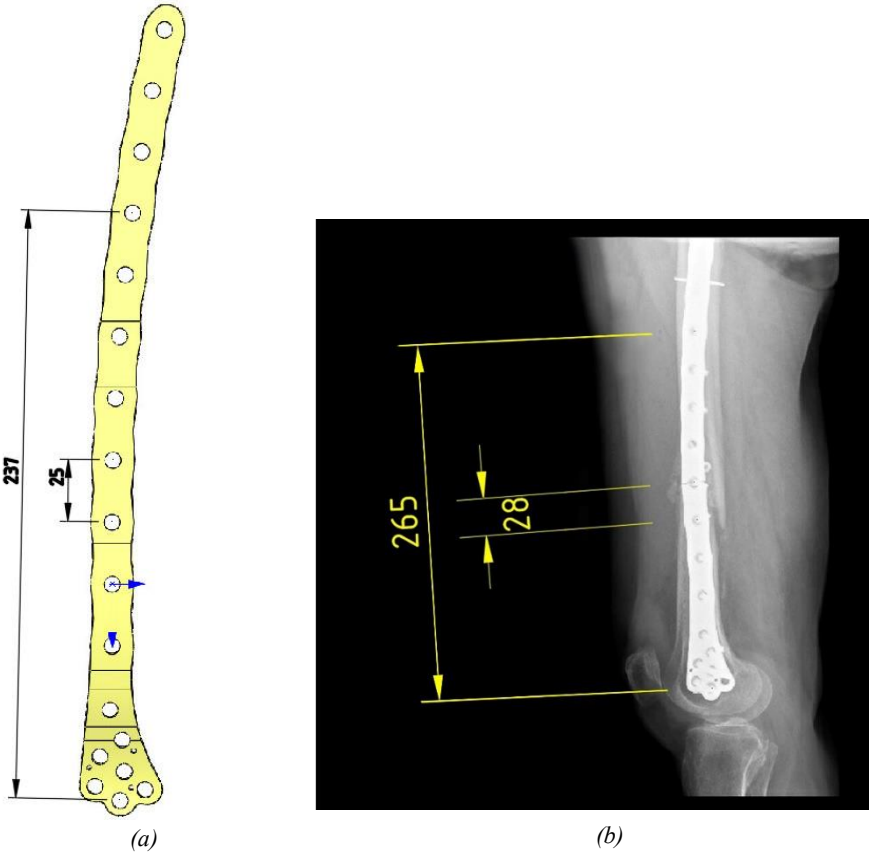


Figure 3.7: Anteroposterior views of the plate model (a) and of the femoral bone with the plate in x-rays (b), with relative measured plate dimensions, in millimeters.

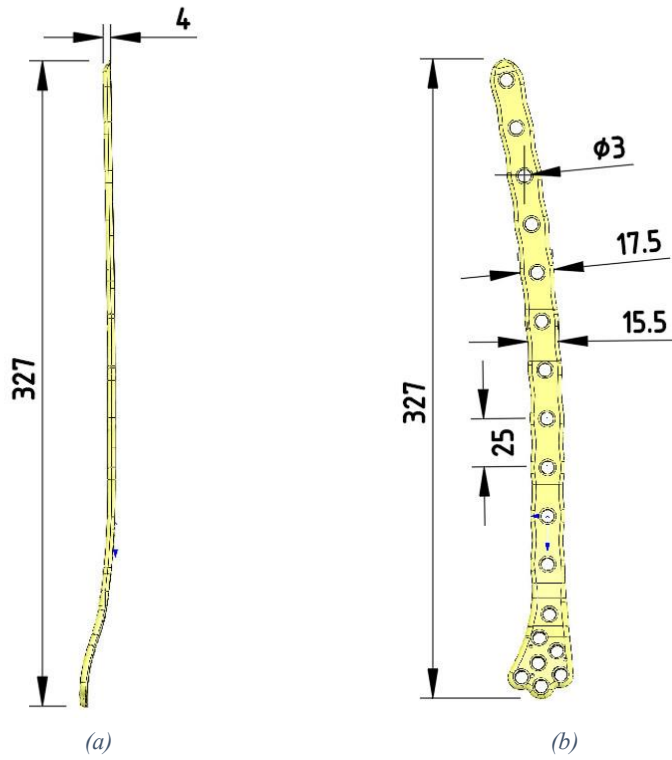


Figure 3.8: Real and CAD plate dimensions, in millimeters, in the lateral (a) and frontal (b) views.

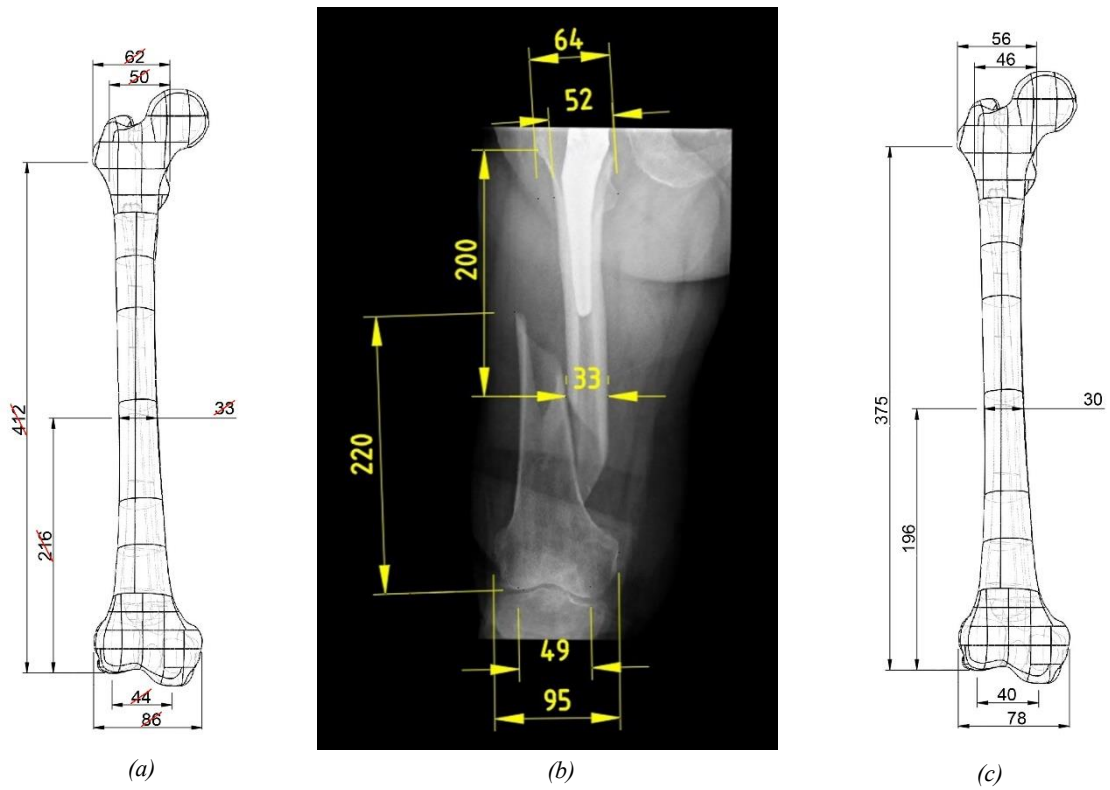


Figure 3.9: Anteroposterior views of the initial (a) and final (c) femur CAD models, and of the femur x-rays (b), with relative reference dimensions expressed in millimeters.

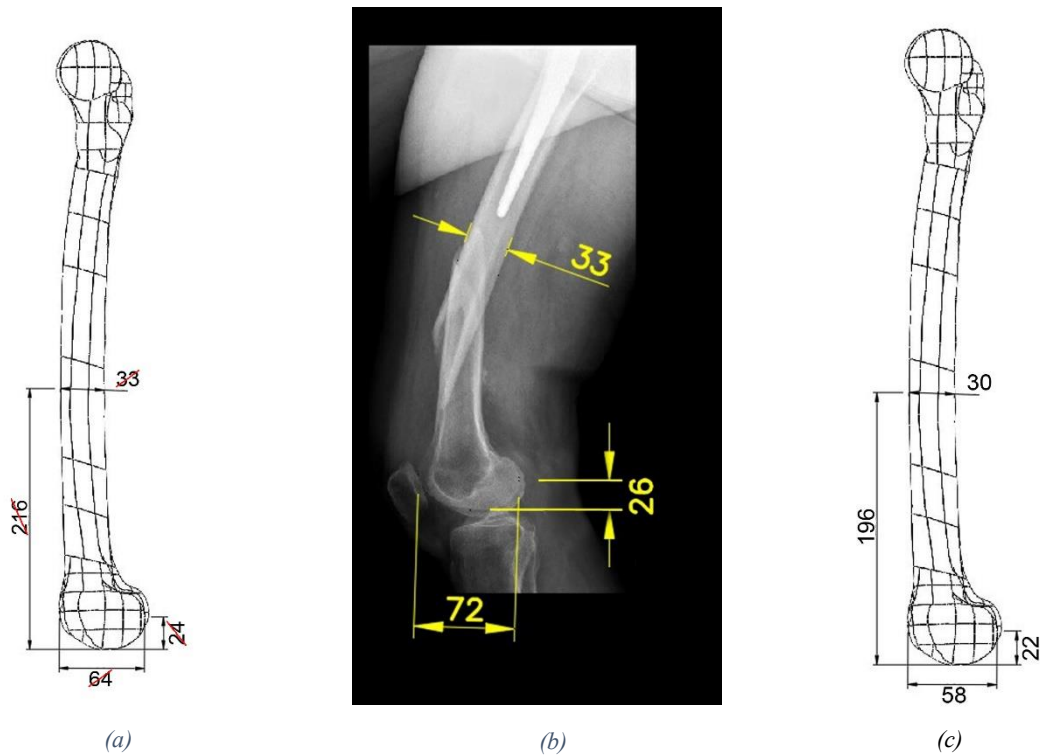


Figure 3.10: Right-left views of the initial (a) and final (c) femur CAD models, and of the femur x-rays (b), with relative reference dimensions expressed in millimeters.

Measure	Direction	Initial CAD model	X-ray	Reality (final CAD model)	SF (x-ray/reality)	LF (x-ray/CAD)
Distance between holes number 1 and 15 (numbered from below)	Longitudinal	237	265	237	$265/237 = 1.12$	-
Distance between two plate holes	Longitudinal	25	28	25	$28/25 = 1.12$	-
Distance between tip of the great trochanter and internal condyle (femur)	Longitudinal	412	420	$420/1.12 = 375$	-	$420/412 = 1.02$

Table 3.1: Main measures from the CAD models and the x-rays, of plate and femur. Calculations of Scale factor (between x-ray and reality) and longitudinal factor (between x-ray and CAD).

3.2.2 Fracture reproduction

To draw the fracture profile on the bone surface some reference points have been identified, their characteristic measurements have been obtained by x-ray and then multiplied by the S scale factor. Specifically, the distances between the aforementioned points and a plane perpendicular to the longitudinal axis of the femur and passing through the lower extremity of the internal condyle were measured (Fig. 3.11a). It has been hypothesized that the four points identified are precisely on the outer surface of the bone and that their projections on the transverse plane are positioned on the extremes of two perpendicular radii of an imaginary circumference, that approximate the diaphyseal transversal section. In the geometric model of the scaled femur the transversal plane passing through the distal end

of the internal condyle (plane 0) has been traced. Four planes (planes 1-4), parallel to it, were then created, using the values calculated from the x-ray measured distances (Fig. 3.11b). On each of these planes the intersection curve with the external bone profile was identified. The four reference points were located and a line crossing them was created. Additional points were added to impose the desired spatial contour. The intersection curves between the four planes and the internal bone profiles were identified, some characteristic points on the internal bone surface were located and the internal profile of the fracture section has been traced (Fig. 3.12a). Using this method a surface fracture with horizontal inclination was obtained, in fact the reference points of the internal curve are situated at the same height with respect to the longitudinal femoral axis of the corresponding points on the external one. Subsequently a surface was created between the two previous curves, whose shape was reproduced at a distance of 10 mm upwards along the longitudinal axis, in order to isolate the fractured bone volume. The bone was then cut and divided into three parts (Fig. 3.12b). The central part was removed. The fracture surfaces obtained are not inclined along the radially direction, as usually occurs in real cases, but it is assumed that this approximation does not over-influence the femur behaviour.

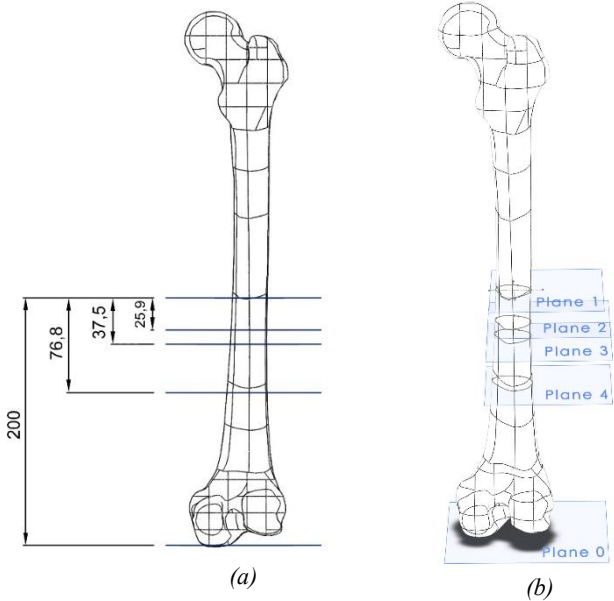


Figure 3.11: Reference measures used for the construction of the femoral fracture (a). Transversal planes created for the definition of the femoral fracture (b).

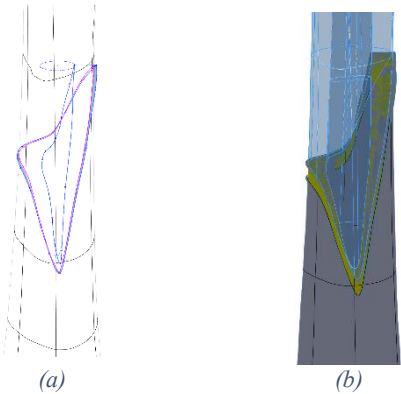


Figure 3.12: External and internal fracture surface profiles created (a). Fracture volume obtained (b).

3.2.3 Femur geometry refinement

The cortical region of the inferior bone diaphysis of the patient is thinner than the superior one, and its thickness decreases downwards along the longitudinal axis (Fig. 3.1). To make the finite element model more similar to the real situation, the thickness of the lower femoral bone previously obtained was reduced.

The aforementioned thickness was reduced as a function of the height along the longitudinal axis of the femur. The distal area of the diaphysis is therefore thinned than the proximal ones. A plane tangent to the higher area of the inferior diaphyseal segment and perpendicular to its longitudinal axis was created. Seven planes parallel to the previous one were then added, according to the indicated distances (Fig. 3.13a). The intersection curves of these planes with the femoral internal and external surfaces were identified. Some profiles have been designed to create a cutting surface inside the cortical region, according to the established thicknesses (Fig. 3.13b). A solid was created through this surface, subsequently subtracted from the lower bone body (Fig. 3.14a, 3.14b).

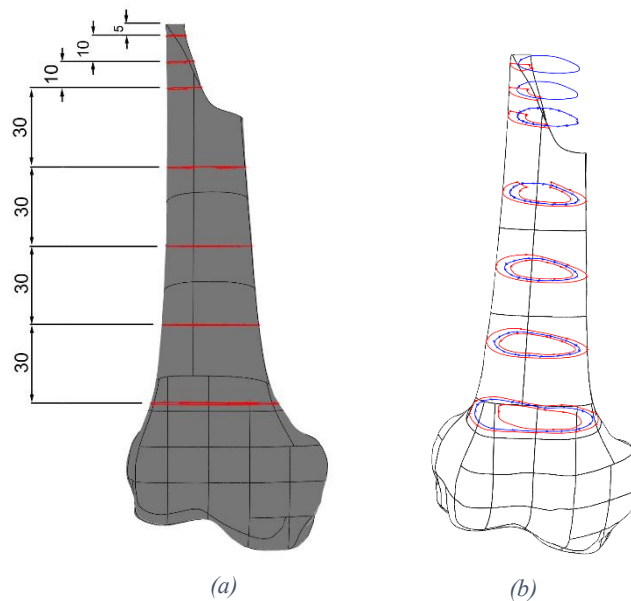


Figure 3.13: Inferior bone segment with the created planes and the relative distances (a). Inferior bone segment with the created profiles of the cutting surface (b).

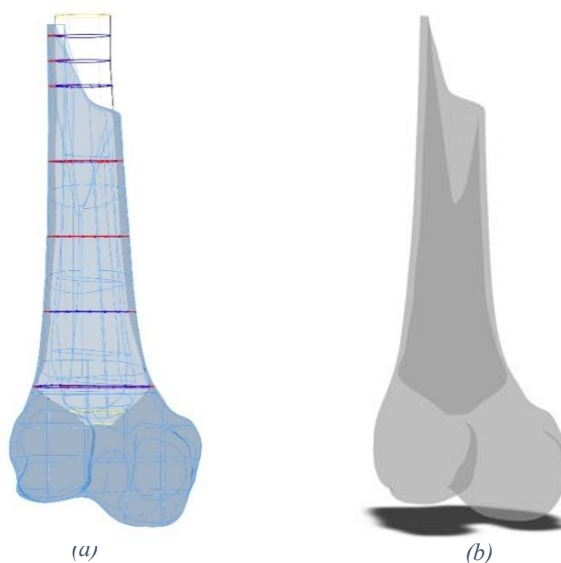


Figure 3.14: Inferior bone segment with the cutting surface internally created (a). Profile of the inferior bone segment with reduced thickness (b).

3.2.4 Prosthesis modification and positioning

As there was no available information on the implanted prosthesis, an available prosthetic stem model, of appropriate size, has been chosen (Fig. 3.15a). Was assumed that this choice does not excessively influence the behaviour of the bone, subjected to load. The femoral head, of suitable size, was added to the prosthetic stem model as follows. The stem body axis and the stem neck axis were identified, and a plan passing for both, was created. On this plane the section profile of the head has been drawn. The central point of the femoral head has been individuated, situated on the neck axis and whose distance respect to the body axis is equal to 36 mm, the nominal offset value of the stem. On the plane a circumference was traced, whose centre is the aforementioned point and whose radius is equal to its 38 mm, value indicated in the stem model file. The circumference was suitably cut in order to obtain the section of the femoral head (Fig. 3.15b). The prosthetic head volume was created through the revolution operation of the femoral head section around the neck axis (Fig. 3.15c).

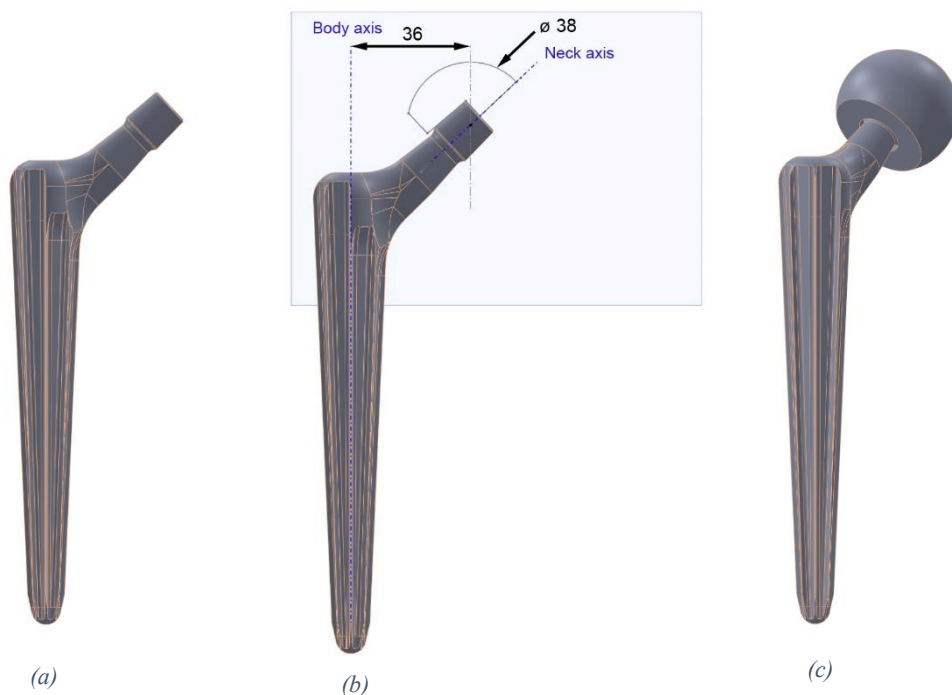


Figure 3.15: Prosthetic stem model (a). Prosthetic stem model with the head section profile (b). Prosthetic stem and head models (c).

The prosthesis and femur components were positioned so that the centre of the prosthetic head coincide with the centre of the femoral head. By rotating the prosthesis around the centre point the stem was rightly directed into the femur medullary canal (Fig. 3.16a). The cavity for the prosthesis seat was obtained by subtracting it respect to the femoral body. The neck and body axes of the prosthesis were duplicated and saved within the model of the upper bone segment.

Within the obtained assembly, the axial symmetry plane of the prosthesis was identified, on which a cutting profile was designed (Fig. 3.16b). Through the extrusion of this profile, in a direction perpendicular to the plane, a resection of the femoral head and of part of the great trochanter was carried out. In this way the femoral head was removed, obtaining a configuration similar to that present at the end of the real implant operation (Fig. 3.17).

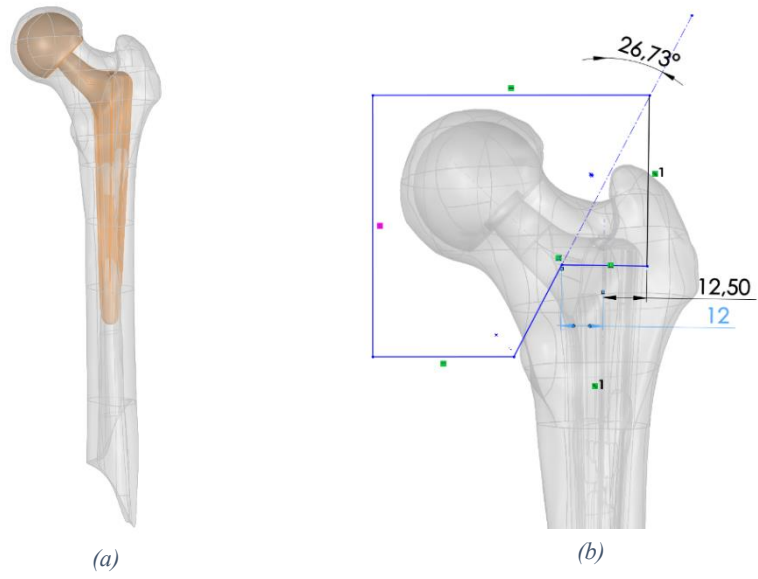


Figure 3.16: Prosthetic model positioned in the femoral bone (a). Cutting profile of the upper femoral model (b).

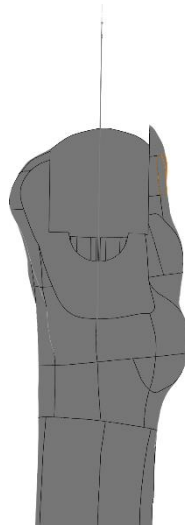


Figure 3.17: Cut bone model, ready for the insertion of the prosthetic stem.

3.2.5 Screws and bushings modification

The plate screws have a diameter of the head measuring 5 mm and a variable length from 12 to 110 mm. A simplification of the initial geometries of screws and bushings has been carried out, in order to reduce the subsequent formation of too small and distracting elements, and therefore the computation necessary in the calculation phase (Fig. 3.18). The screws diameter has been slightly increased in order to compensate for the loss of stiffness caused by the thread removal.

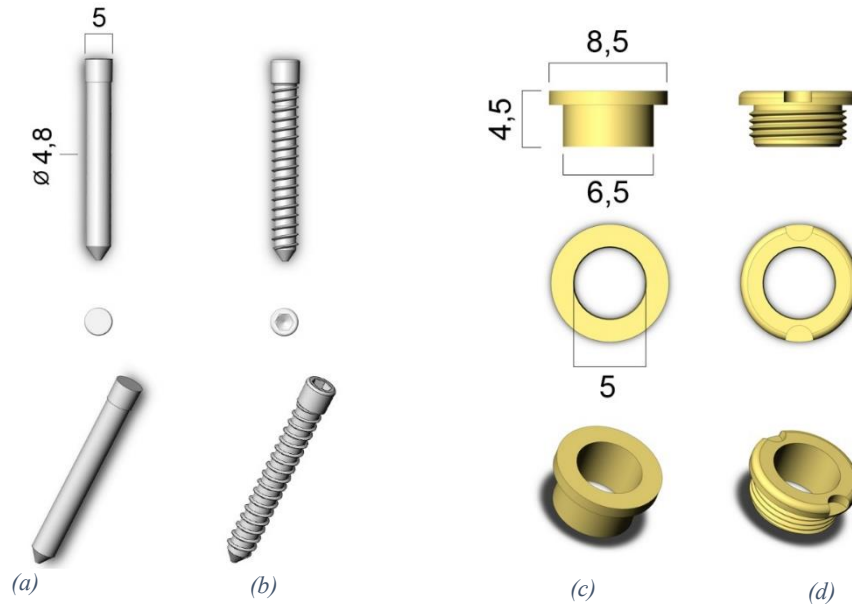


Figure 3.18: Geometry of a simplified (a) and an original (b) screw models. Geometry of a simplified (c) and an original (d) bushing models.

The type of the implanted interfragmentary screw is unknown. For this reason, an available screw geometric model was used, to which some simplifying were apported. The thread has been removed as follows. A plan has been identified containing the screw longitudinal axis, on which a rectangular cut profile has been drawn. Through a revolution of the profile around the longitudinal axis a volume was created, subsequently subtracted from the screw model. Finally, the remaining carvings were removed through the revolution of a further profile, contouring the screw (Fig. 3.19a, 3.19b).

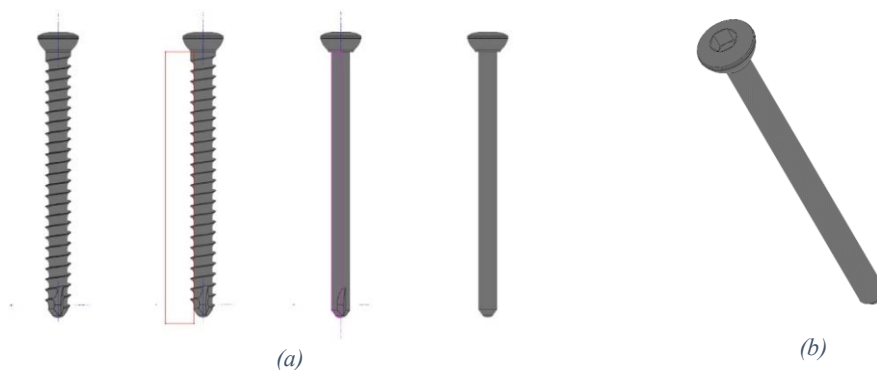


Figure 3.19: Demonstration of the procedure for the simplification of the interfragmentary screw model (a), simplified interfragmentary screw model (b).

3.2.6 Femoral plate features

The plate used, as previously specified, is of the O'Nil distal femur model, produced by the "Intrauma" company. The extra-long size was chosen (Fig. 3.8). This model has 7 holes in the condylar area and 11 along the diaphyseal one. The screws, relative to each hole, were individuated (Table 3.2). In order to simplify the explanation, the holes were numbered in ascending order from the plate bottom to the top (Fig. 3.20).

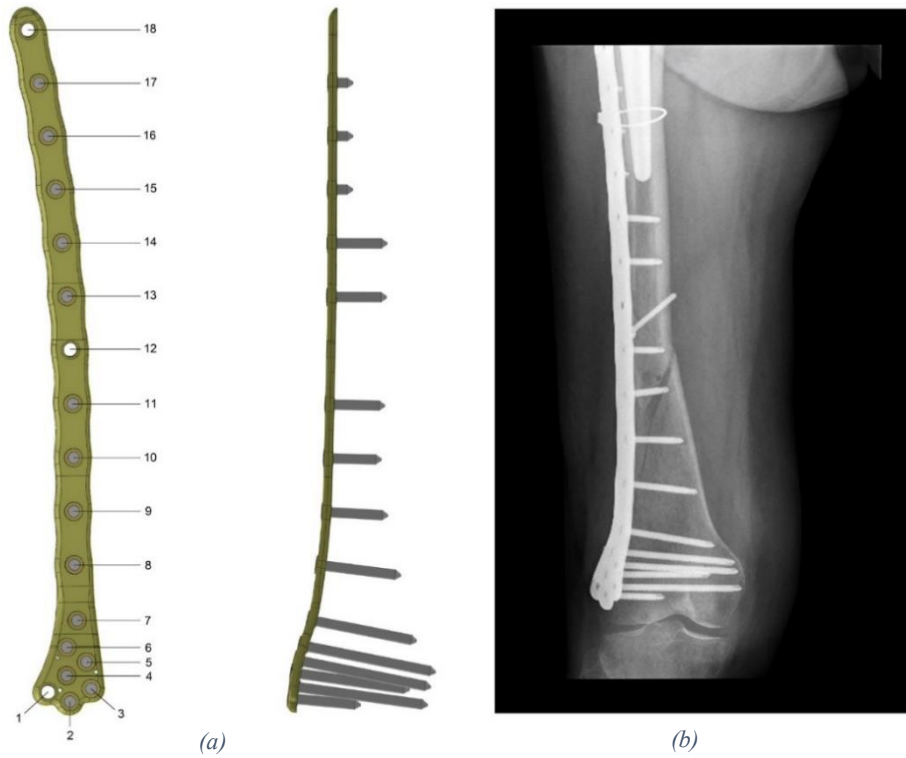


Figure 3.20: Plate model frontal and lateral views, with holes numeration (a). Plate x-ray image, demonstrative of the chosen screw lengths (b).

Hole number	Screw length [mm]
2	40
3	80
4	70
5	80
6	80
7	65
8	50
9	38
10	34
11	30
13	30
14	30
15	12
16	12
17	12

Table 3.2: Screws lengths and corresponding holes number.

3.2.7 Geometry assembly

Through the coupling of axes and surfaces, screws and bushings were positioned inside the corresponding holes. The axis of each plate hole was coupled with the one of the corresponding bushing and screw, and the annular plate-bushing and screw-bushing surfaces were overlapped (Fig. 3.21).

The plate was positioned relatively to the femur according to the x-ray images, by means of displacements and rotations around the Cartesian axes. In order to avoid the overlap between the two models, a minimum limit of distance between them of 1 mm was defined.

The inferior bone segment of the patient was slightly inclined with respect to the diaphyseal axis (Fig. 3.20b), so it was necessary to modify its position in the model by means of a slight rotation.

The prosthetic stem was constrained to the upper femoral segment through the coupling of the neck and body axes, present in both models. The femoral head was constrained to the stem by overlapping the joint surfaces. The resulting assembled model was compared with the x-ray images on order to verify the correct positioning (Fig. 3.22-3.25).

After the positioning phase, subtraction was performed between the femur and the screws volumes. The geometric models of upper femur, lower femur, prosthetic stem, prosthetic head, bushings, plate screws, interfragmentary screw and plate were isolated and saved. The obtained files were converted and imported into the finite element pre-processor software Hypermesh 13.0 (Simulia, Dassault Systèmes, Providence, RI). It is highlighted, that the presence of the cerclage, situated near the area comprised between the holes 16 and 17 of the plate, has been neglected as it is not stressed. Therefore, it would not bring variations in the analysis of the behaviour of the femur and plaque.

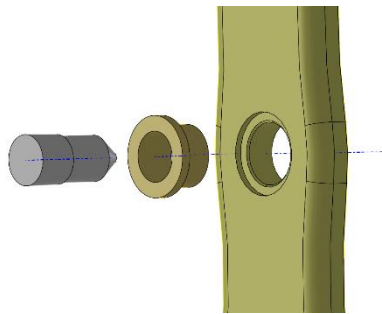


Figure 3.21: Screw, bushing and plate hole relative positioning.

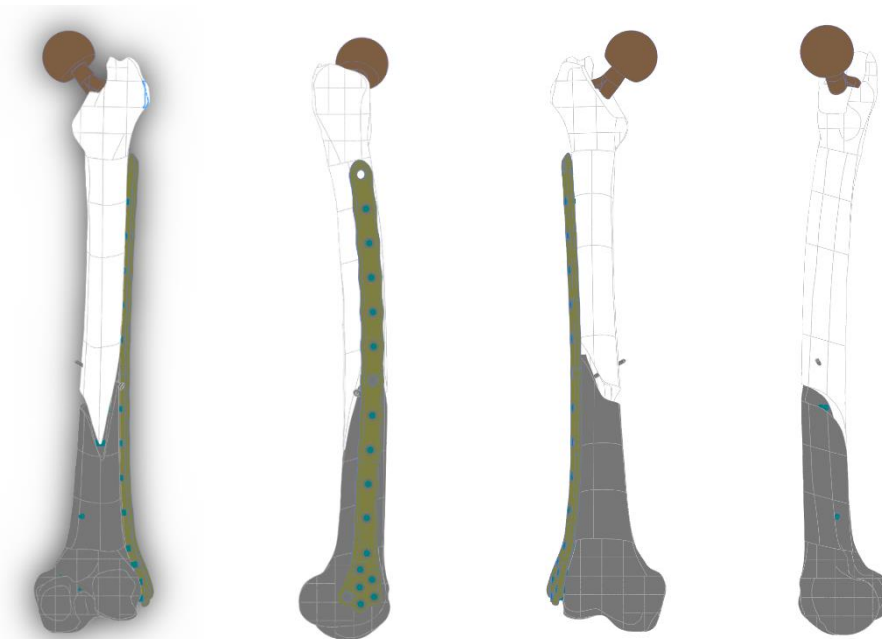


Figure 3.22: The resulting assembled geometrical model, in different views.

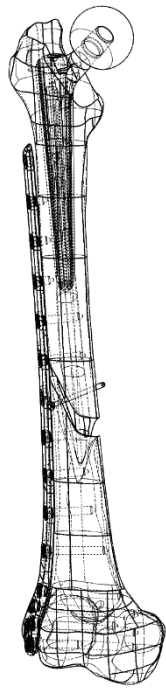


Figure 3.23: Resulting assembled geometrical model compared with the corresponding x-ray image.

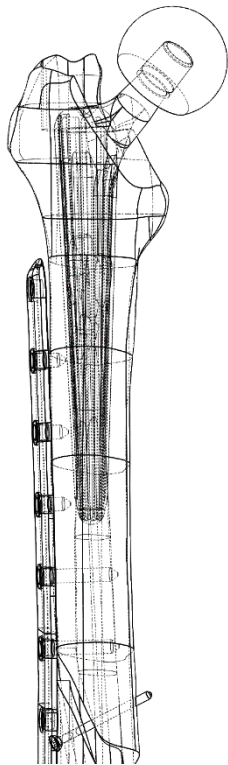


Figure 3.24: Resulting assembled geometrical model compared with the corresponding x-ray image.

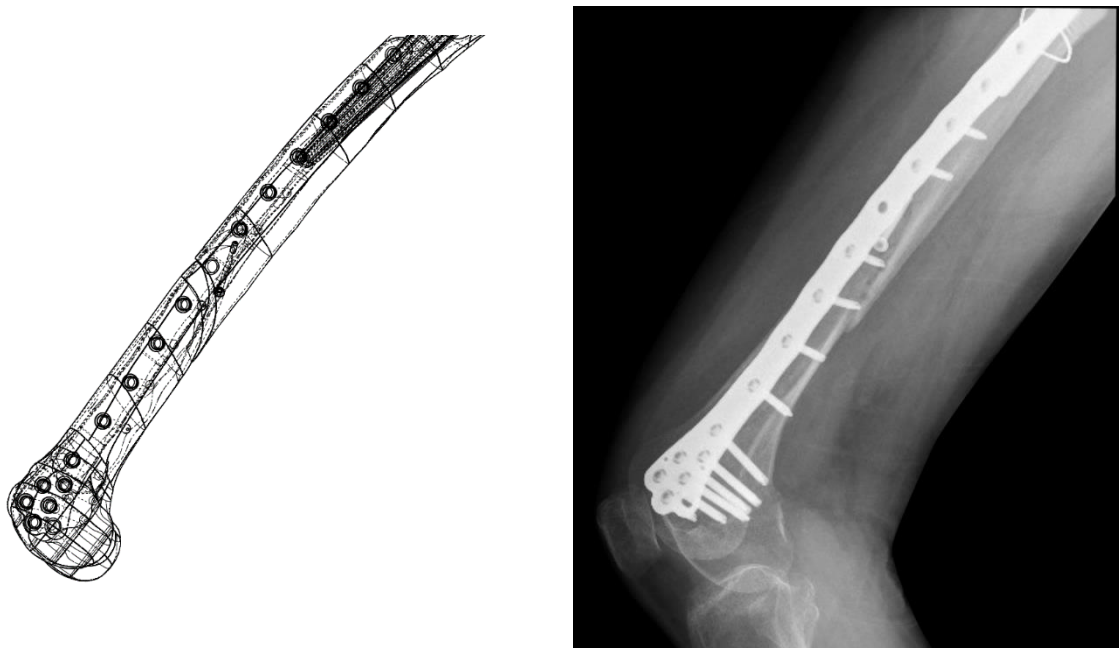


Figure 3.25: Resulting assembled geometrical model compared with the corresponding x-ray image.

3.3 Preprocessing phase

3.3.1 Mesh creation

The surface mesh was created using triangular elements with side size of 2 mm, allows to obtain a double layer of tetragonal elements along the thickness of the plate, and therefore to observe the variation of the stress along it. Furthermore, according to the sensitivity analysis performed, this size guarantee a good precision regarding the maximum stress values calculated in the plate.

In order to reduce the calculation errors in the subsequent processing phase, the mesh quality control was performed and the excessively distorted elements were improved or eliminated and replaced. The chosen mesh quality criterion admit triangles with internal angles higher than 15° and lower than 130° , and aspect value³ lower than 5. Consequently, the volume mesh was created using tetrahedral elements Tetra-4, having four nodes each, linear displacement behaviour and six degrees of freedom at each node (Fig. 3.26). The chosen 3D mesh quality criterion admits elements with a tetra-collapse³ value higher than 0.1. The tetragonal shape was considered the most suitable because it fits well to the irregular femur volume.

A study on the advantages and disadvantages of using hexahedral, tetrahedral or cubic mesh in the modelling of femurs, was published by M. Viceconti et al. According to it, a tetrahedral mesh requires a clean solid model with well-defined surfaces. Gaps or overlaps between surface patches and other surface irregularities can produce bad quality triangles and consequently distorted tetrahedrons. If the quality of the geometry is good, tetra-meshing is a precise method [43]. According to A. Ramos et al. tetrahedral and hexahedral elements are both good alternatives to model the femoral shape. However, analysing Von Mises stresses and principal strains on some points of the femoral surface, the tetrahedral ones reported more precise results. This precision is much more effective in the diaphyseal zone, of greater interest in this thesis [44]. The same results are again compared using the ten-node quadratic tetrahedral (Tetra-4) and four-node tetrahedral (Tetra-10) elements. The variation obtained is very low,

³ Measure of mesh element's deviation from having all sides of equal length.

and is reduced with the increase of the mesh refinement. This was also affirmed by K. Polgar et al. that compared the performances of linear and quadratic tetrahedral elements modelling a femur-prosthesis system. The CPU time needed to solve the model increased rapidly and non-linearly with the number of degrees of freedom. Therefore, obtain the solution for meshes having the same number of degrees of

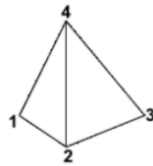


Figure 3.26: Tetra-4 element shape.

freedom can take up to 2.08 times longer in the case of a T4 than in the one of a T10 (K. Polgar et al. [45]). Nevertheless, the size of the mesh is small enough to consider the use of first-order elements to be sufficient in the present study. Furthermore, the computational weight of the model is so reduced as to allow the use of a relatively refined mesh.

In order to simulate bonding contacts between the components it is necessary that the surface meshes of the interface areas coincide. The two-dimensional mesh of the lower and upper femoral components was initially created. The internal surface mesh of the upper femoral component was reproduced and substituted to the external surface mesh of the prosthetic stem (Fig. 3.27). The same procedure was used to define the contact surfaces between bone and screws, bushings and screws, plate and bushings, prosthetic stem and head. In order to obtain the contact, the coincidence of the corresponding nodes between the overlapping surfaces was imposed.

The surface mesh belonging to the fracture site was constructed by copying the contact interfaces present in the upper femur, lower femur and interfragmentary screw components, and completed by filling functions.

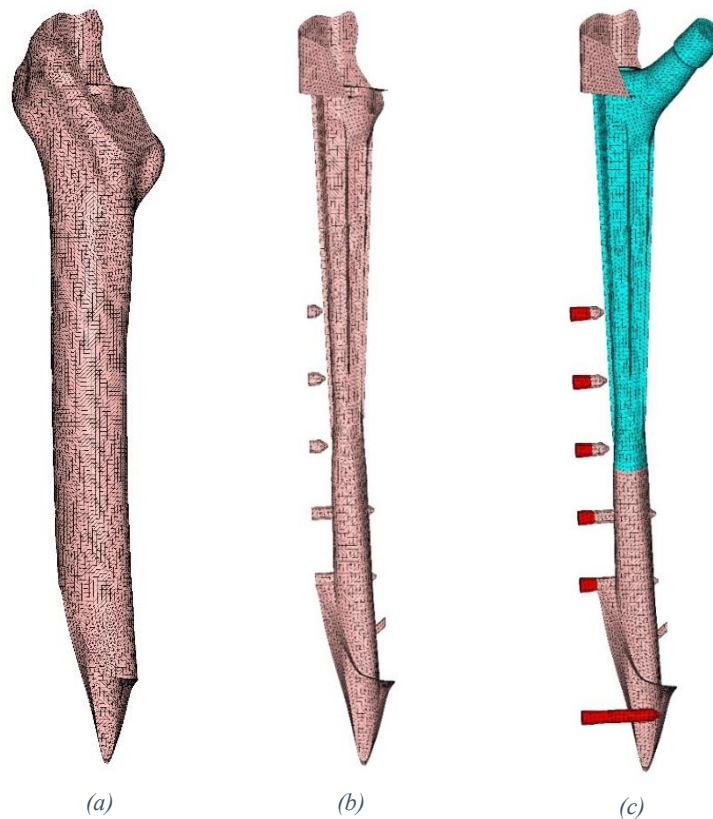


Figure 3.27: External (a) and internal (b) surface meshes off the upper femur (a), internal surface mesh of the upper femur reproduced in order to crate part of the surface meshes of prosthetic stem and plate screws (c).

The obtained volume mesh are showed (Fig 3.28, 3.29).

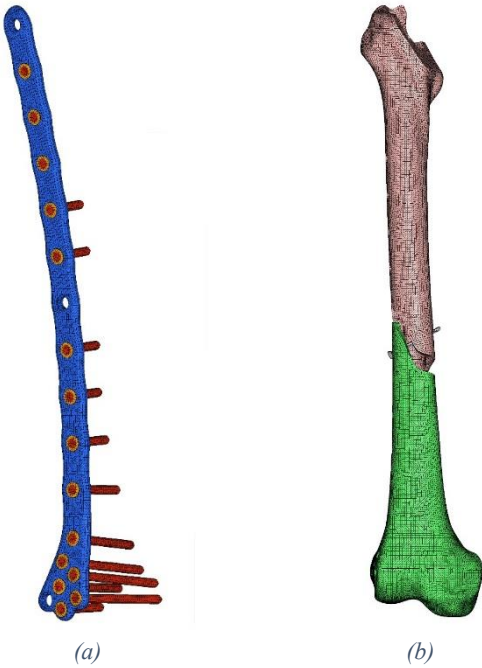


Figure 3.28: Plate, bushings and screws volume meshes (a), upper and lower femur, and interfragmentary screw meshes (b).

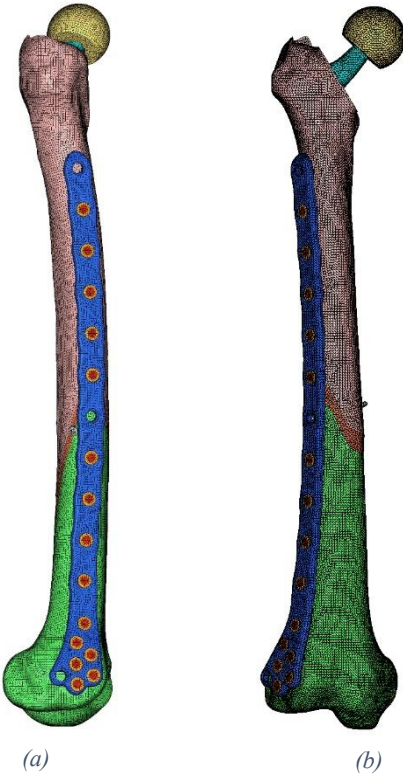


Figure 3.29: Right-left and anteroposterior views of the obtained mesh volumes.

The interfragmentary screw crosses the fracture. For this reason, to suppose that the relative position between the two is equivalent to the real one, is inaccurate.

Two alternative models to the reference one have been implemented, in which the mesh in the fracture zone has been modified, to evaluate the dependence of the analyzed results on the position of the interfragmentary screw (Fig. 3.30).

The models implemented are the following:

- The reference situation considers a 1 cm thick fracture.
- A second model includes a 2 cm thick fracture
- A third model includes a 2 cm thick fracture with a geometry that completely surrounds the interfragmentary screw body.

Analyzing the results it was observed that the relative position between fracture and screw does not greatly affect the stress distributions and values within the plate and the deformations of the model.

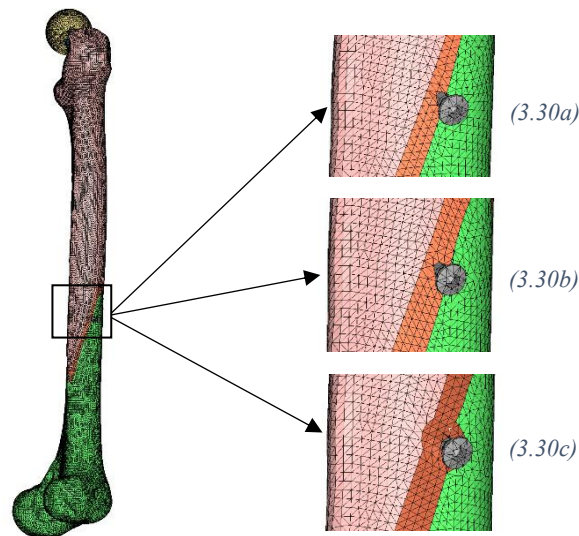


Figure 3.30: Implemented conditions of the interfragmentary screw position respect to the fracture geometry. Conditions with a 1 cm thick fracture (a), with a 2 cm thick fracture (b) and with a geometry that surrounds the interfragmentary screw body (c).

3.3.2 Material properties assignment

The fractures of the implemented materials were specified. The relative properties were created and assigned to the model components. The used materials are stainless steel, cortical intact bone, cortical fracture bone and a titanium-aluminium-vanadium alloy (Table 3.3).

Component	Assigned material	Elastic modulus [Mpa]	Poisson modulus	Mechanical behaviour
Prosthetic head	Steel	210000	0,3	Linear elastic
Prosthetic stem	Steel	210000	0,3	Linear elastic
Superior bone	Intact bone	18160	0,3	Linear elastic
Central bone	Weak cortical bone	Variable	0,3	Linear elastic
Inferior bone	Intact cortical bone	18160	0,3	Linear elastic
Plate	Steel	210000	0,3	Linear elastic
Plate bushings	Ti6Al4V alloy	110000	0,3	Linear elastic
Plate screws	TiAlV alloy	110000	0,3	Linear elastic
Single screw	Ti6Al4V alloy	110000	0,3	Linear elastic

Table 3.3: Materials assigned to the model components and corresponding features [23].

Stainless steel

The material constituting the plate is the stainless steel ISO 5832-1, whose chemical composition and mechanical properties are indicated (Tables 3.4, 3.5). It is an austenitic steel, poor in carbon, extra-soft and with high ductility. Oxidability is conferred by the high percentages of nickel and chromium which act on corrosion resistance. It has medium hardness (HRC = 30.5) and a wide range of plasticity. The yield and breakage stresses are greater than in austenitic steels with similar composition, due to the very fine grain size. Regarding the stem and prosthetic head components, the material used is unknown. For this reason it was decided to assign them the same material composing the plate, the AISI-316L american grading steel, usually used also in the prosthetic field. Despite the plastic character of the steel, the mechanical behavior has been assumed linearly elastic since the analysis in question was carried out in a stress range below the plate and prosthesis yield point.

<i>Element</i>	<i>Chemical composition [%]</i>
<i>C</i>	<i>0,0130</i>
<i>Si</i>	<i>0,2900</i>
<i>Mn</i>	<i>1,6400</i>
<i>P</i>	<i>0,0200</i>
<i>Si</i>	<i>0,0003</i>
<i>N</i>	<i>0,0940</i>
<i>Cr</i>	<i>17,5500</i>
<i>Ni</i>	<i>14,5500</i>
<i>Mo</i>	<i>2,7600</i>
<i>Cu</i>	<i>0,0500</i>

Table 3.4: Chemical composition of the ISO 5832-1 stainless steel.

<i>Mechanical property</i>	<i>Nominal value</i>
<i>Elastic modulus [MPa]</i>	<i>210000</i>
<i>Poisson modulus</i>	<i>0,3</i>
<i>Tensile strength [Mpa]</i>	<i>1014</i>
<i>Yield strength [Mpa]</i>	<i>859</i>
<i>Elongation (A50mm) [%]</i>	<i>14,6</i>
<i>HRC</i>	<i>30,5</i>
<i>Grain size [G]</i>	<i>6,0</i>

Table 3.5: Mechanical properties of the ISO 5832-1 stainless steel.

Titanium-aluminium-vanadium alloy

The material constituting plate bushings and screws is the Ti6Al4V – ISO 5832-3 alloy. Ti6Al4V alloys have a composition mainly of titanium, 6% in weight on average of aluminum, 4% in weight on average of vanadium and a variable micro quantity of other elements. It has american designation ASTM F136. It has high mechanical strength, corrosion resistance and good biocompatibility. Its elastic modulus is smaller respect to many other metal alloys and closer to the one of the bone with which it must interface directly. Inside the model the material has been simplified as linearly elastic because in the conducted analysis the maximum stress in screws and bushes remains far below the yield point. The values of breakage and yield stresses are not specified because are not necessary and very dependent on the forging thermal treatment. The available mechanical properties are indicated (Table 3.6). Since the

material constituting the single screw is unknown, it was decided to assign it the same titanium-based alloy used for the plate screws.

<i>Mechanical property</i>	<i>Nominal value</i>
<i>Elastic modulus [Mpa]</i>	<i>110000</i>
<i>Poisson modulus</i>	<i>0,3</i>

Table 3.6: Mechanical properties of the Ti6Al4V alloys.

Cortical bone

As previously explained, the femoral model don't comprehends the trabecular component, therefore only the characteristics of the cortical bone are considered, which vary according to the patient's age and to the possible presence of bone pathologies. According to R.K. Nalla et al. the age-related changes in the mechanical properties of cortical bone have been mainly attributed to increased porosity and hypermineralization, which are strictly correlated with Young's modulus and fracture toughness. The strength of cortical bone under traction and compression declines by approximately 2% per decade beginning in the third decade of life, and fracture toughness decreases approximately 4% per decade [46, 47]. Increasingly common diseases such as osteoporosis and diabetes involve marked changes in cortical bone's mechanical behavior. As information regarding the age of the patient and the presence of bone pathologies were not made available, a material whose mechanical characteristics correspond to those of an adult individual, in absence of deteriorating pathologies, was implemented.

The cortical femur material was modelled as homogeneous, linear elastic and isotropic. It was assumed that these simplifications does not excessively affect the bone behaviour in the conducted analysis.

Usually, in finite element models based studies, the femoral bone is divided into a sufficient number of regions to which different material properties are assigned. This process is effectuated basing on bone images previously obtained by computerized tomography, in which the level of grey-value belonging to each pixel allows to assign it to the corresponding material. Wei Sheng et al. affirm that use a two materials model (for trabecular and cortical bone), is sufficient to obtain acceptable values regarding bone stresses. In fact, a two materials model, loaded axially, can attain the precision of a 180 materials model with less than a 2% error [48]. Model that, as previously said, can be correctly replaced by removing its cancellous region. A study developed by F. Taddei et. al, analyses the stresses in the superficial epiphyseal zone of the femoral bone, within a non-homogeneous model constructed by computed tomography and a homogeneous two-materials model. This femur was tested in vitro under different loading scenarios and the results of these tests were used to verify how the adoption of the simplified model would change the accuracy with respect to the inhomogeneous one. The density-based model was more precise, as expected, with an average error of 8,6% regarding the maximum measured stress, with respect to the experimental value. The two materials model, anyway, maintained the average error under the 10% of the maximum value.

However, it is reasonable to consider that this agreement between the experimental data measured on the bone surface and the global model performance cannot guarantee that the isotropic material approach will predict the behaviour of the internal portion of the bone with the same accuracy. In fact, the variation between the stress field distributions predicted inside the bone by the two models was higher than the ones regarding the surface. It is expected that the diaphyseal zone results maintain a better similarity with respect to the real case, respect to the epiphyseal ones. For the purpose of this thesis, furthermore, an hypothetical average error of 10% is considered acceptable. Moreover, the author affirm that the bone could be assumed to behave on a linearly elastic way [49].

The behaviour of the cortical bone material is anisotropic. Nevertheless, his strenght and traction and compression moduli along the longitudinal direction are greater than those along the radial and circumferential ones, so it can be assumed transversely isotropic [47]. Nowadays most of the FE models simulate bone tissue as an isotropic material due to the simplicity of its implementation. Liang Peng et. al, investigated the effects of orthotropic material property assignment on a femoral finite element model

by comparing it with isotropic material property assignment. Under two loading conditions, double-leg standing and single-leg standing, the maximum equivalent Von Mises stress and the maximum nodal displacement were similar, differing of values lower than 1.2% [6]. H. Yang et al. investigated the differences in maximum Von Mises stresses and maximum nodal displacements between isotropic and orthotropic models, under different loading conditions, on some proximal and diaphyseal zones of a femur surface. The results were significantly different depending on the applied loading condition, but in the diaphyseal area these were lower than 1% in all the cases [50]. Moreover, in an orthotropic model, stress and strain distributions are relatively influenced by the orientation directions of the mechanical properties [51]. According to W.S. Enns-Bray, anisotropy have a minimal impact on macroscopic measurements, but alter the internal strain behaviour. This suggest that studies considering failure of internal structures should include anisotropy to their model, but CT-based FE models measuring femoral stiffness have little to gain from the addition of anisotropy. Since the densitometry information of the femur in question is not available, and the interested diaphyseal area is little affected by the material properties orientation, the isotropy assumption is considered sufficient [52].

Different values of the cortical bone elastic modulus and Poisson modulus are available from literature. D.C. Wirtz et al. conducted a literature analysis concerning the relationship between Young’s modulus and apparent density of the cortical femoral bone. They affirmed that the elastic modulus vary, depending on the bone density, within values between 8 and 20 GPa [53]. F. Taddei et al. in their study implemented a femur finite element model whose cortical bone elastic and Poisson’s modulus were equal to 19,3 GPa and 0,3 [49]. The modules chosen values were taken from an article published in the journal “Annual Review of Biomedical Engineering”, edition of the year 2018 (Table 3.7) [47].

<i>Mechanical property</i>	<i>Nominal value</i>
<i>Elastic modulus [Mpa]</i>	<i>18160</i>
<i>Poisson modulus</i>	<i>0,3</i>

Table 3.7: Mechanical properties of the femoral cortical bone.

With regard to the fracture bone callus, the mechanical properties are dependent on the specific situation. Bone tissue, in fact, has a remarkable ability for self-repair and regeneration after an injury and is able to completely restore its mechanical function. The time needed for the bone regeneration is different for every person, and early controlled by intrinsic genetic factors.

Manjubala et. al conducted a study in order to correlate the nanoindentation modulus of the callus formed over the course of bone healing. The nanoindentation module is the elastic modulus calculated through measures taken from the nanoindentation tests. Midshaft tibial samples, obtained from a bone healing experiment performed on sheeps with an osteotomy gap of 3mm at time points of 2, 3, 6 and 9 weeks after fracture, were employed. The nanoindentation test was performed and the nanoindentation modulus was calculated. The resulted modulus, was comprise between 6 and 10 GPa after 3 weeks and exceeded 10 GPa after 9 weeks [54].

Considering the dependence of the elastic modulus of bone callus during healing, from the morphologic and genetic factors, and the uncertainty regarding the patient's correct bone reduction, different values were assigned to the central femoral component. These values were selected according to some proportionality factors, up to the lower limit of 181.6 MPa (Table 3.8). Considering that the fracture occurred after three months from the plate implant, an elastic modulus value equal to half of that of healthy bone was considered representative of the situation of higher bone reduction. The Poisson’s modullus value was considered to be equal to that of healthy bone in all the situations.

<i>Reduction factor [%]</i>	<i>Elastic modulus [Mpa]</i>	<i>Poisson modulus</i>
50	9080	0,3
20	3632	0,3
10	1816	0,3
2	363,2	0,3
1	181,6	0,3

Table 3.8: Mechanical properties of the femoral cortical bone.

3.3.3 Boundary conditions assignment

To test the functioning of the plate, some commonly and accidentally load configurations have been simulated. Specifically, the effects of the forces acting on the femur during walking, lateral falling and stumbling, were analysed. To distribute the loads on the application surfaces, one-dimensional rigid elements of the RBE3⁴ type have been used. Through these, the nodes belonging to the application volumes were connected to a further node outside the model, on which the forces were then applied. Consequently, the forces resulted equally distributed among the connected nodes. As regards the analysis of walking and stumbling, a distal portion of the lower femur has been constrained according to all the degrees of freedom to guarantee the achievement of balance to the model. Some nodes of the femoral base were connected to a further one, external to the model, by means of one-dimensional rigid elements of the RBE2⁵ type. The external node was then constrained (Fig. 3.31).

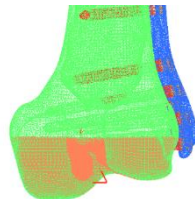


Figure 3.31: Constraint applied to the femur base, during walking and stumbling configurations.

Walking boundary conditions

Walking is a cyclic pattern of movements. A single gait cycle is constituted by different phases. By convention, the cycle begins when one of the feet (is here considered the right foot) makes contact with the ground. The gait cycle is mainly divided in stance and swing phases. During the first one the considered foot is on the ground, whereas in the swing phase that same foot is swinging through in preparation for the next foot strike. The stance phase occupies the first 60% of the walk cycle, and is further divided into events, based on the movement of the considered foot. The cycle begin with the heel strike of the foot on the ground. Subsequently, during the “loading response”, the plantar surface of the foot touches the ground, during the 10% of the cycle. The “midstance” event, between the 10% and the 30%, occur during the swing phase of the contralateral foot. During the “terminal stance”, between the 30% and the 50%, the heel loses contact with the ground. Finally occur the “toe off”, in which the contact of the foot with the ground terminate [55]. During the stance phase the contact force acting on the hip surface is varying, and assume two peaks values during the midstance event and just before the toe off instant. A graphic representation of the hip contact force variation, in function of the gait cycle percentage is showed, indicative of the general trend that the force assume (Fig. 3.32).

⁴ Element that induce a motion in a node as a function of the weighted average of other nodes.

⁵ Element that create a rigid connection between nodes, in which the dependent node assume the same motion as the independent one on the degrees of freedom that have been linked.

To analyse the effect of contact forces due to walking on the stresses present in the plate, load configurations from two different studies were applied. First of all, three characteristic instants are considered during the walk cycle, which do not correspond to the situations of greatest load on the prosthetic head, but are useful to understand the variation of the plate behaviour during the cycle. Subsequently the time instant in which the greatest contact force on the head is applied, is considered. Since no information is available regarding the mass of the patient, it was decided to assume this amounting to 95 kg for two reasons. This value is greater than the mean body weight of the european women, so it guarantees a safety margin with respect to the most probable real situation. Furthermore, the amount of the available data, regarding the forces applied to the femur under the analysed conditions, is wide, for a subject with body mass equal to the chosen value.

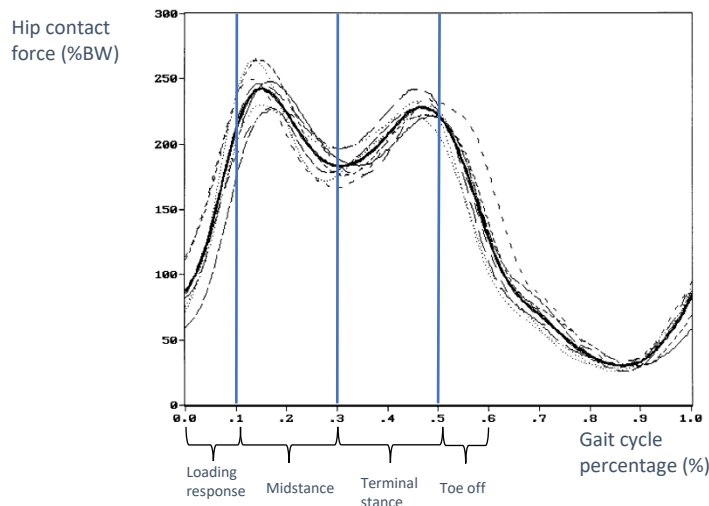


Figure 3.32: Trend of the multiplicative factor of body weight, for the calculation of the contact force applied to the hip, in function of the gait cycle percentage, from different subjects. The loading events occurring during the stance phase of the walking cycle are highlighted. Figure modified from [56].

Walking forces – A configuration

In the first loading phase, the effect of the loads acting on the bone during three moments of the walking cycle, was studied. The phases analysed, are expressed like percentage of the gait cycle time. The considered instants are equal to the 10% of the cycle, during the beginning of the midstance, the 30% of the cycle, during the beginning of the terminal stance, and the 45% of the cycle, just before the toe off. A complex loading configuration that includes all the muscles that act around the hip joint is infeasible, therefore a choice should be made to include only those ones that have a major influence during the considered walking cycle. A. Correa et. al. conducted a study that investigates the muscle-force contribution to hip joint loading during normal walking. The force developed by each muscle plus its contribution to the ground reaction force were used to determine the muscle's contribution to hip contact force. The muscle excitation patterns for normal walking were determined by solving a dynamic optimization problem, in which the performance criterion minimize the metabolic energy consumed per unit distance traveled. Four muscles that span the hip – gluteus medius, gluteus maximus, iliopsoas, and hamstrings – contribute most significantly to the three components of the hip contact force. Gluteus maximum and medius influence mainly the components in the superior-inferior direction, while iliopsoas and hamstrings the one in the anterior-posterior direction. Gluteus maximum contributes in early stance, gluteus medius contributes throughout stance, iliopsoas and hamstrings contribute during swing (Fig. 3.33) [57]. The maximum, middle and minimum gluteal abductors muscles were included in the model, assuming that these bring a sufficient approximation of the muscular forces acting on the femoral head, during the considered stance phase. Furthermore, is a common simplification in the femur FE models to

represent only the hip joint contact and abductor muscle forces, acting on the femur head and the greater trochanter respectively [6, 50, 58, 59].

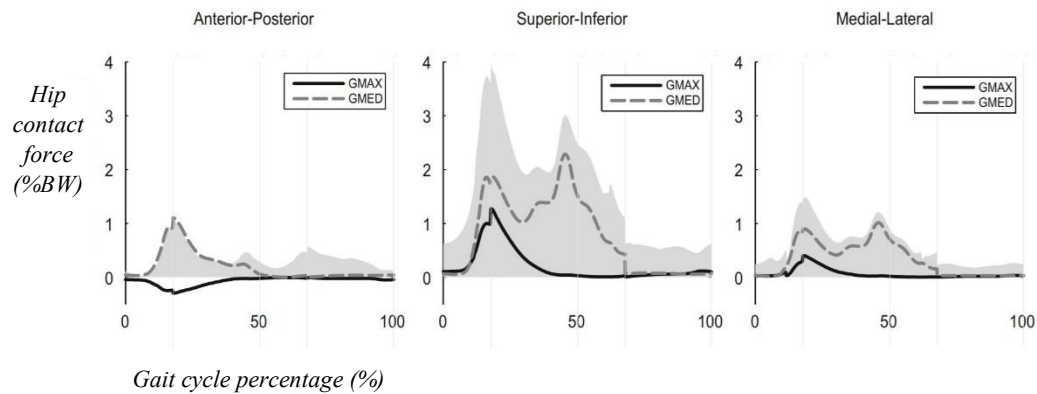


Figure 3.33: Contribution of the gluteus maximum (GMAX) and minimum (GMIN) muscular forces, to the hip contact force acting on the femur, in the anterior-posterior, superior-inferior and medial-lateral directions, in function of the percentage of the gait cycle. Figure taken from [57].

This assumption is confirmed by J. Stolk et al, who performed a study investigating which muscle group acting around the hip joint affect most prominently the stress/strain distributions in bone and prosthesis, and the maximum displacement of the femoral head, during walking. A fem model was created and load were applied as occurring during the three analysed phases of walking. The results produced with the application of contact force alone were compared with the ones produced adding the abductors, and subsequently the iliotibial, adductor and vastii muscles. Was concluded that inclusion of the gluteal abductor-muscle forces in addition to the hip-joint force has a major impact on the femur displacement, whereas the additional inclusion of the iliotibial tract, the vastii and the adductors has relatively small effects [60]. Then, a loading configuration including the hip-joint contact force and the abductors forces can adequately reproduce the in vivo load acting on the THA implanted prosthesis.

T. San Antonio et al. and Bitsakos et al. proposed two studies regarding the orientation of orthotropy material properties in human femur and the bone remodelling in proximal human femur [51, 61]. In these ones, the multi load scenarios comprising the contact force and seven muscle forces, corresponding to 10%, 30% and 45% of the gait cycle, of a person with body mass equal to 95 Kg, were used (Fig. 3.32). Through the values obtained from the study conducted by T. San Antonio et al, the application of contact and gluteal forces on prosthetic head and large trochanter respectively, was implemented for each of the 3 configurations. The gluteal force was represented as a single vector acting in the center of the great trochanter, whose components are the sum of the contributions of maximum, medium and minimum gluteus (Table 3.9). The simplification of the forces of the abductor muscles to a single point of application is not entirely correct, the maximum gluteus, in particular, acts on a surface of the femur inferior to the great trochanter. Considering the level of precision required by the thesis in question, this approximation is sufficient. The information regarding the validity of the chosen point of insertion of the muscular force, was obtained (Fig. 3.34) [51, 58]. The components of the muscular and contact forces were expressed in the global coordinate system of the FE model implemented in the study conducted by T. San Antonio et al. (Table 3.9, 3.10). For this reason an orthogonal locale coordinate system has been created in which the z axis is parallel to the longitudinal femur direction and the x axis is the projection on the xy plane of the prosthetic neck direction (Fig. 3.35).

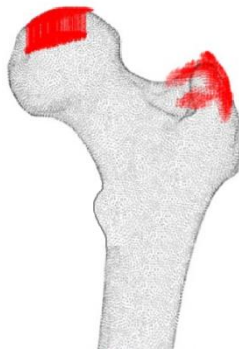


Figure 3.34: Areas of application of the hip contact force and muscular force, acting respectively on the prosthetic head and on the greater trochanter. Figure modified from [39].

Force	10% gait cycle			30% gait cycle			45% gait cycle		
	x	y	z	x	y	z	x	y	z
Gluteus maximum [N]	-103,9	213,4	334,9	-36,3	200,3	244	-12,8	201,4	203,8
Gluteus medium [N]	-152,5	118,4	260	-70,9	146,6	220,3	-55,1	255,6	297,8
Gluteus minimum [N]	-36,1	28,3	35,5	-41,4	75,2	38	-29,1	100,3	22,4

Table 3.9: X, y and z components of the maximum, medium and minimum muscular forces, acting on the greater trochanter during instants corresponding to the 10%, 30% and 45% of the walking cycle, expressed in the local coordinate system of the relative study [39].

Force	10% gait cycle			30% gait cycle			45% gait cycle		
	x	y	z	x	y	z	x	y	z
Total muscular force [N]	-292,5	360,1	630,4	-148,6	422,1	502,3	-97	557,3	524
Hip contact [N]	823,1	-470,2	-1722,5	699,5	-561,7	-2056,9	531,6	-376,9	-2868,7

Table 3.10: X, y and z components of muscular and hip contact forces, acting on the greater trochanter and on the prosthetic head respectively, during instants corresponding to the 10%, 30% and 45% of the walking cycle, expressed in the local coordinate system of the relative study [39].

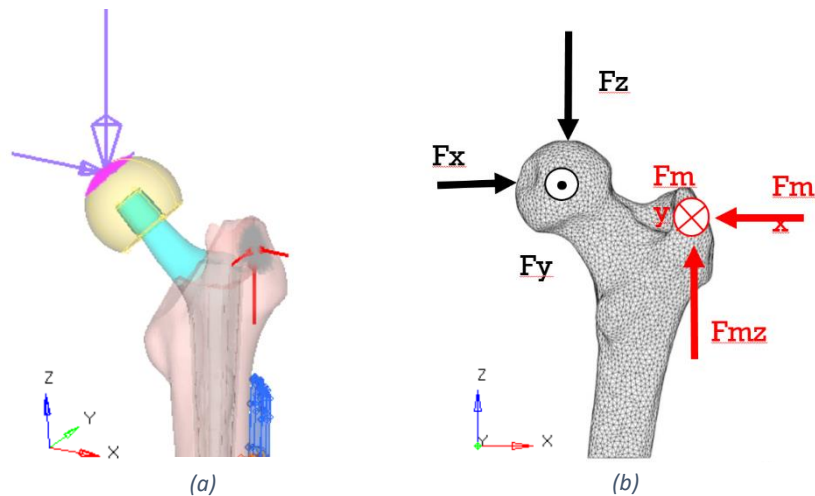


Figure 3.35: Partial model of the upper femur and prosthesis, representing the forces applied on the prosthetic head and greater trochanter respectively (a). Graphic representation of the components of the forces (b), figure modified from [39].

Walking forces – B configuration

In the second loading configuration, the only the contact force acting on the femoral head was implemented, referring to a different study conducted by G. Bergmann et al. [56]. Was so possible to compare the stress distribution within the plate during gait, according to two different approaches. According to this configuration, the instant of the walking cycle in which the first of the two peaks of the contact force takes place, is considered (Fig. 3.32). Bergmann et al. get the contact force amplitude as a function of time, of the average patient, obtained through experiments on four subjects with instrumented hip implants (Fig. 3.36). The components of the contact force used are expressed in the global coordinate system of the considered study. For this reason an orthogonal locale coordinate system was created in which the z axis is parallel to the longitudinal femur direction and the x axis is tangent to the condyles profile (Fig. 3.37). During the considered instant, the force has a modulus equal to 238% of the body weight, and inclinations equal to 13° with respect to the Z axis in the frontal plane and of 30° with respect to X axis in the transversal plane. Considering a body mass of 95 Kg, the body weight is equal to 932,0 N. In accordance with the previous observations, the force modulus results to be 2218,0 N. Its components along the three axis were calculated as follows.

$$F_x = F_{xy} * \cos(\alpha_x) \quad (3.1)$$

$$F_y = F_{xy} * \sin(\alpha_x) \quad (3.2)$$

$$F_z = F_{xz} * \cos(\alpha_z) \quad (3.3)$$

$$F_x = F_{xz} * \sin(\alpha_z) \quad (3.4)$$

$$F^2 = F_{xy}^2 * (\cos \alpha_x)^2 + F_{xy}^2 * (\sin \alpha_x)^2 + F_{xz}^2 * (\cos \alpha_z)^2 \quad (3.5)$$

In which the force F is the force modulus, α_z is the angle between the force direction and the Z axis in the frontal plane, and α_x is the angle between the force direction and the X axis in the transversal plane. F_{xy} , F_{xz} and F_{yz} are the projections of the contact force on the frontal, transversal and lateral planes. The F_x , F_y and F_z components force F are equal respectively to 494. 5 N, -297.1 N, -2141.7 N.

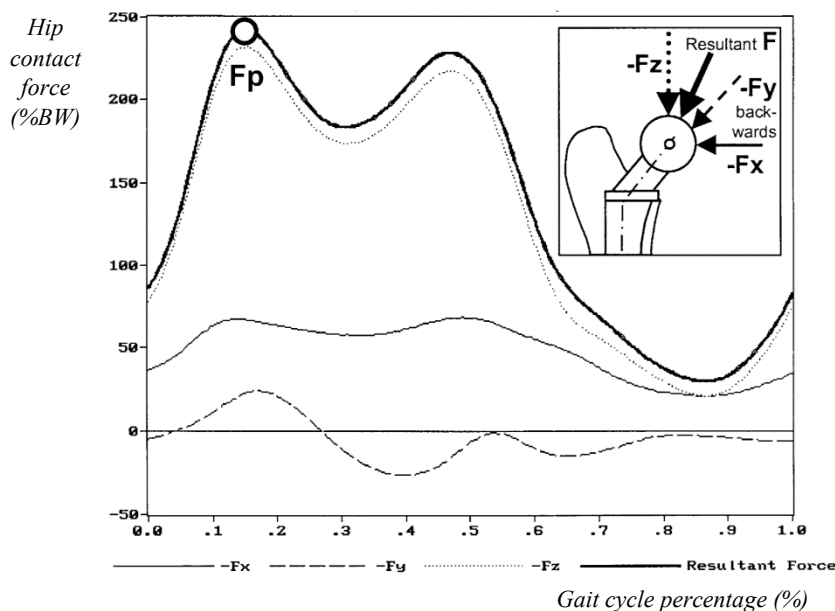


Figure 3.36: Components of the hip contact force used in the walking B configuration. Figure taken from [56].

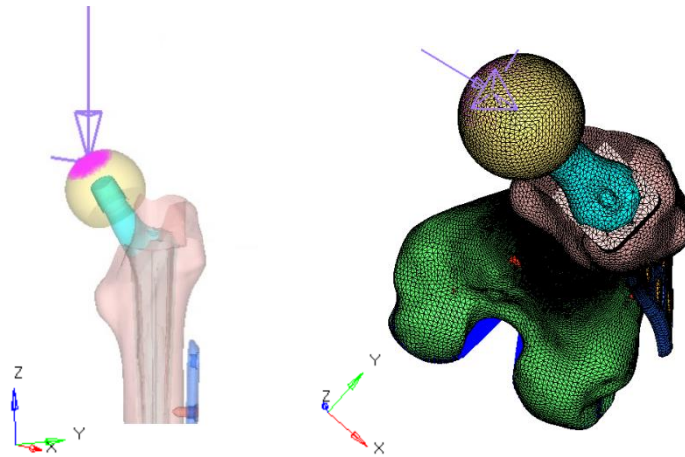


Figure 3.37: Partial model of the upper femur and prosthesis (a) and total model (b), representing the force applied on the prosthetic head.

Stumbling boundary conditions

Bergmann et al, conducted a second study, after the aforementioned one, in which the stumbling gesture was simulated in laboratory conditions [62]. The study was based on a patient with hip replacement implant. The patient stumbled missing a step attempting to climb stairs, but used the handrails and did not fall. Through instrumented prosthesis, data on the contact force on the femur surface was obtained. The maximum resultant force was approximately 290%BW during normal walking but rose to 720%BW during stumbling. The total range of force directions was very similar for walking and stumbling, and the directions of peak forces were nearly identical in both cases. The aforementioned article is based on information previously obtained, by the same authors, regarding the peak force during walking. The direction of the peak force during stumbling is therefore the same used in the previous study by Bergmann et al. The force components are expressed according to the reference system used in the B walking configuration, and are equal to 1495.9 N, 898.8 N, 6479.1 N. Like previously specified, a part of the femur base volume was constrained along all the degrees of freedom.

Lateral fall boundary conditions

The lateral fall situation was modeled assuming the beat of the great trochanter on the ground. To justify the realistic nature of the selected boundary conditions, reference is made to several studies. In order to simplify the explanation, an orthogonal local reference system is defined, in which the z axis is parallel to the longitudinal femur direction and the x axis is tangent to the condyles profile (Fig. 3.38).

A study recently conducted at the Polytechnic University of Turin, had the scope to validate a criterion that predict osteoporotic hip fractures caused by lateral falls. A load was applied on the greater trochanter towards the negative x direction, while the head nodes were bounded to the ground by

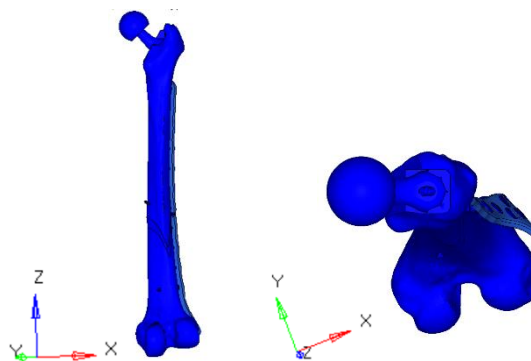


Figure 3.38: Representation of the local coordinate system implemented for the definition of the falling load.

means of spring elements with a 10,000 N/mm stiffness. This value represents the articular cartilage stiffness. The model included only the proximal part of the femur. The distal nodes of the proximal femur models were connected through link elements to a reference node, having all the translational degrees-of-freedom fixed [63]. Usually, experiments analysing lateral fall force implement mathematical models, which are based on factors such as the impact velocity of the hip and the effective mass, stiffness, and damping of the tissues surrounding it, during the contact with the ground. In fact, increased soft tissues thickness over the hip and impacting the ground in a relaxed state can decrease the stiffness of the body, and reduce peak impact forces. An example of mass-spring-damper model was implemented by Robinovitch et al. in order to simulate the oscillatory response of the body in pelvis release experiments for different subjects [64]. On the basis of the previous model, the formula (8), which describes the impact force acting on the greater trochanter, according to average values of impact velocity, stiffness and damping of the body, was derived [65]. In the formula h is the height of the subject in centimeter and w is his body weight in Newton.

$$F_{impact} = 8,25 * BW * \sqrt{\frac{h}{170}} \quad (3.6)$$

Supposing h and BW equal respectively to 170 cm and 95 Kg, the impact force results equal to 7688,6 N. The study in question is aimed at analysing the behaviour of the femur subject to lateral fall, through the use of a finite element model of an entire femur. To simulate the sideways fall configuration, the femur distal end was fixed along all the degrees of freedom, the femoral head surface was fixed along the load direction, and a force acting on the greater trochanter surface, towards the negative x semi-axis, was applied.

The force consequent to lateral fall, is influenced by many factors such as position and impact speed, mass and height of the subject (or BMI), mass of the part of the body that undergoes the impact, thickness, stiffness and damping of the soft tissues covering the hip. Each study is therefore dependent in the first analysis on the constitution and age of the subjects analysed, and on the context of the incident [66]. A. J. van den Kroonenberg et al. compared different models in order to identify which one simulated side fall more realistically. Basing on the impact velocity of the hip, the mass of that part of the body that is moving prior to impact and the stiffness of the tissue overlying the hip, the peak impact force was found. Masses and velocity involved ranged from 15,9 to 70 kg, and from 2,47 to 4,34 m/s. Predicted values for the peak force applied to the greater trochanter ranged from 2900 N to 9990 N [67].

Analysing the current state of the art, regarding the simulation of a lateral fall with beat on the large trochanter, it was chosen to implement four different simulation models, called A and B configurations. In each of these the previously calculated impact force was applied towards the negative x semi-axis on the large trochanter, with the addition of different constraint conditions (Fig. 3.39).

Falling A configuration

A connection of the base nodes, through RBE2 link elements, to a reference node having all the translational degrees of freedom fixed, was implemented. A bond to an external node through RBE3 link elements was applied to the prosthetic head surface nodes. This reference node was then bonded to the ground by means of a spring element with a 10,000 N/mm stiffness acting along the x-axis. The spring simulates the stiffness of the soft tissues that surround the hip in order to dampen the impact that occurs during the fall.

Falling B configuration

A connection of the base nodes, through RBE2 link elements, to a constrained node was implemented. The constraint allows the only rotation around the y axis. A bond to the ground by means of RBE3 spring elements, with a 10,000 N/mm stiffness, acting along the x-axis was applied to the prosthetic head surface.

Falling C configuration

This configuration is similar to the A one, with the only difference that the femoral head is constrained along all the degrees of freedom. The implementation of the connection to the ground, through a spring element, is therefore omitted.

Falling D configuration

This configuration is similar to the C one, with the only difference that the femoral base is constrained with a spherical joint.

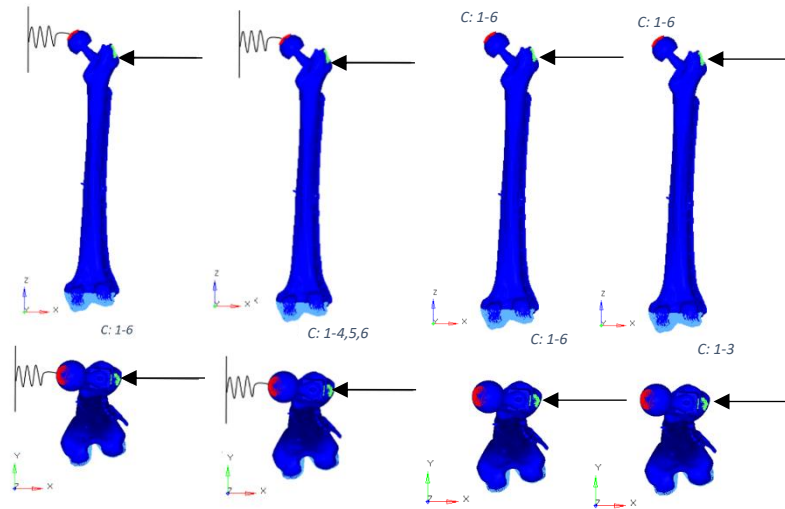


Figure 3.39: Representation of the implemented A (a), B (b), C (c) and D (d) load conditions of lateral fall walking. The number of constrained degrees of freedom is highlighted by the c letter.

According to the literature analysis conducted, on the boundary conditions applied for the simulation of lateral fall with the beat of the great trochanter, is believed that the implemented models cover the whole range of possible cases, regarding the distributions and peak values of the resulting stresses inside the plate.

As will be specified later, the results of the models C and D are neglected. The stress values inside the plate are fact very low compared to those obtained in the other analyzed conditions and, for the purpose of the thesis, it would be superfluous to deepen its analysis.

3.3 Results analysis

Resuming, four different load conditions were analysed: two walking configurations, stumbling and falling (Fig. 3.40).

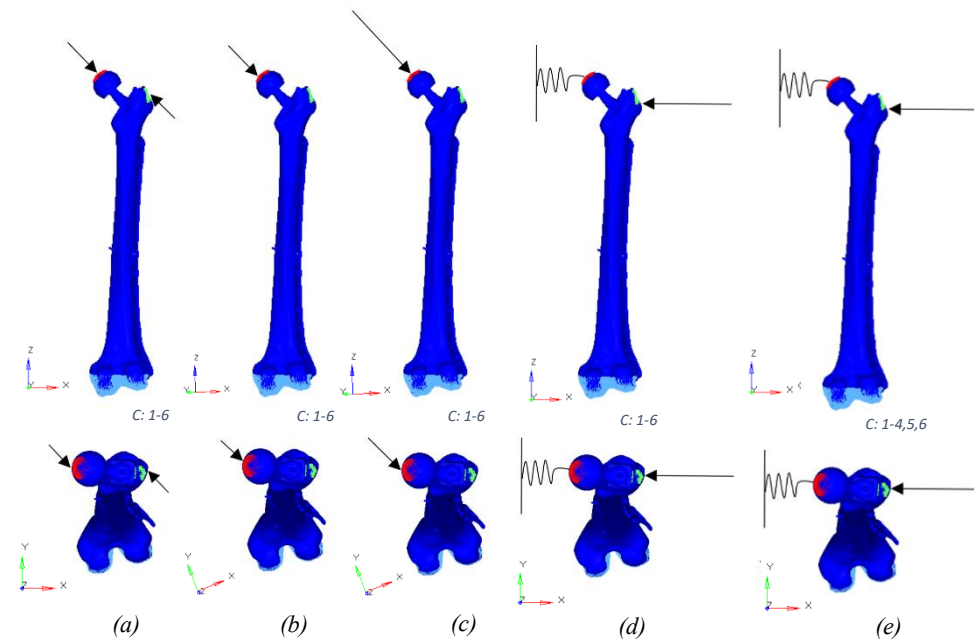


Figure 3.40: Representation of the implemented load conditions: walking A (a), walking B (b), stumbling (c), falling A (d), falling B (e). The number of constrained degrees of freedom is highlighted with the c letter.

In the walking A configuration the hip contact force and the abductor muscular force were applied respectively on the surfaces of the prosthetic head and of the greater trochanter. The femur base was constrained along all the degrees of freedom (Fig. 3.40a). Three steps were implemented during 10%, 30% and 45% in time, of the walking cycle, corresponding to the instants during the beginning the midstance, during the end of it, and just before the toe off.

In the walking B configuration, just the hip contact force was applied on the surface of the prosthetic head (Fig. 3.40b). The femur base was constrained along all the degrees of freedom. The instant of the walking cycle in which the maximum force acts on the hip, was implemented.

In the stumbling configuration the hip contact force have the same direction with respect to the one applied during the walking B configuration, but the intensity of it is amplified (Fig. 3.40c).

In the falling configuration, a horizontal force was applied to the greater trochanter. The prosthetic head was connected to the ground through a spring element that acts along the force direction. Four different models were implemented, in which the second two were neglected. In the first one the femur base was constrained along all the degrees of freedom (Fig. 3.40d), in the second one it was constrained through an hinge element that permit the only rotation along the force direction (Fig. 3.40e).

A resume of the implemented forces is presented (Table 3.11). Is specified that these are expressed in two different reference systems. We will refer to the system 1 when the z axis is the longitudinal femur direction and the x axis is the projection of the prosthetic neck on the xy plane. We will refer to the system 2 when the z axis is the longitudinal femur direction and the x axis is tangent to the condyles profiles in the xy plane. Since the results of the study, such as main and Von Mises stress within the plate, are not dependent on the chosen system, it is not necessary to set a single reference for all load conditions.

In the A loading configuration the F_c and F_m parameters refer to the hip contact forces and muscular abductor forces respectively. The F parameter refers to the sum of the previous ones along each direction, representing a fictitious resulting force.

For each of the implemented boundary condition configurations, the entities and types of the deformations assumed by the model, the Von Mises stress distributions within the plate and their peak values were analysed. These parameters were evaluated according to the bone reduction level of the fracture. Five models have been implemented for each configuration, whose elastic modules of the fracture material assume values equal to 9080 MPa, 3632 MPa, 1816 MPa, 363.2 MPa, 181.6 MPa. To simplify the results presentation, the volumes of the plate between each pair of holes were numbered, depending on the distance from the bone fracture, which is located, respect to the plate, at the height of the hole 12 and extends downwards to the height of the hole 10. The language used in the results presentation recalls the left and right sides of the plate, assuming that it is positioned in the frontal plane with the front side facing the observer (Fig. 3.41).

		Force type	X component [N]	Y component [N]	Z component [N]	Reference system
A walking configuration	Step 1	Fc	823,1	-470,2	-1722,5	1
		Fm	-292,5	360,6	630,4	
		F	530,6	-109,6	-1092,1	
	Step 2	Fc	699,5	-561,7	-2056,9	
		Fm	-148,6	422,1	502,3	
		F	550,9	-139,6	-1544,6	
	Step 3	Fc	531,6	-376,9	-2868,7	
		Fm	-97,0	557,3	524,0	
		F	434,6	180,0	-2344,7	
B walking configuration		F	494,5	-297,1	-2141,7	2
Stumbling configuration		F	1495,9	-898,8	-6479,1	
Falling configuration		F	-7688,6	0	0	1

Table 3.11: Resume of the component of the implemented forces, in every of the load configurations.

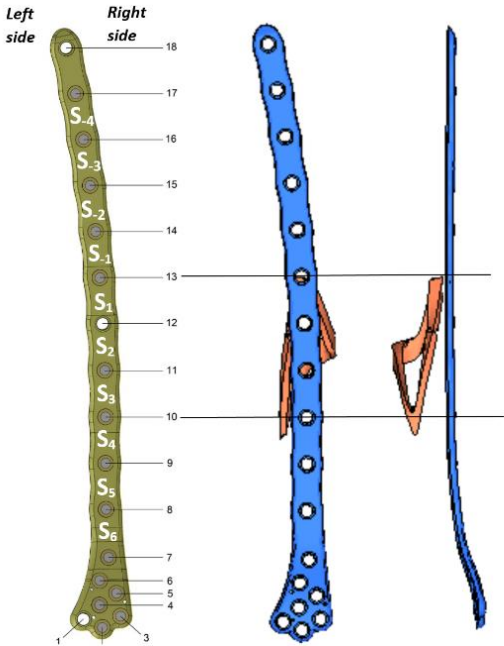


Figure 3.41: Indication of the numbering assigned to holes and areas of the plate (a). Frontal (b) and lateral (b) views of plate and fracture models. The longitudinal extension of the fracture is highlighted.

2.3.1 Walking - A configuration

10% of the walking cycle

The distributions of the nodal displacements of the model, which simulates the initial midstance of the walking cycle, are similar in all the tested healing conditions of the fracture. Approximately zero displacements are obtained below the fracture and growing upwards along the longitudinal direction of the femur, meaning that the femoral body flexes more in the most yielding area (Fig. 3.42a). In each cross section of the diaphysis, above the fracture zone, the values increase according to the distance

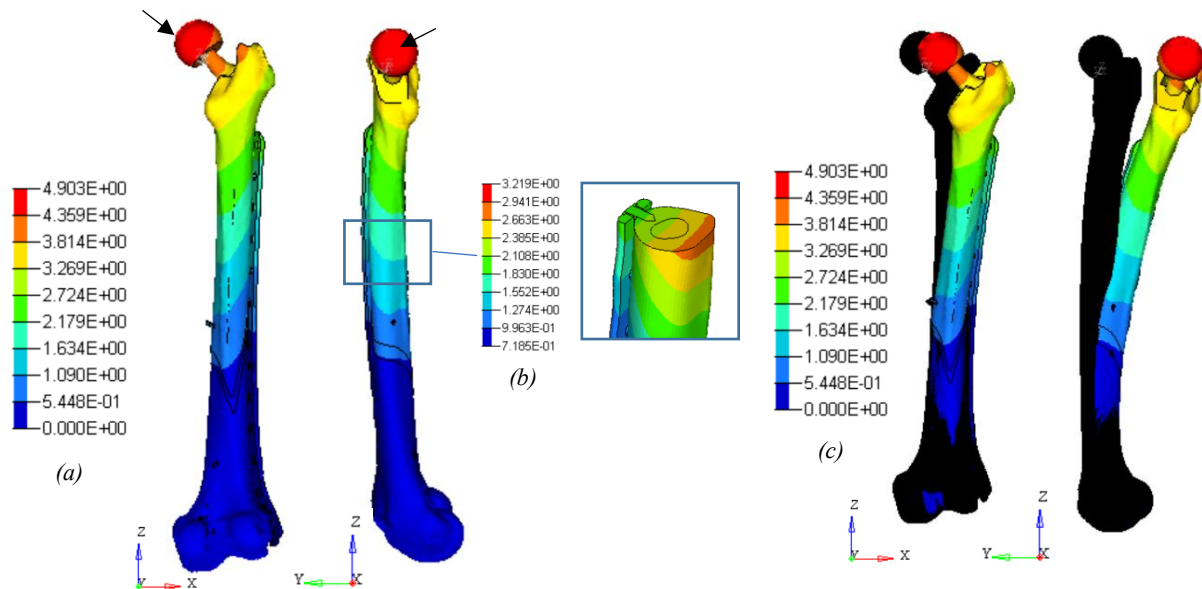


Figure 3.42: Magnitude of the nodal displacements [mm] of the entire model (a) and of a diaphyseal section above the fracture zone (b), with fracture elastic modulus 9080 MPa. The arrows indicate the point of maximum displacement. Magnitude of the nodal displacements [mm] of the entire model with addition of the undeformed shape (c), and deformations amplified by a factor of 10.

from the plate (Fig. 3.42b). It, in fact, due to the higher elastic modulus, stiffens the anterior and distal side of the femur. The point of the model in which the nodal displacement is maximum lies on the anterior surface of the femoral head. The exact position is not relevant as it is strictly dependent on the application points of the contact and muscular forces, which require a more precise analysis as they differ according to the subject's muscular geometry. The displacement of this node has preponderant components x and y and is negligible along the z axis (Fig. 3.43, 3.44). The F_x and F_y forces generate bending moments with respect to the base of the femur. The F_{cy} and F_{my} forces generate a torsional moment around the longitudinal femoral axis. The F_z force, despite having greater value than the previous ones, causes a compression stress whose consequent deformation have a reduced value. The maximum nodal displacement value decreases by a few millimeters, as the elastic modulus of the fracture increases within the chosen range. This behaviour is comprehensible on the basis of the dependence of the deformation on the stiffness of the bone segment (Fig. 3.44, Table 3.12). The fact that the values of the nodal displacements are not representative, as strictly dependent on the points of application of the forces, is again highlighted. Useful information concerns its orders of magnitude and its spatial distributions. The deformed model shape confirms what was argued as it shows the femoral torsion and flexion with maximum displacement at the level of the prosthetic head (Fig. 3.42c). To simplify the understanding of the image the deformations are amplified by a factor of 10.

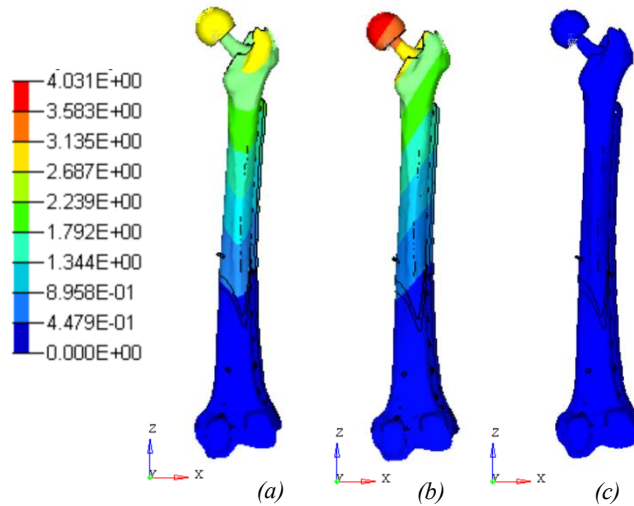


Figure 3.43: Absolute values of the x, y and z components of the nodal displacements [mm] of the model with fracture elastic modulus 9080 MPa.

Fracture elastic modulus [MPa]	Maximum displacement magnitude [mm]	Maximum displacement x[mm]	Maximum displacement y[mm]	Maximum displacement z[mm]
181,6	8,1	5,3	-6,0	0,9
363,2	7,1	4,6	-5,4	0,8
1816,0	5,6	3,4	-4,4	0,6
3632,0	5,2	3,1	-4,2	0,5
9080,0	4,9	2,8	-4,0	0,4

Table 3.12: Total and components of the maximum nodal displacements values varying the fracture elastic modulus.

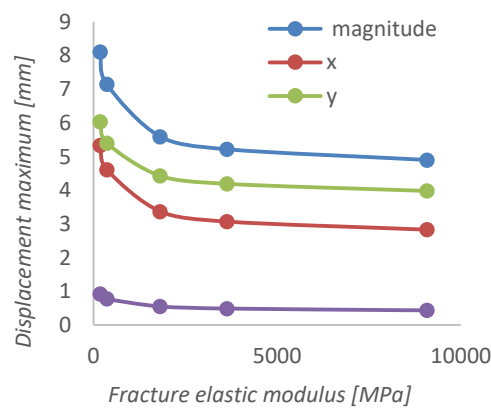


Figure 3.44: Total and components of the maximum nodal displacements varying the fracture elastic modulus.

The most stressed surfaces of the plate, under every loading situation, are lateral to the volumes whose cross sections are smaller. This means that the geometry of the plate stiffens the areas surrounding the holes and prevents that the presence of these from promoting the rupture. The distributions of Von Mises stresses within the plate vary according to the level of healing achieved. For low elastic modulus values of the fracture, the lateral surfaces belonging to the S_2 area are more stressed. As the bone segment stiffness increases, the greater stresses move downwards, affecting the lateral surfaces of the S_4 and S_5 areas. In the central volume of the plate, instead, the stresses are lower (Fig. 3.45). The influence of the

fracture reduction level on the maximum stresses obtained in the lateral S_2 and S_5 lateral area, were analysed (Table 3.13).

The right and left sides of the plate, according to the reference specified above, were identified. As the elastic modulus of the fracture increases, the values of lateral stresses in the zone S_2 are reduced, with initially precipitous progression. The left S_2 area is slightly more stressed than the right S_2 one (Fig. 3.46).

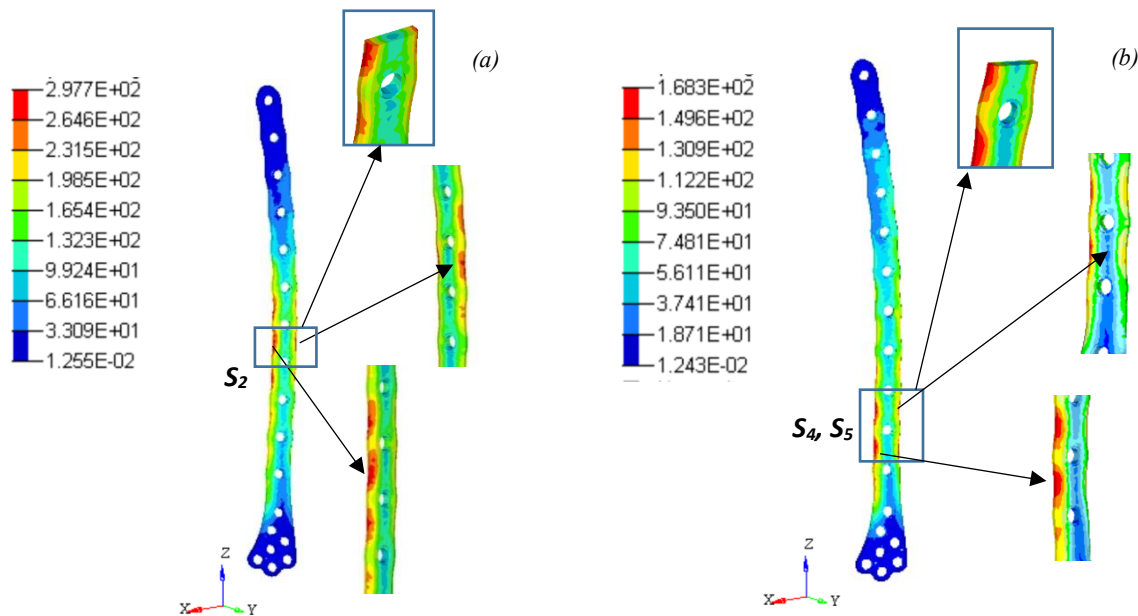


Figure 3.45: Von Mises stresses in the S_2 and S_5 plate zones from the models with elastic fracture modulus of 181,6 MPa (a) and 9080 MPa (b).

The lateral stresses in the S_5 zone decrease slightly with similar trends, but with clear superiority of the left values compared to the right ones (Fig. 3.46). It is natural how the greater values are detected in the left area, in fact here the compression stress acting on the whole femur, generated by the F_z force, is added to those acting in restricted areas, caused by the bending moment. The maximum stress reached, in the case of fracture stiffness of 181.6 MPa, is equal to 297.7 MPa, and does not exceed the plaque yield point. In the configurations with less consolidated fracture the load acting on the femur is transferred to the lower area through the plate which, having a very high elastic modulus compared to that of the weak bone, is less yielding and has greater affinity to sustain the loads. For this reason, areas of high stress are generated between the holes number 10 and 13, at heights corresponding to the extent of the fracture. When the level of healing is greater, the distal areas of the plate are the most stressed. Here there is the most thinned diaphyseal area and, for this reason, after the consolidation of the fracture, the most yielding. Furthermore, the bending moment given by the x and y components of the forces is maximum in the distal zone, the plate would therefore be, in the case of healthy bone, more loaded at the heights of the areas S_5 and S_6 . In this case, however, the overall bone model is more rigid, and therefore has greater capacity to transfer loads.

Within the distribution of the maximum principal stress, it is possible to identify the boundary that divides the area subjected to a significant traction level (3.47a). In the model with more solid bone configuration the maximum principal stress, on the right side of the plate, reaches values in the order of hundreds of MPa. Within the distribution of the minimum principal stress it is possible to identify the boundary that divides the area subjected to compression (Fig 3.47b). In the model with more solid bone configuration the minimum main stress, on the right side of the plate, reaches values in the order of hundreds of MPa.

Fracture elastic modulus [MPa]	Maximum Von Mises left s2 [Mpa]	Maximum Von Mises right s2 [Mpa]	Maximum Von Mises left s5 [Mpa]	Maximum Von Mises right s5 [Mpa]
181,6	297,7	293,2	202,0	149,6
363,2	248,0	245,2	191,7	141,5
1816,0	162,8	159,5	176,0	131,5
3632,0	142,2	137,6	172,1	129,5
9080,0	126,2	120,6	168,3	127,6

Table 3.13: Von Mises maximum stresses values in the S_2 and S_5 zones varying the fracture elastic modulus.

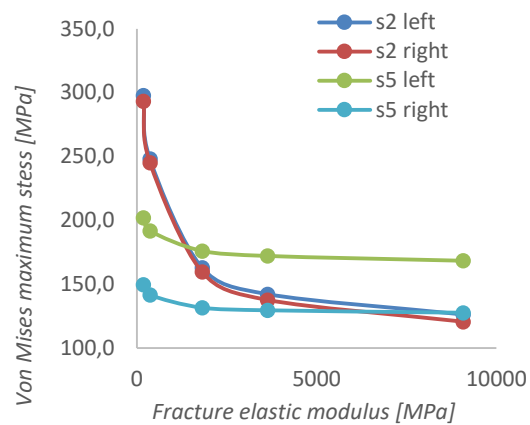


Figure 3.46: Von Mises maximum stresses in the S_2 and S_5 zones varying the fracture elastic modulus.

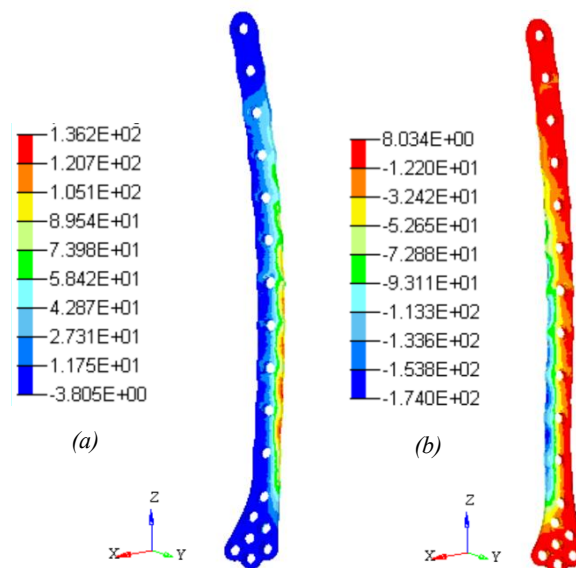


Figure 3.47: Maximum (a) and minimum principal stress distributions (b) [MPa] from the model with elastic fracture modulus of 9080 MPa.

30% of the walking cycle

The distributions of the nodal displacements of the model, which simulates the end of the midstance walking phase, are similar to those generated during the beginning of it. The results obtained regarding the overall deformations of the model and the stresses inside the plate are shown below, whose justifications refer to the previous paragraph. The bending curvatures caused by the moment generated by the F_x force is reduced compared to the previously analysed phase (Fig. 3.48, 3.49, Table 3.14). Respect to the previous case, the resulting F_y force has a slightly higher modulus and the F_z force has grown by about 40%. The reduction of the bending along the x axis is caused by the growth of the z component of the resulting force, whose compression contrasts the flexional deformation in a greater way. The slight increase in flexion along the y axis, on the other hand, is justified by the growth of the F_y force modulus. The bending moment generated by the force F_z with respect to the arched central diaphysis, whose arm is not null, could also be influential.

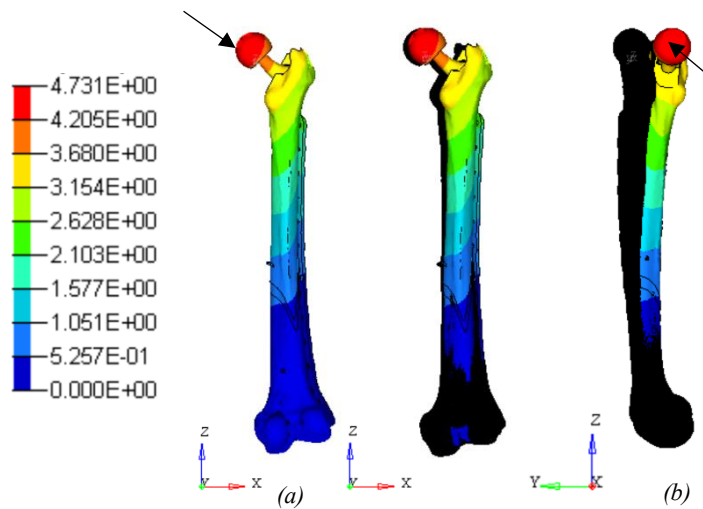


Figure 3.48: Magnitude of the nodal displacements without (a) and with (b) the deformed shape, from the model with fracture elastic modulus 9080 MPa [mm]. The arrows indicate the maximum displacement point. The deformations are amplified by a factor of 10.

Fracture elastic modulus [MPa]	Maximum displacement magnitude [mm]	Maximum displacement x[mm]	Maximum displacement y[mm]	Maximum displacement z[mm]
181,6	7,9	3,5	-7,1	0,5
363,2	6,9	3,2	-6,1	0,4
1816,0	5,4	2,3	-4,8	0,3
3832,0	5,0	2,1	-4,6	0,2
9080,0	4,7	1,9	-4,3	0,2

Table 3.14: Total and components of the maximum nodal displacements values varying the fracture elastic modulus.

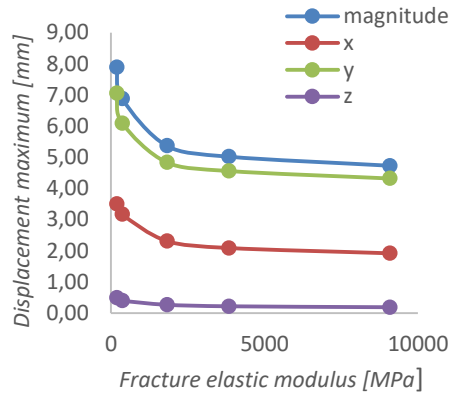


Figure 3.49: Total and components of the maximum nodal displacements varying the fracture elastic modulus.

The maximum stress, for values of fracture elastic modulus lower than 1816 MPa, are in the left side of the S_2 zone. The maximum value reached in the weakest bone model is 284.7 MPa, lower than the plate yield limit. For high values of fracture elastic modulus the lower area of the plate is stressed, mostly on the left side (Fig. 3.50, 3.51, Table 3.15).

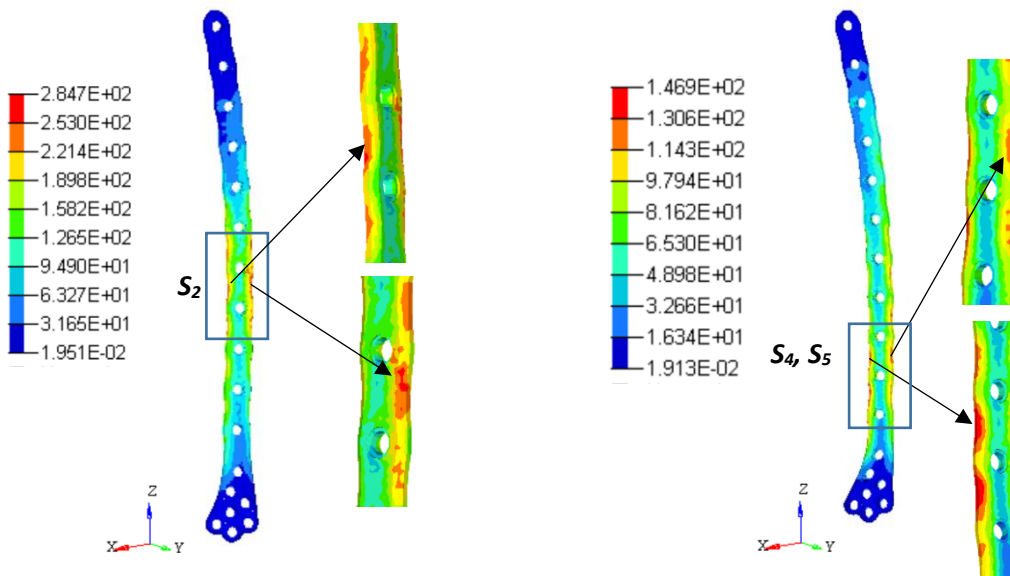


Figure 3.50: Von mises stresses in the plate from the models with elastic fracture modulus of 181,6 MPa (a) and 9080 MPa (b). The most stressed areas are highlighted.

Fracture elastic modulus [MPa]	Maximum Von Mises left s2 [Mpa]	Maximum Von Mises right s2 [Mpa]	Maximum Von Mises left s4 [Mpa]	Maximum Von Mises right s4 [Mpa]
181,6	284,7	280,3	195,5	181,2
363,2	228,2	233,2	177,9	163,9
1816,0	139,8	153,3	155,9	139,3
3832,0	120,5	134,0	151,4	134,0
9080,0	106,4	119,0	146,5	129,1

Table 3.15: Von Mises maximum stresses values in the S_2 and S_5 zones varying the fracture elastic modulus

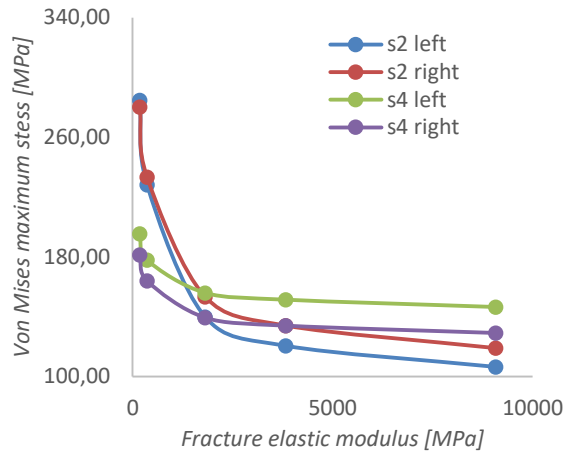


Figure 3.51: Von Mises maximum stresses in the S_2 and S_5 zones varying the fracture elastic modulus.

Within the distribution of the maximum and minimum principal stresses it is possible to identify the areas subjected to compression and traction. It is confirmed that, in any condition of bone reduction, the compressive stress on the left side exceeds those of traction on the right side. In the model with more solid bone configuration, the minimum and maximum principal stresses, reaches values in the order of hundreds of MPa (Fig. 3.52).

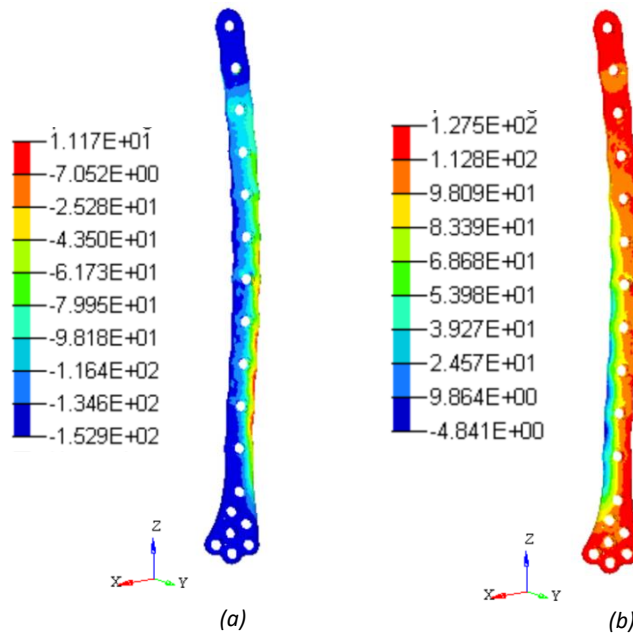


Figure 3.52: Maximum (a) and minimum principal stress distributions (b) [MPa] from the model with elastic fracture modulus of 9080 MPa.

45% of the walking cycle

Respect to the walking phases previously analysed, the resulting F_x force has slightly higher modulus, the F_y force has opposite direction and the F_z force has widely grown. Consequently, the distributions of the nodal displacements of the model, which simulates an instant just before the toe-off walking phase, are quite different. The femur is subjected to bending towards the negative x semi-axis and towards the positive y semi-axis, together with a slight torsion around the y-axis. The x and y components of the nodal displacements are opposite to the previous cases. Regarding the y component this is due to the opposite direction assumed by the resulting force F_y . Muscle strength, in fact, exceeds the femoral contact force. The bending moment generated by the F_x force with respect to the femur base is overwhelmed by the moment generated by the F_z force. The F_{cy} and F_{my} forces generate a torsional moment around the longitudinal femoral axis. Displacements of less than one millimeter are associated with the nodes below the fracture, and growing upwards along the longitudinal femur direction (Fig. 3.53). The point of the model in which the nodal displacement is maximum lies on the superior surface of the femoral head, and its components signs represent the model bending side (Table 3.16, Fig. 3.54). The exact position of this point, as previously specified, is not relevant.

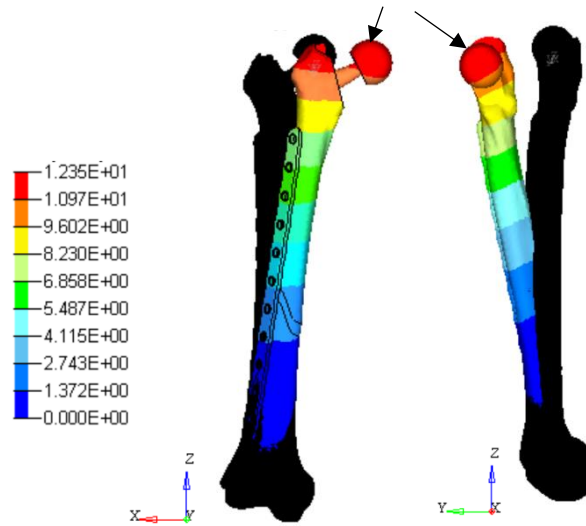


Figure 3.53: Magnitude of the nodal displacements with the deformed shapes from the model with fracture elastic modulus 9080 MPa [mm]. The arrows indicate the maximum displacement point. The deformations are amplified by a

Fracture elastic modulus [MPa]	Maximum displacement magnitude [mm]	Maximum displacement x[mm]	Maximum displacement y[mm]	Maximum displacement z[mm]
181,6	12,4	-9,9	6,8	-2,8
363,2	11,4	-8,8	6,7	-2,6
1816,0	9,6	-7,1	6,1	-2,0
3632,0	9,1	-6,6	5,9	-1,9
9080,0	8,7	-6,3	5,7	-1,8

Table 3.16: Total and components of the maximum nodal displacements values varying the fracture elastic modulus.

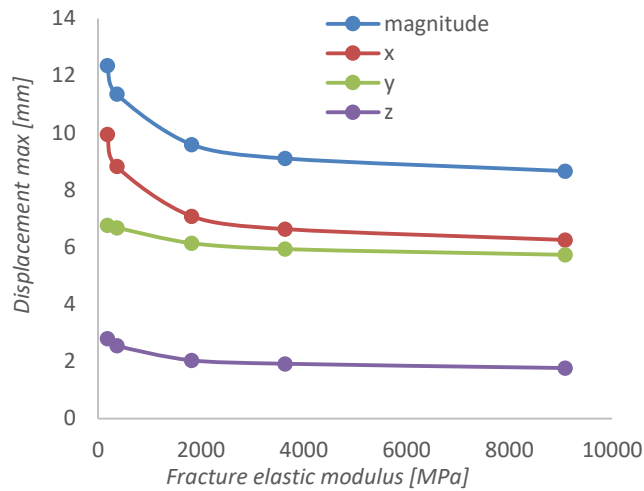


Figure 3.54: Magnitude and x, y and z components of the maximum nodal displacement, with fracture elastic modulus 9080 MPa.

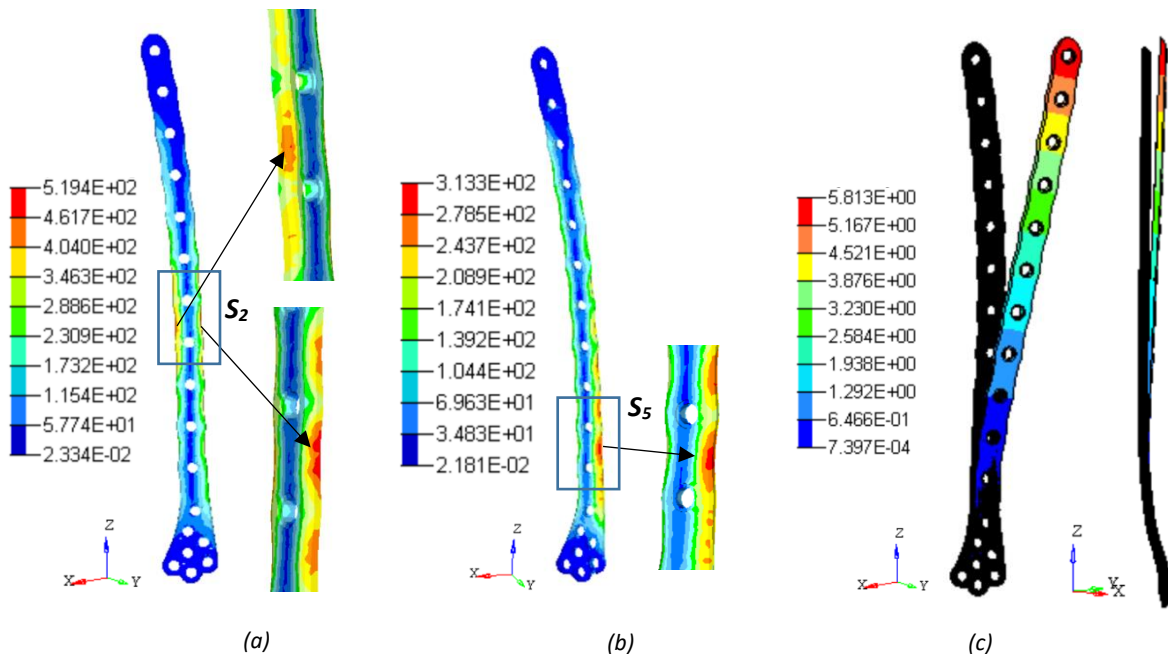


Figure 3.55: Von Mises stresses in the S_2 and S_5 plate zones from the model with elastic fracture modulus of 181,6 MPa (a) and 9080 MPa (b). Magnitude of the plate nodal displacements [mm] with the deformed shapes from the model with fracture elastic modulus 9080 MPa (c). The deformations are amplified by a factor of 10.

In the plate, areas of high stress are generated around the fracture, when it is less reduced, and in the lower part, when it is more healed (Fig. 3.55, Table 3.17). The stress is higher in the right side of the plate, subjected to compression. For the identification of the causes of this behavior reference is made to the analysis of the walking phase 1.

The maximum Von Mises stress inside the plate, according to the chosen range of fracture stiffness values, is equal to 519 MPa. This value, even if greater than those obtained in the previous phases, remains far below the yield point. The distribution of the maximum principal stress in the plate, and its deformed shape, show how, in the situation with a fracture elastic modulus of 9080 MPa, the entire left side is subjected to traction (Fig. 3.55c, 3.57a). The distribution of the minimum principal stresses shows that the right area of the plate, in case of elastic modulus of fracture equal to 9080 MPa, is subjected to compression, mostly in the lower part (Fig. 3.57b).

Fracture elastic modulus [MPa]	Maximum Von Mises left s2 [Mpa]	Maximum Von Mises right s2 [Mpa]	Maximum Von Mises left s5 [Mpa]	Maximum Von Mises right s5 [Mpa]
181,6	470,2	519,4	271	348,1
363,2	400,3	444,3	261	341,2
1816,0	282,9	309,8	242	324,4
3632,0	256,3	276,2	237,1	318,9
9080,0	229,4	145,8	232	313,3

Table 3.17: Von Mises maximum stresses values in the S₂ and S₅ zones varying the fracture elastic modulus

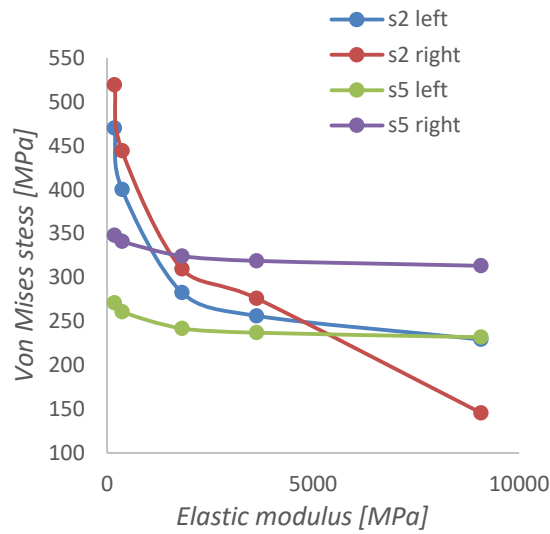


Figure 3.56: Von Mises maximum stresses in the S₂ and S₅ zones varying the fracture elastic modulus.

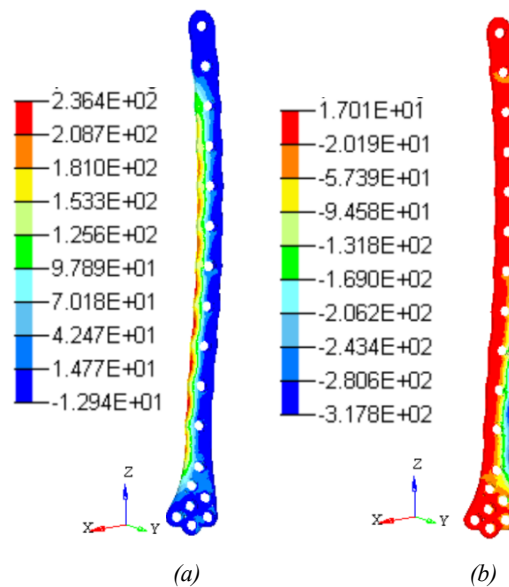


Figure 3.57: Maximum (a) and minimum principal stress distributions (b) [MPa] from the model with elastic fracture modulus of 9080 MPa.

2.3.2 Walking - B configuration

The instant of walking in which the contact load on the hip assumes the maximum value, occur approximately between 10% and 20% in time of the cycle. It is expected that the results do not vary significantly with respect to phase 1 of the A walking configuration, which occur in the instant immediately preceding the peak of the hip contact load. The displacements of the nodes along the x and z directions are almost zero (Table 3.18). The total maximum nodal displacement was plotted (Fig. 3.59). The femoral body bending is caused by the moments generated by the y and z components of the resulting force. The F_y force generate a bending moment with respect to the femoral base and the F_z force generate a moment with the same bending direction, with respect to the central diaphyseal area (Fig. 3.58).

The stresses inside the plate have distributions and peak values similar to those obtained in phase 1 of the A configuration. As previously, in the case of more yieldable fractured bone the stresses are higher in the S_2 area and, with the increase of the bone healing, these move downwards (Table 3.19, Fig. 3.60). The distribution of the maximum and minimum principal stresses confirms that the left area of the plate is subjected to compression while the right one to traction (Fig. 3.61). The maximum compression stress values are just above the traction ones, due to the reasons explained above. The maximum stresses, anyway, stay widely below the yield limit value.

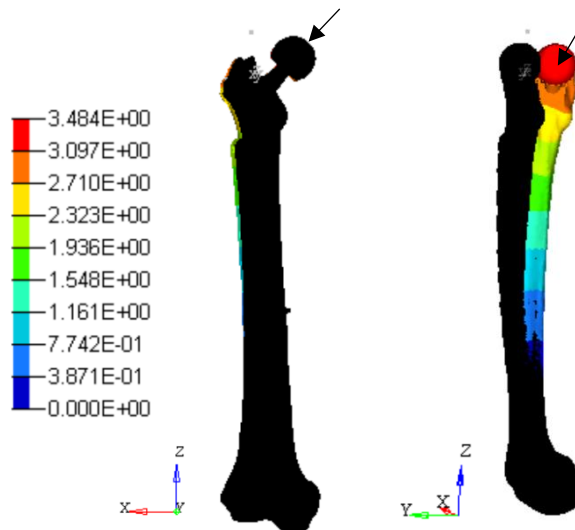


Figure 3.58: Magnitude of the nodal displacements with the deformed shapes from the model with fracture elastic modulus 9080 MPa [mm]. The arrows indicate the maximum displacement point. The deformations are amplified by a factor of 10.

Fracture elastic modulus [MPa]	Maximum displacement magnitude [mm]	Maximum displacement x[mm]	Maximum displacement y[mm]	Maximum displacement z[mm]
181,6	5,5	0,1	-5,4	0,0
363,2	4,8	0,1	-4,8	0,0
1816,0	3,9	0,3	-3,9	0,1
3632,0	3,7	0,3	-3,7	0,0
9080,0	3,5	0,2	-3,5	0,0

Table 3.18: Total and components of the maximum nodal displacements values varying the fracture elastic modulus

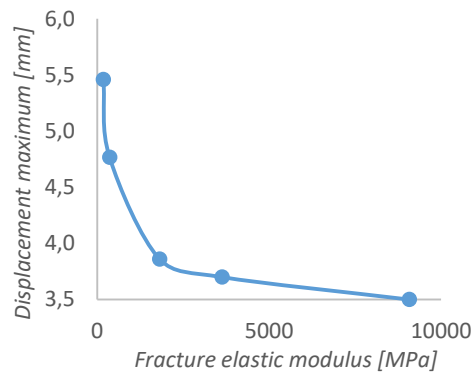


Figure 3.59: Total maximum nodal displacement varying the fracture elastic modulus.

Fracture elastic modulus [MPa]	Maximum Von Mises left s2 [Mpa]	Maximum Von Mises right s2 [Mpa]	Maximum Von Mises left s5 [Mpa]	Maximum Von Mises right s5 [Mpa]
181,6	209,6	190,1	145,2	114,6
363,2	172,1	162,1	140,6	108,0
1816,0	117,2	117,8	133,0	99,3
3632,0	106,0	106,4	131,3	97,4
9080,0	95,0	96,20	129,4	95,2

Table 3.19: Von Mises maximum stresses values in the S₂ and S₅ zones varying the fracture elastic modulus.

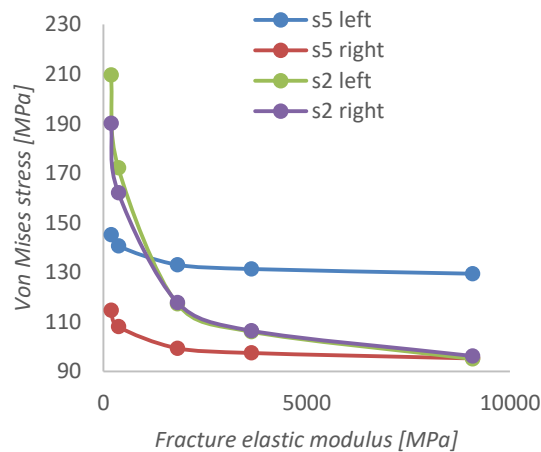


Figure 3.60: Von Mises maximum stresses in the S₂ and S₅ zones varying the fracture elastic modulus.

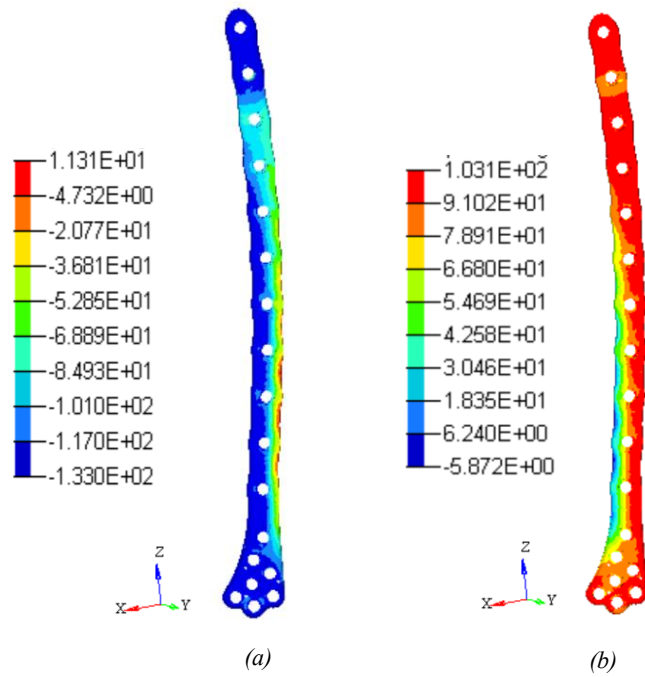


Figure 3.61: Maximum (a) and minimum principal stresses (b) [MPa] from the model with elastic fracture modulus of 9080 MPa [MPa].

Through two different approaches, has been deduced that the stress generated in the plate during walking is not sufficient to take it to break, even in the case of poor fracture bone quality. In fact, the simulations were conducted including a very low elastic modulus value of the fracture, whose stiffness is equal to the 1% of the completely healed bone. The first phase of the A configuration and the B configuration result series were compared. The order of magnitude of the nodal displacement and of the stress distributions into plate were similar, demonstrating that these are representative of the real situation.

2.3.3 Stumbling

The load acting on the femur during stumbling from standing position have the same direction as those during walking and amplified module. The deformation obtained is mainly caused by the bending of the femoral segment in the yz plane. The maximum nodal displacement belongs to the frontal surface of the femoral head and is of the order of tens of millimeters (Fig. 3.62, Table 3.11). The high z component of the contact force causes a bending moment with respect to the central diaphysel area, due to the arched femur shape. The F_z force, moreover, generates a bending moment with respect to the base of the femur whose lever arm is represented by the prosthetic neck. This moment is opposed to that generated by the F_x force with respect to the base itself. For this reason the bending of the femur in the xz plane is a minimal component of the total model deformation, which is almost entirely caused by the bending towards the y positive semi-axis (Fig. 3.63, 3.64).

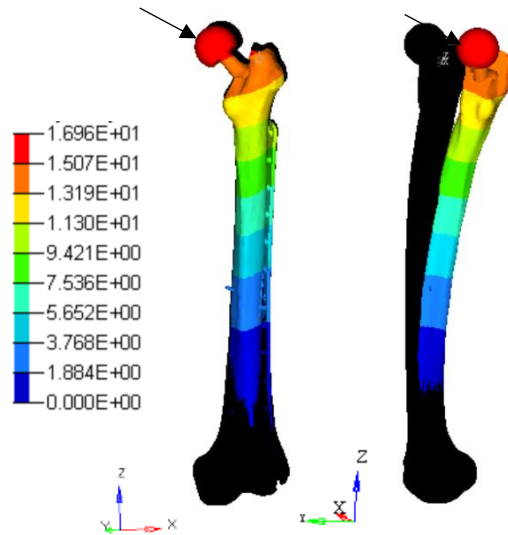


Figure 3.62: Magnitude of the nodal displacements with deformed shapes from the model with fracture elastic modulus 9080 MPa [mm]. The arrows indicate the maximum displacement point. The deformations are amplified by a factor of 3.

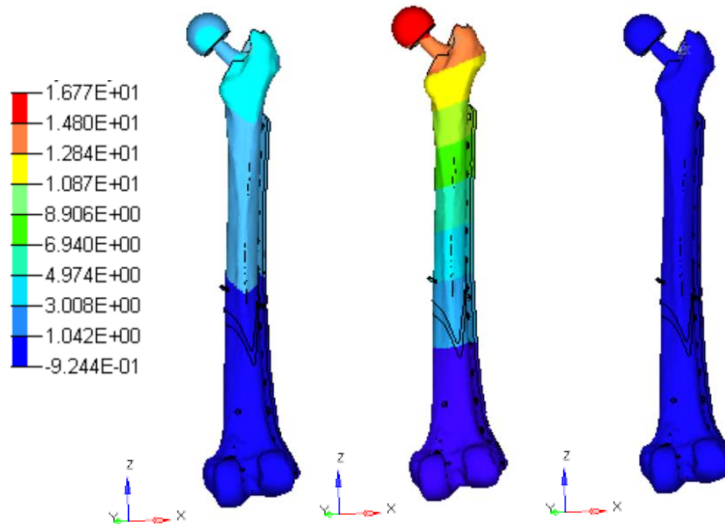


Figure 3.63: Absolute values of the x, y and z components of the nodal displacements [mm] of the model with fracture elastic modulus 9080 MPa.

Fracture elastic modulus [MPa]	Maximum displacement magnitude [mm]	Maximum displacement x[mm]	Maximum displacement y[mm]	Maximum displacement z[mm]
363,2	29,9	5,5	29,4	0,8
726,4	24,5	4,6	24,0	0,8
1816,0	20,3	3,5	20,0	0,8
3632,0	18,5	2,9	18,2	0,7
9080,0	17,0	2,5	16,8	0,6

Table 3.21: Total and components of the maximum nodal displacements values varying the fracture elastic modulus

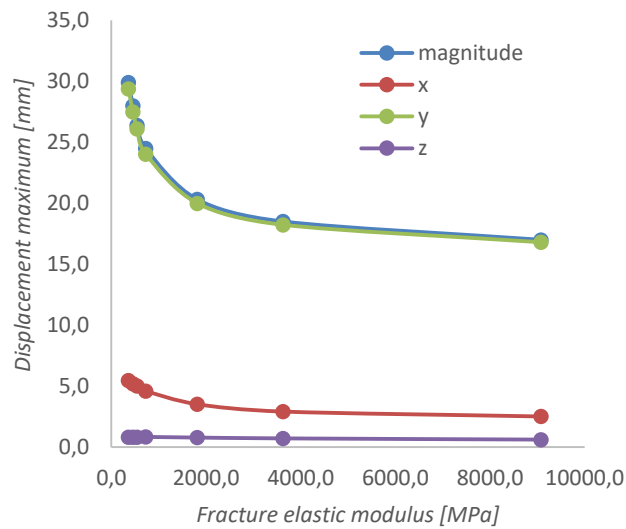


Figure 3.64: Magnitude and x, y and z components of the maximum nodal displacement, with fracture elastic modulus 9080 MPa.

In the models with fracture elastic modulus greater than 1816 MPa, the lateral S_4 and S_5 areas assume higher stresses because the most yielding area is situated at the thinnest diaphyseal section. In situations of poor bone reduction, high stress areas appear on the lateral S_2 and S_3 surfaces of the plate (Table 3.22, Fig. 3.65). This in fact acts as a means of transferring the loads to the lower diaphysis. The magnitude of the stresses is here greater than the ones caused by walking, which is amplified by almost 5 times.

Fracture elastic modulus [MPa]	Maximum Von Mises left s2 [Mpa]	Maximum Von Mises right s2 [Mpa]	Maximum Von Mises left s3 [Mpa]	Maximum Von Mises right s3 [Mpa]
363,2	1047,3	1118,6	1023,5	1048,6
726,4	791,3	866,8	818,1	833,3
1816,0	591,4	661,7	653,8	664,2
3632,0	505,0	570,1	582,0	588,2
9080,0	436,9	496,3	520,3	521,7

Table 3.22: Von Mises maximum stress values in the S_2 and S_3 zones varying the fracture elastic modulus. The values close to the yield stress are highlighted.

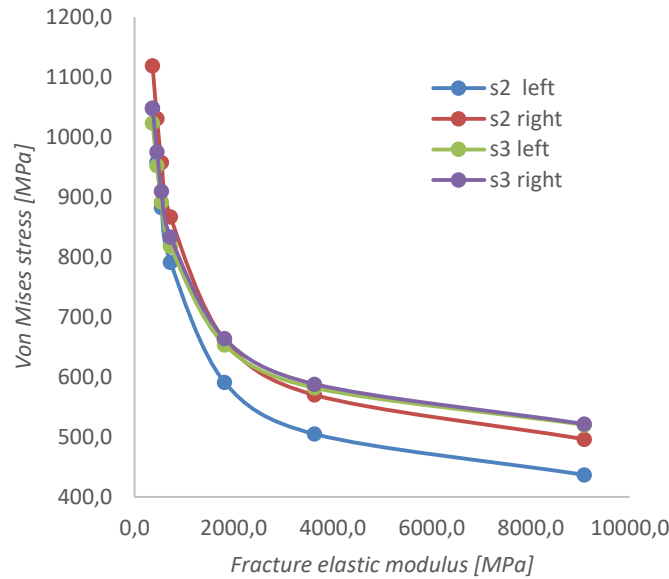


Figure 3.65: Von Mises maximum stresses in the S_2 and S_3 zones varying the fracture elastic modulus.

For fracture elastic modulus equal to 1816 the maximum stress, on the right side of the S_2 zone, is close the yield point of the steel constituting the plate. An additive model was implemented, in which the elastic modulus value of the fracture is equal to 726,4 MPa, to better understand which level of bone healing would correspond to the plaque break (Fig. 3.66). This value corresponds to a stiffness equal to 4% of that of healthy bone. The value 181,6 was removed as it would not bring significant information because of the very high stresses it would be subjected to. The yield limit, equal to 690 MPa, is exceeded if the elastic modulus of the fracture is equal to 726 MPa. The stress distributions in the sections where the real fracture occurred are demonstrative of how the yield strength under the stumbling load may have been reached (Fig. 3.67). The maximum stresses are found in the lateral areas, distally respect to the hole, and decrease towards it. The oblique bands of stress levels are due to the bending moment caused by the F_x and F_y forces so that the femur rotates around an inclined axis in the xy plane. As the elastic modulus decreases, the zone which stress values exceed the yield limit, move closer the hole. The yield causes the reduction of the plate section and the subsequent break. It is assumed that the conducted static simulation, in which the loads have been chosen taking into account the entity of the present inertia, is representative of the dynamic condition of force applied in an impulsive way. If the femur is subjected to this type of load, the resulting stress distribution suggests that is probable that the plate break would be caused in the section where it actually occurred.

The maximum and minimum principal stresses distributions confirm that the right volume of the plate is subject to traction and is slightly more stressed than the left one, subject to compression (Fig. 3.68). Is here demonstrated that the stumbling activity during the walk loads the femur with a force with a predominantly vertical component, whose moment generates the flexion of the same and of the plate in the yz plane. This deformation corresponds to lateral plaque tensile stresses that exceed the yield point and cause it to break. This load situation, combined with a very poor fracture reduction situation, could be the cause of bone the fracture and plate rupture.

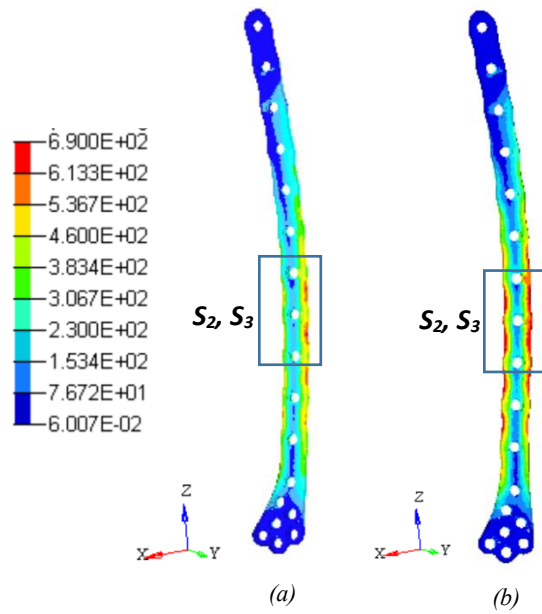


Figure 3.66: Von Mises stress distribution [MPa] in the plate from the models with elastic fracture modulus of 1816 MPa (a) and 726,4 MPa (b). In the red areas the stress exceeds the yield point.

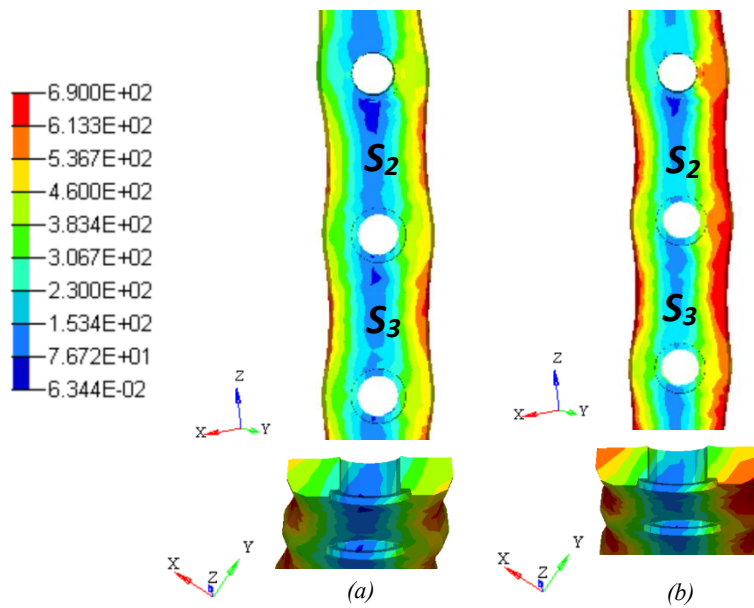


Figure 3.67: Von Mises stresses [MPa] in the S_2 and S_3 areas and fracture section from the models with fracture elastic modulus of 726,4 MPa (a) and 1816 MPa (b). Reference is made to figure 3.66.

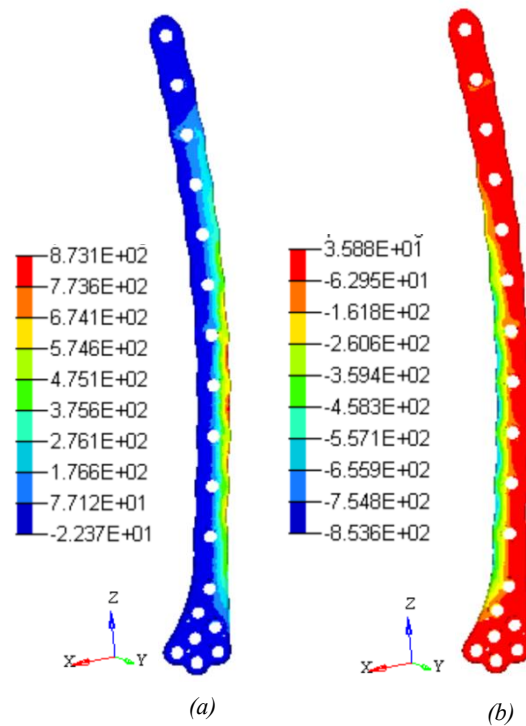


Figure 3.68: Maximum (a) and minimum principal stress distributions (b) [MPa] from the model with elastic fracture modulus of 726.4 MPa.

For this loading condition, a further model was created whose body weight value is equal to 75 Kg, representative with greater probability of the real situation. This value is in fact equal to the average body weight of the European female individual. The loads acting on the hip were calculated using the formulas 3.1 – 3.5. The analysis of the stress in the plate was carried out in order to observe the variations with respect to the reference model. The distributions of Von Mises stress are similar with respect to the previous case and the high values are concentrated in the real breaking section. The peak stresses are lower, and reach the yield point in the case of elastic modulus of the fracture of approximately 300 MPa (Table 3.23).

Fracture elastic modulus [MPa]	Maximum Von Mises right s2 [Mpa]
242,1	713,5
363,2	632,5
726,4	518,1

Table 3.23: Von Mises maximum stress values in the S₂ and S₅ zones varying the fracture elastic modulus, for a subject of body weight equal to 75 Kg. The values close to the yield stress are highlighted.

2.3.4 Falling

Falling A Configuration

According to this configuration, which simulates the lateral fall with beat on the greater trochanter, the femur base is constrained along all the degrees of freedom, and the prosthetic head is connected to the ground through a spring-type element that acts along the x direction. A force, directed towards the negative x semi-axis, is applied to the greater trochanter.

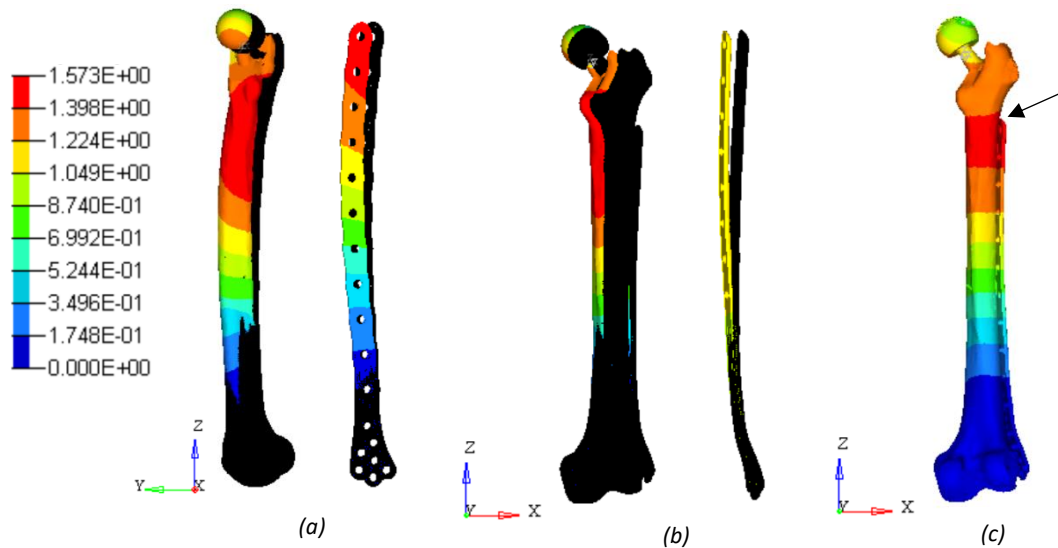


Figure 3.69: Magnitude of the nodal displacements with (a,b) and without (c) deformed shapes from the model with fracture elastic modulus 9080 MPa [mm]. The arrow indicate the maximum displacement point. The deformations are amplified by a factor of 10.

The femoral body, as well as the plate, undergoes a bending displacement and the central area deforms forming a hump directed towards the negative x semi-axis. The point at which the maximum displacement occurs is on the upper end of the plate (Fig. 3.69). The module of this displacement is approximately constant and directed towards the negative x semi-axis (Table 3.24) .

Fracture elastic modulus [MPa]	Maximum displacement [mm]	Maximum displacement x [mm]	Maximum displacement y [mm]	Maximum displacement z[mm]
181,6	1,5	-1,5	0,1	0,0
363,2	1,5	-1,5	0,2	0,0
1816	1,5	-1,5	0,5	0,0
3632	1,6	-1,5	0,5	0,0
9080	1,6	-1,5	0,6	-0,2

Table 3.24: Positions, total values and components values of the maximum displacement points of the model varying the fracture elastic modulus.

Two areas of the plate show high stress values. Considering the lower fracture elastic modulus, high stress values are found in the upper area of the left side in correspondence of S_3 , and in the lower area of the same side in correspondence of S_6 (Fig. 3.70). As the consolidation of the bone increases, the distribution of the stresses is similar, but the lower area takes on more weight from the femur. Therefore the stress located in S_6 decrease, and the one located in S_3 increase, reducing the fracture stiffness (Table 3.25, Fig. 3.71). The present is the only case, among the here presented ones, in which the plate displacement grows with the fracture healing level. As consequence the peak Von Mises stress grows with the increase of the fracture elastic modulus.

The presence of a superiorly stressed area is caused by the lateral compression of the plate during bending. The lower area is stressed because the constraint prevents its bending movement.

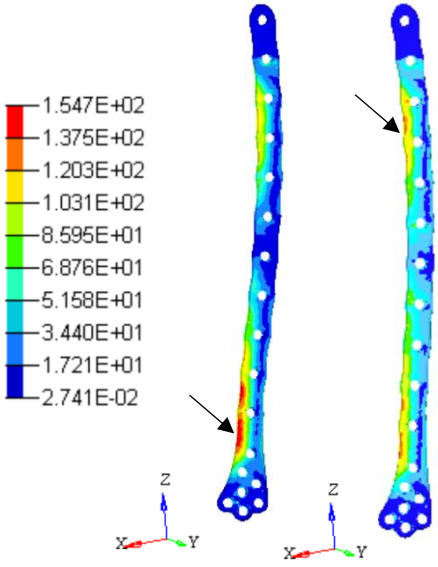


Figure 3.70: Von Mises stresses distributions [MPa] from the models with fracture elastic modulus of 9080 MPa (a) and 181.6 MPa (B). The arrows indicate the maximum stress points.

Fracture elastic modulus [MPa]	Maximum Von Mises s6 [MPa]	Maximum Von Mises s3- [MPa]
181,6	132,6	134,1
363,2	137,5	131,5
1816	147,8	126,0
3632	151,3	124,1
9080	154,7	122,1

Table 3.25: Von Mises stresses values in the S₆ and S₃ plate areas, varying the fracture elastic modulus.

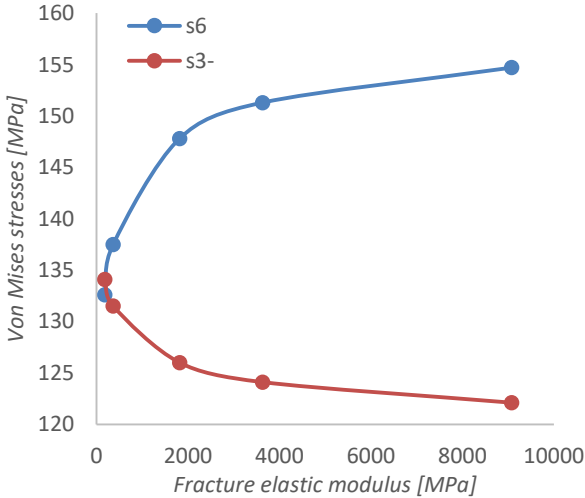


Figure 3.71: Von Mises maximum stresses, into the plate, varying the fracture elastic modulus.

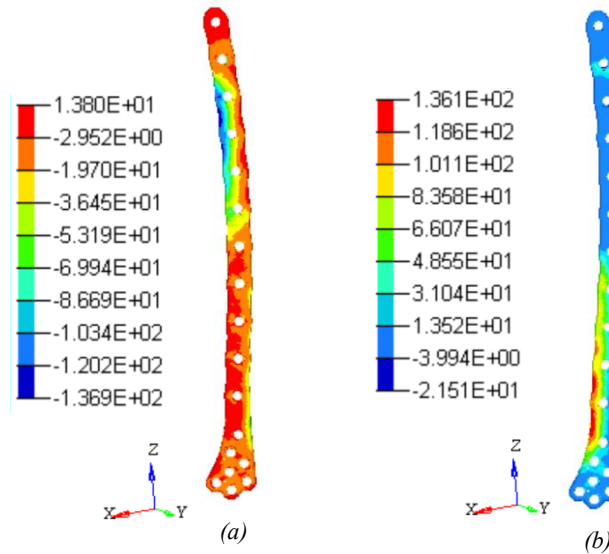


Figure 3.72 Maximum (a) and minimum (b) principal stresses [MPa] from the model with elastic fracture modulus of 181,6 MPa.

The distribution of the maximum principal stresses shows the traction zones present in the upper left plate frontal area and, in a reduced way, in the lower right side. The distribution of the minimum principal stresses shows the areas subject to compression located on opposite sides with respect to the previous ones. The maximum compression stress is present in the lower part due to the opposition to the movement by the constraint (Fig. 3.72).

This load configuration would not cause the plate to break according to the case in question since the values and distributions of the maximum stresses deny it. The stress values are very low, not exceeding the two hundred of MPa, and their distributions along the plate are inconsistent with the position of the occurred break.

Falling B Configuration

According to this configuration, which simulates the lateral fall with beat on the greater trochanter, the femur base is constrained through a hinge that allows the only rotation around the y axis, and the prosthetic head is connected to the ground through a spring-type element acting along the x direction. A force, directed towards the negative x semi-axis, is applied to the greater trochanter. The deformation

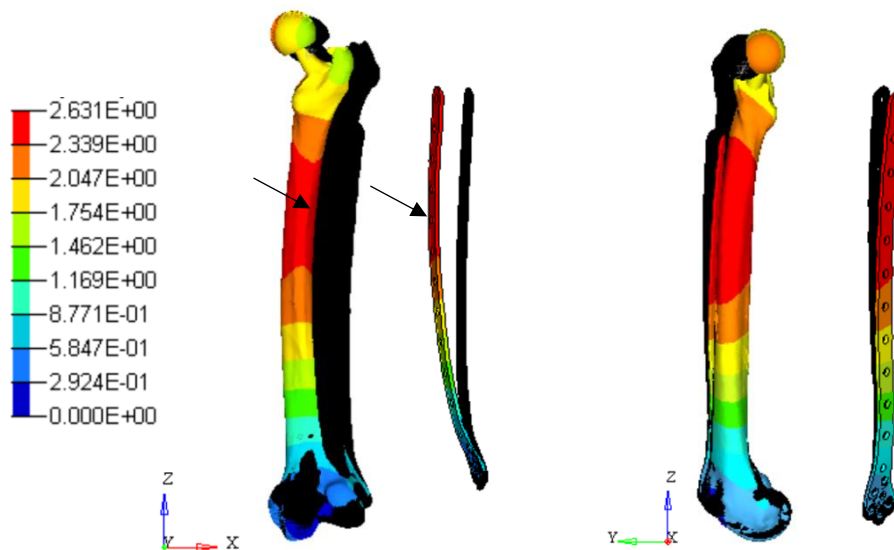


Figure 3.73: Magnitude of the nodal displacements [mm] with deformed shapes from the model with fracture elastic modulus 9080 MPa. The arrows indicate the maximum displacement point. The deformations are amplified by a factor of 10.

undergone by the model is similar to that obtained in the previous stage, unlike the zone close to the constraint where the displacements are significant. The femoral body, as well as the plate, undergoes a bending displacement and the central area deforms forming a hump directed towards the negative x semi-axis (Fig. 3.73). Along the femoral diaphysis the nodal displacements are almost totally influenced by the x component, representing the body femur flexion (Fig. 3.74). This behavior is caused by the bending moment generated by the applied force, with respect to the femur base. The prosthetic head, in contact with the spring, undergoes a vertical and lateral shift towards the negative y semi-axis. The node with greater displacement belongs to the plate and its position varies according to the elastic modulus of the fracture. For slightly reduced fractures the model bending is higher and the maximum displacement is near the hole number 14. For more consolidated fractures the bending is minor and the

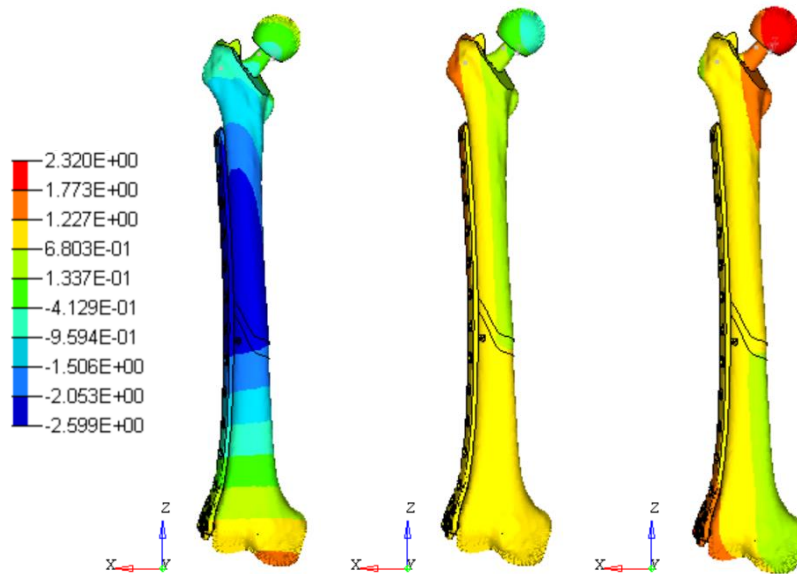


Figure 3.74: X, y and z components of the nodal displacements with fracture elastic modulus 9080 MPa [mm].

Fracture elastic modulus [MPa]	Maximum displacement [mm]	Maximum displacement x [mm]	Maximum displacement y [mm]	Maximum displacement z [mm]	Corresponding hole number
181,6	4,5	-4,4	-0,1	-0,1	14
363,2	3,7	-3,7	-0,3	0,0	14
1816	2,9	-2,9	-0,4	0,0	15
3632	2,7	-2,7	-0,4	0,0	16
9080	2,6	-2,6	-0,5	0,0	16

Table 3.26: Positions, total values and components values of the maximum displacement points of the model varying the fracture elastic modulus.

considered node moves towards the upper holes (Table 3.26). Since the area in which this node is positioned is subject to predominant deformation along the x axis, the module of the displacement vector in function of the level of fracture healing, was plotted, neglecting its components along the three axes (Fig. 3.75).

Stress distributions within the plate vary according to the level of bone reduction. The greatest stresses are found, in any case, in the upper left side volume. These stresses grow and move downwards when the fracture elastic modulus is reduced. For a fracture with stiffness of 181.6 MPa, the maximum stress area covers the lateral surface of the hole number 12 (Fig. 3.76, 3.77, Table 3.27).

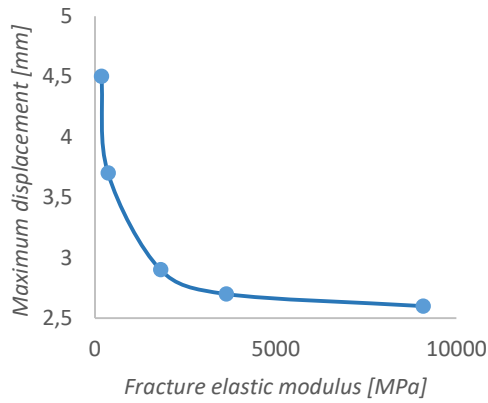


Figure 3.75: Maximum displacement values of the model varying the fracture elastic modulus.

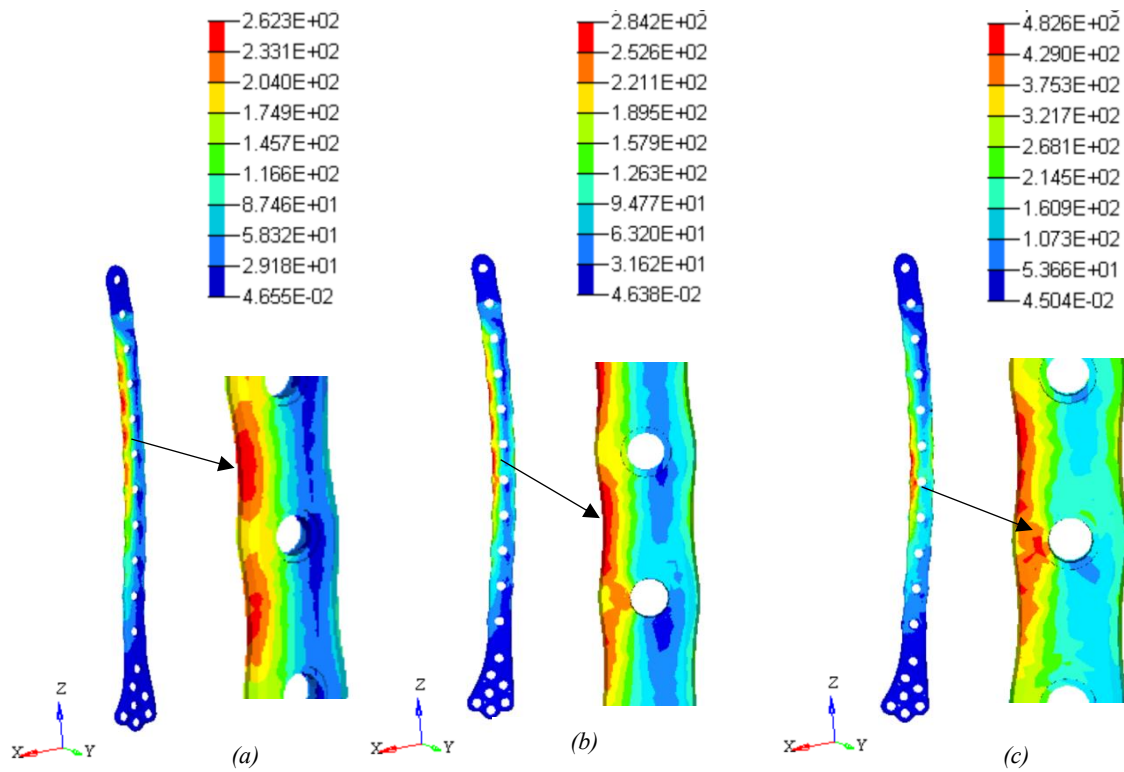


Figure 3.76: Von Mises stresses distributions from the models with fracture elastic modulus of 9080 (a), 1816 (b) and 181.6 (c)

Fracture elastic modulus [MPa]	Maximum Von Mises stress [Mpa]	Corresponding area
181,6	482,6	S_I
363,2	388,2	S_I
1816	284,2	S_I
3632	266,9	S_{-I}
9080	262,3	S_{-I}

Table 3.27: Von Mises maximum stresses values and positions, into the plate, varying the fracture elastic modulus

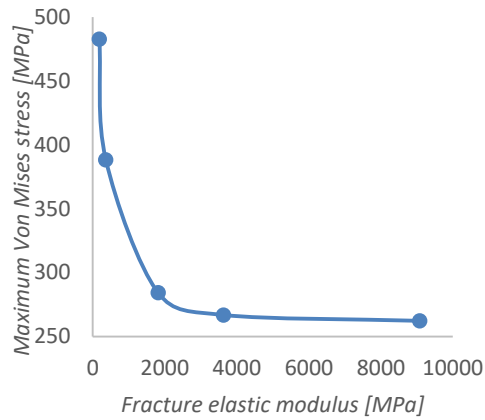


Figure 3.77: Von Mises maximum stresses, into the plate, varying the fracture elastic modulus.

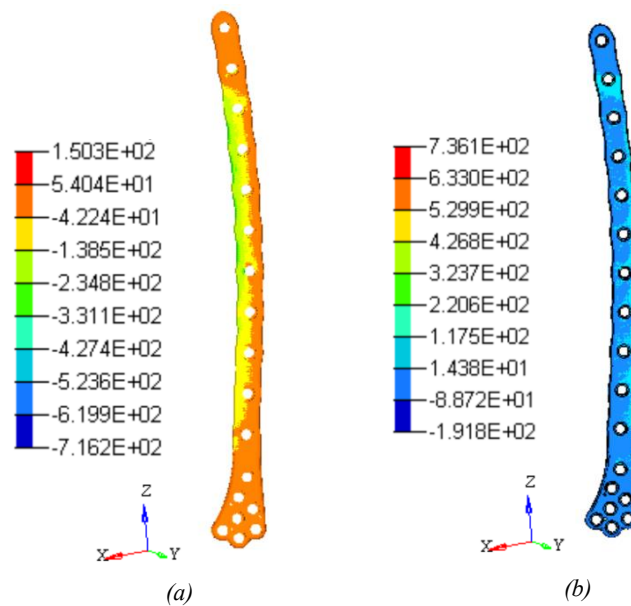


Figure 3.78: Maximum (a) and minimum (b) principal stresses [MPa] from the model with elastic fracture modulus of 9080 MPa.

According to the deformation profiles and the principal maximum and minimum stresses, in the left and front areas the plate is subjected to compressive stresses, while in the right and rear areas traction stresses are present (Fig. 3.78).

This configuration does not cause the plate break in the observed real conditions for two reasons. The maximum stress value remain below the yield point even for very weak fracture bone situations. Even if the fall caused a greater impact than the one simulated here, or the level of fracture reduction is very low, the plaque break would occur in a higher area than that in which the rupture actually occurred.

2.3.5 Sensitivity analysis

It was necessary to verify that the size of the selected tetragonal elements guarantee a sufficient precision of the results. For this reason, a two further model were constructed, whose mesh have a side length of 75% and 150% compared to the reference model (1,5 mm and 3,0 mm). The values of the peak stress inside the plate for each loading configuration, in the most yielding models, were compared. The percentage variability of these values with respect to model with the greatest number of degrees of freedom, were calculated (Table 3.28-3.34).

<i>Walking A - Step 1 - E = 181,6</i>		
<i>Element size</i>	<i>Maximum Von Mises stress [Mpa]</i>	<i>Percentage variation [%]</i>
3	273,9	12,8
2	297,7	5,3
1,5	314,2	

Table 3.28: Von Mises maximum stress values, varying the element lateral size, in the load configuration walking A / step 1, with fracture elastic modulus equal to 181,6. The variability with respect to the most refined model is highlighted.

<i>Walking A - Step 2 - E = 181,6</i>		
<i>Element size</i>	<i>Maximum Von Mises stress [Mpa]</i>	<i>Percentage variation [%]</i>
3	243,2	15,5
2	284,7	1,1
1,5	287,8	

Table 3.29: Von Mises maximum stress values, varying the element lateral size, in the load configuration walking A / step 2, with fracture elastic modulus equal to 181,6. The variability with respect to the most refined model is highlighted.

<i>Walking A - Step 3 - E = 181,6</i>		
<i>Element size</i>	<i>Maximum Von Mises stress [Mpa]</i>	<i>Percentage variation [%]</i>
3	11,6	9,9
2	12,4	2,6
1,5	12,7	

Table 3.30: Von Mises maximum stress values, varying the element lateral size, in the load configuration walking A / step 3, with fracture elastic modulus equal to 181,6. The variability with respect to the most refined model is highlighted.

<i>Walking B - E = 181,6</i>		
<i>Element size</i>	<i>Maximum Von Mises stress [Mpa]</i>	<i>Percentage variation [%]</i>
3	169,7	23,9
2	209,6	5,9
1,5	222,9	

Table 3.31: Von Mises maximum stress values, varying the element lateral size, in the load configuration walking B with fracture elastic modulus equal to 181,6. The variability with respect to the most refined model is highlighted.

<i>Stumbling - E = 726,4</i>		
<i>Element size</i>	<i>Maximum Von Mises stress [Mpa]</i>	<i>Percentage variation [%]</i>
3	704,3	19,0
2	866,8	0,4
1,5	870,0	

Table 3.32: Von Mises maximum stress values, varying the element lateral size, in the stumbling load configuration with fracture elastic modulus equal to 726,4. The variability with respect to the most refined model is highlighted.

<i>Falling A - E = 181,6</i>		
<i>Element size</i>	<i>Maximum Von Mises stress [Mpa]</i>	<i>Percentage variation [%]</i>
3	130,6	3,5
2	134,1	0,9
1,5	135,3	

Table 3.33: Von Mises maximum stress values, varying the element lateral size, in the falling A load configuration, with fracture elastic modulus equal to 181,6.

<i>Falling B - E = 181,6</i>		
<i>Element size</i>	<i>Maximum Von Mises stress [Mpa]</i>	<i>Percentage variation [%]</i>
3	410,0	16,7
2	482,6	1,9
1,5	492,1	

Table 3.34: Von Mises maximum stress values, varying the element lateral size, in the falling B load configuration, with fracture elastic modulus equal to 181,6. The variability with respect to the most refined model is highlighted.

3.4 Conclusions

Comparing the entities and the locations of the peak stresses to which the plate would be subjected in the analysed situations, was concluded that, there is a good probability that the break occurred due to the application of a load higher than 6000 N and with a predominant vertical component. In fact, this would cause a concentration of the stress converging towards the eleventh hole, which was the breaking section. These assumptions are valid for elastic modulus values of the healing fracture below approximately 1500 MPa. This value is low compared to what should be the level of bone reduction achieved after 3 months since the fixation operation. Observing an x-ray acquired two months after the fixation, it seems that the reduction was absent in the posterior area as the line that divides the bone stumps is clearly visible (Fig. 3.79). Some of the possible causes could have been malalignment during surgery, incorrect distribution of stress that does not allow bone rehabilitation or pathologies that reduce bone metabolism. The value of the elastic modulus that applied to the fractured bone would best simulate the real situation is not known. Despite this lack, has been deduced that a compromise of insufficient bone reduction and load applied to the prosthetic head with a predominant vertical component, is the most probable cause of the fracture occurrence. According to the present study, considered a patient with normal bone reduction and body mass of 95 Kg, after 3 months from the fixation (supposed to be 9080 MPa), subjected to the most common physiological activity such as walking, the maximum stress value the O'Nil plate for distal femur would be about 230 MPa, equal to one third of the yield strength (reference is made to the step 3 of the walking A configuration). In this situation the plate would have been designed to sustain the load with a safety coefficient equal to 3.

In conclusion, neglecting any possible but rare defects that could arise during the manufacturing phase, the O'Nil plate model for distal femur is safe and functional for the treatment of periprosthetic fractures related to THA.



Figure 3.79: Femoral x-ray after two months from the surgical implant. The sign of non-consolidation of the bone fracture is highlighted.

It is emphasized that the lower value of the chosen elastic modulus of the fracture, equal to 181.6 MPa, does not represent a limit to refer to for the evaluation of plaque break. This value is in fact related to a very yielding material, the use of which makes the model in question unrealistic. This value was chosen for the sole purpose of setting a lower limit for the evaluation of the stress and deformation distributions as a function of the fracture healing level.

As previously mentioned, the results obtained from configurations C and D representing the lateral fall have been neglected. In both cases, the values of nodal displacement and stress within the plate do not exceed the tenths of a millimeter and tens of megaPascals respectively. Furthermore, the stress and strain distributions of models C and D regarding the fall, are very similar to those obtained in the models A and B respectively. This is confirmed by the similarities between the boundary conditions. The stiffness of the implemented spring, representing the soft tissues surrounding the hip, causes an effect comparable to those obtained through a constraint acting along all degrees of freedom.

The analysis of the results obtained varying the finishing level of the mesh, confirms that the tetragonal element with chosen size guarantees a sufficient precision of results for the type of analysis performed. The variability of the Von Mises stress values, between the reference model and that with a lateral mesh dimension of 1.5 mm, remains in all cases below 6%.

4. Analysis on a generic oblique periprosthetic fracture

In this section, six femoral models have been implemented with a planar fracture located in the middle height of the diaphysis, with variable inclination with respect to the horizontal plane. For each of the implemented load configurations, the total deformation assumed by the model, the Von Mises stress distribution within the plate and its peak values were analysed. These parameters were evaluated in relation to the inclination and bone reduction level of the fracture. Thirty models have been implemented for each load configuration, whose elastic modules of the bone material inside the fracture assume values equal to 9080.0, 3632.0, 1816.0, 363.2, 181.6, and whose fracture inclinations assume angles between 15.0° and 52.5° , varied with 7.5° intervals. To simplify the presentation of the results, the numbering of the plate holes and the names of the right and left sides of it, indicated in the previous section, were used (Fig. 3.41).

The distributions of displacements and stresses, for each load configuration, are often similar to those obtained in the same simulation phase with the femoral model relative to the real case. The conclusions drawn regarding the distributions of femoral displacements and stresses within the plate, when not explained, refer to the corresponding analyses previously carried out.

4.1 Models creation

The models creation procedure was similar to the one presented in the previous chapter of the thesis. In this case, however, the bone geometry was generalized as much as possible, in order to obtain results not influenced by the features of the patient. The femoral bone available model was reduced according to the scale factor previously individuated (SF), to permit the correct adaptation of the plate, of size extra-long, on it. Subsequently, the oblique fracture was inserted, cutting the bone through two parallel planes, whose relative distance was equal to one centimeter (Fig. 4.1). Varying the inclination of the planes with respect to the transverse femoral plane, the seven aforementioned models were constructed. The positions and lengths of the screws, as well as the fracture insertion area, refer to the previous case.

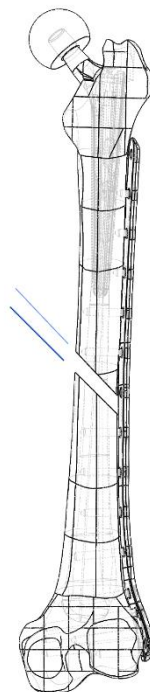


Figure 4.1: Femur model cutted by two oblique planes with relative distance equal to one centimeter.

4.2 Results

4.2.1 Walking - A configuration

10% of the walking cycle

During the first walking phase the femoral body is flexed towards the positive x semi-axis and towards the negative y semi-axis and undergoes a torsion around its longitudinal axis (Fig. 4.2a). This determines the flexion of the plate directed anteriorly and towards the left side (Fig. 4.3). The maximum Von Mises stresses inside the plate are located on the left posterior side between the holes number 12 and 13 (Fig. 4.2b, Table 4.1). Exceptions are the cases in which the elastic modulus is equal to 9080, in which a stress peak is concentrated on the left side of the area between the holes 10 and 11. These are compression stresses. The maximum stress within the plate is reduced as bone healing increases. With the same variation of the elastic modulus of the fracture, for small values of this there is a big difference of the peak stresses in the plate, for great values of this the difference is reduced (Fig. 4.4b). When the elastic modulus changes within the chosen range, the peak stress undergoes variations of about 200 MPa. When the fracture is less reduced, the influence of the angle of inclination on the peak value of Von Mises stress is greater (Fig. 4.4c). In the model in which the fracture is more yielding we observe the reduction of the maximum stresses in the plate as the fracture inclination increases. The maximum variation of the peak stress, in the case of more yielding bone, is just over 50 MPa. For more reduced femur models the influence of the inclination of the fracture becomes negligible. Summarizing, the areas of maximum stress within the plate assume increasing values, and move downwards, as the level of bone healing decreases, for the reasons already explained during the analysis of the same loading phase in the previous section. The growth of the inclination angle of the fracture determines the increase of the maximum stress inside the plate, negligible in case of greater bone reduction. The maximum stresses obtained inside the plate applied to oblique fracture, during the beginning of the midstance walking phase, vary between 129.8 and 367.1 MPa.

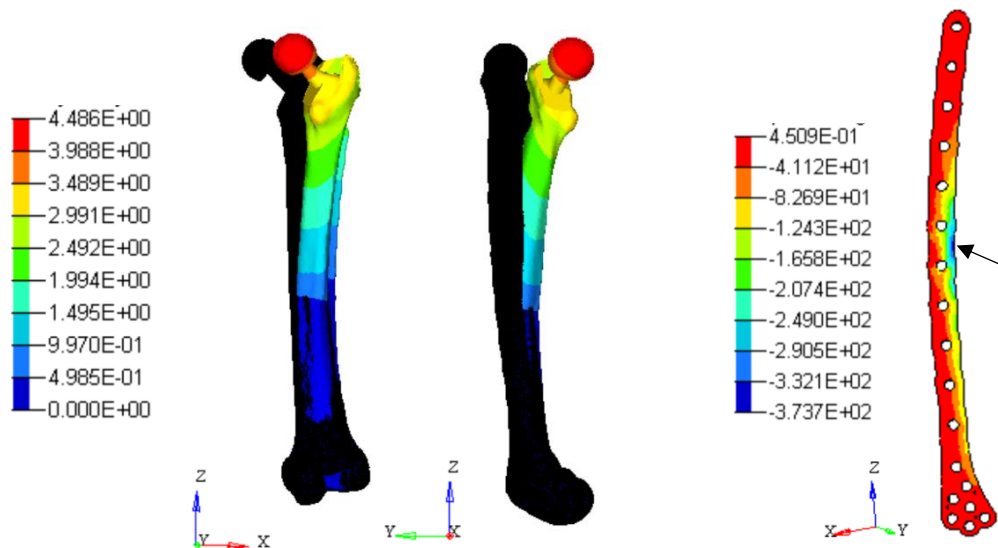


Figure 4.2: Nodal displacements [mm] of the model with non-deformed shape of the model with fracture elastic modulus of 181.6 MPa and fracture inclination of 30° (a). The displacements are amplified by a factor of 3. Minimum principal stress distribution (b) within the plate of the model with fracture elastic modulus of 181.6 MPa and fracture inclination of 30°, view of the posterior side. The arrow indicate the point with maximum stress.

Fracture elastic modulus [MPa] / Fracture inclination [°]	181,6	363,2	1816	3632	9080
15	366,1	298,6	169,8	139,2	132,4
22,5	367,1	300,4	171,8	140,6	132,3
30	363,9	298,8	173,4	141,8	132,1
37,5	354,6	291,8	172,9	142,1	131,3
45	339,4	279,9	171,0	142,3	131,0
52,5	310,0	256,8	165,6	141,1	129,8
Peak area	12 – 13 l	10 – 11 l			

Table 4.1: Von Mises maximum stress in the plate varying the fracture elastic modulus and inclination. The “peak area” field indicate the number of the holes near the peak zone and the side of it (left, right) respect to the plate.

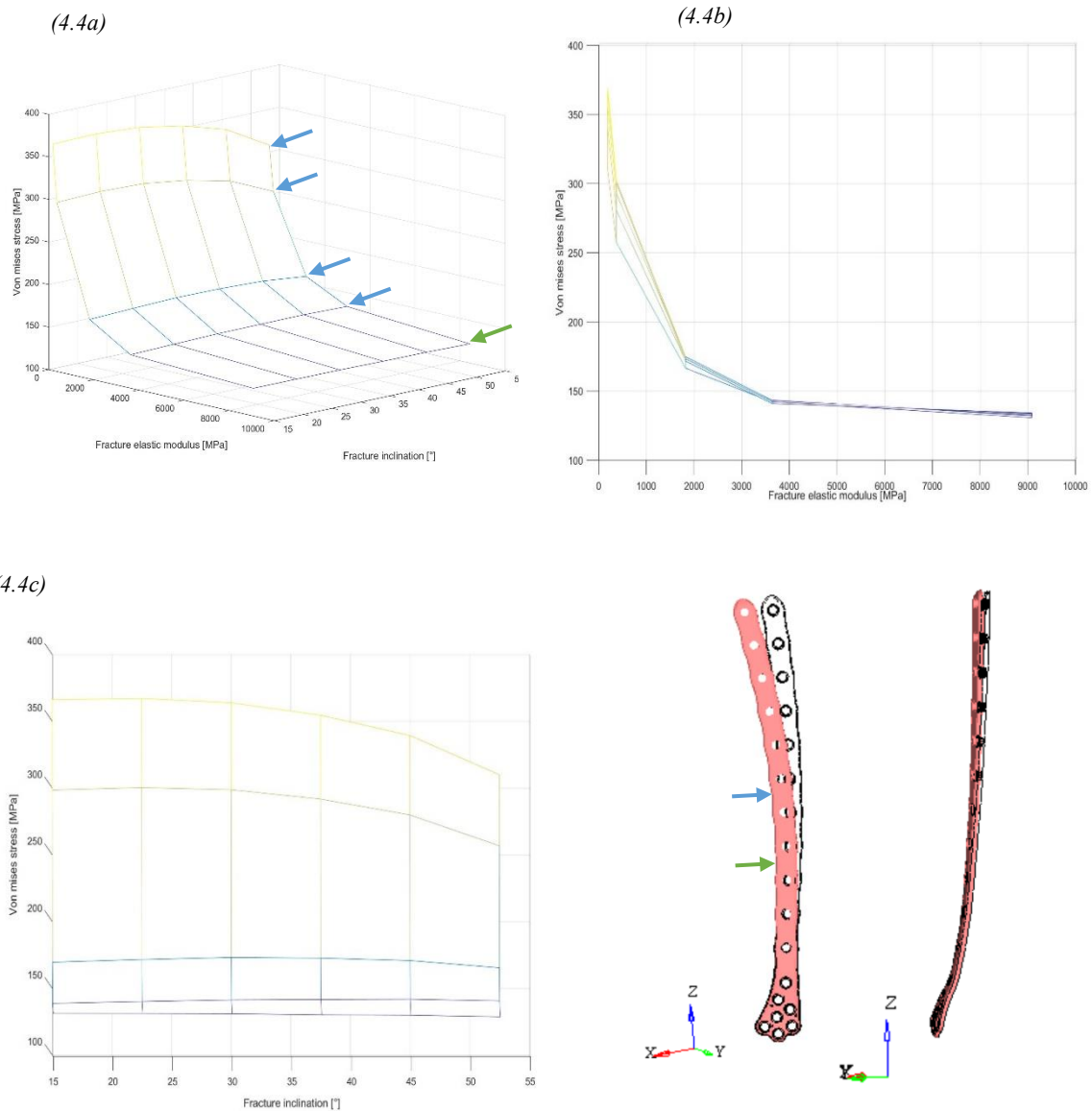


Figure 4.4: Von Mises maximum stresses in the plate varying the fracture inclination and elastic module. Tridimensional (a), xy plane (b) and yz plane (c) views. The arrows represents the stressed areas with reference to figure 4.3.

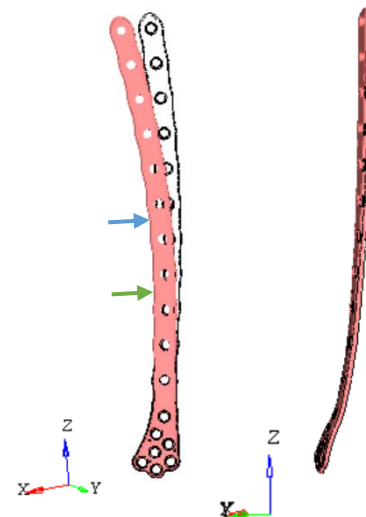


Figure 4.3: Plate deformed and non-deformed shapes, with amplified nodal displacements. The arrows represent the areas of maximum Von Mises stress, varying the fracture elastic modulus.

30% of the walking cycle

During the second walking phase, the femoral body is flexed towards the positive x semi-axis and towards the negative y semi-axis and undergoes an important torsion around its longitudinal axis (Fig. 4.5a). This determines the flexion of the plate directed posteriorly and towards the left side (Fig. 4.6). The maximum Von Mises stress distributions within the plate are located, depending on the elastic modulus, on similar areas than the ones of the previously analysed case (Table 4.2). Here, however, the maximum stress value, is alternated between traction and compression zones. For module values lower than 363.2 MPa, mainly the right side of the plate between the holes 12 and 13 is stressed, subject to traction (Fig. 4.5b). For module values comprised between 1816 MPa and 3632 MPa, the left area of the plate between the holes 12 and 13 is more stressed, subjected to compression. For elastic modulus equal to 9080 MPa the most stressed area moves between the holes 10 and 11, remaining on the left side, and is subjected to compression. The maximum stress within the plate is reduced as the fracture healing level increases. With the same variation of the elastic modulus of the fracture, for small values of this there is a big difference of the peak tensions in the plate, for great values of this this difference is reduced (Fig. 4.7b). When the modulus of elasticity varies within the chosen range, the peak stress undergoes variations greater than 200 MPa. When the fracture is less reduced, the influence of its inclination angle on the Von Mises stress peak value is greater. In the model in which the fracture is more yielding we observe the growth of the maximum stresses in the plate with the increase of the fracture inclination, for angles inferior to 30°. Instead, the maximum stresses are reduced for angles increasing above 30° (Fig. 4.7c). The maximum peak stress variation in the case of more yielding bone is just over 40 MPa. For more reduced femur models the influence of the inclination of the fracture becomes negligible. Summarizing, the zones of maximum stress within the plaque assume increasing values, and move downwards, as the level of bone healing decreases, for the reasons already explained during the analysis of real fracture. The inclination of the fracture determines the increase of the maximum tension for angles close to 30°, negligible in case of greater bone reduction. The maximum tensions obtained inside the plate applied to an oblique fracture, at the end of the mid-stance walking phase, vary between 114.7 and 397.2 MPa.

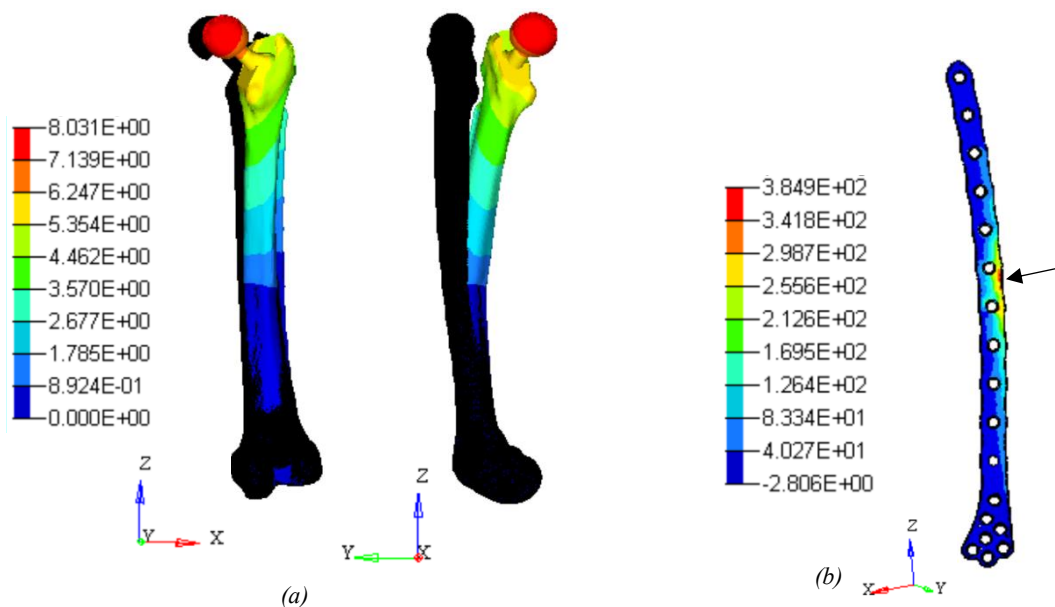


Figure 4.5: Nodal displacements [mm] of the model with non-deformed shape of the model with fracture elastic modulus of 181.6 MPa and fracture inclination of 30° (a). The displacements are amplified by a factor of 3. Maximum principal stress distribution (b) within the plate of the model with fracture elastic modulus of 181.6 MPa and fracture inclination of 30°. The arrow indicate the point with maximum stress.

Fracture elastic modulus [MPa] / Fracture inclination [°]	181,6	363,2	1816,0	3632,0	9080,0
15,0	388,0	302,7	158,2	125,8	116,2
22,5	394,7	307,9	160,8	127,2	116,1
30,0	397,2	309,7	162,7	128,7	116,0
37,5	392,6	305,7	162,5	129,4	115,5
45,0	380,6	296,3	160,9	129,8	114,9
52,5	350,6	274,0	155,5	128,7	114,7
Peak area	12 - 13 r	12 - 13 r	12 - 13 l	12 - 13 l	10 - 11 l

Table 4.2: Von Mises maximum stress in the plate varying the fracture elastic modulus and inclination. The “peak area” field indicate the number of the holes near the peak zone and the side of it (left, right) respect to the plate.

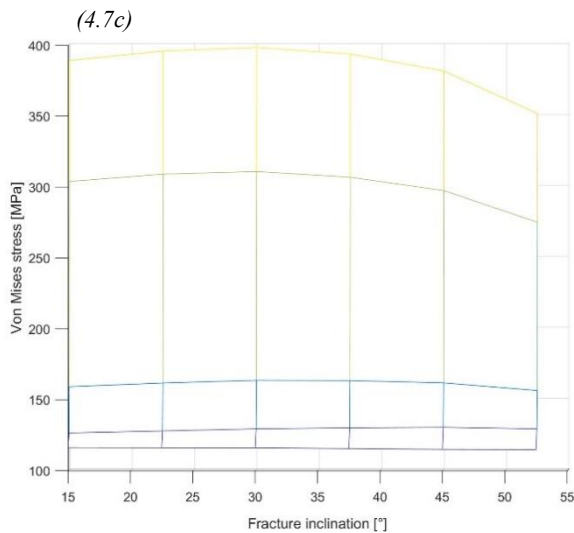
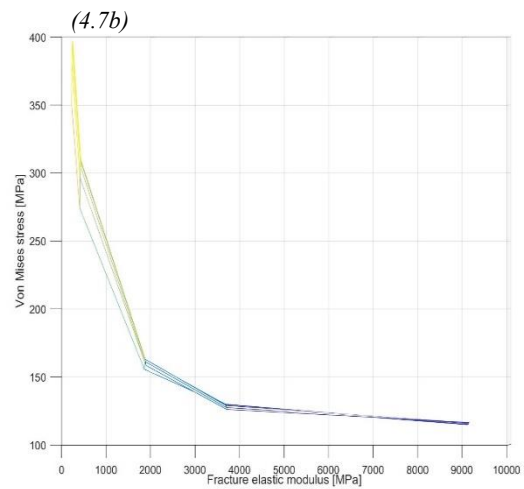
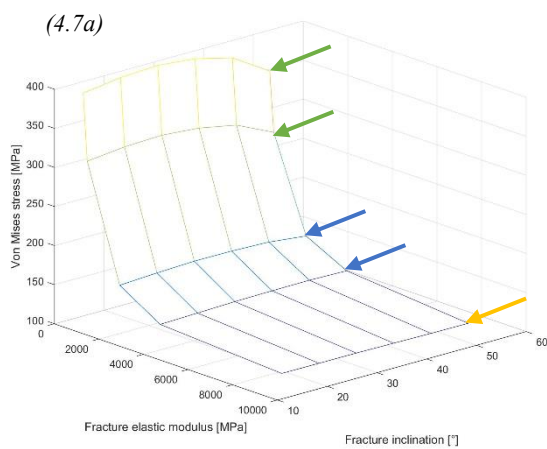


Figure 4.7: Von Mises maximum stresses in the plate varying the fracture inclination and elastic module. Tridimensional (a), xy plane (b) and yz plane (c) views. The arrows represents the stressed areas with reference to figure 4.6.

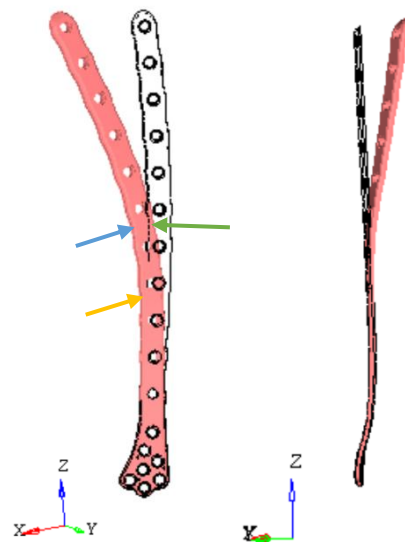


Figure 4.6: Plate deformed and non-deformed shapes, with amplified nodal displacements. The arrows represent the areas of maximum Von Mises stress, varying the fracture elastic modulus.

45% of the walking cycle

During the third walking phase the femoral body is flexed towards the negative x semi-axis and towards the positive y semi-axis and undergoes a slight torsion around its longitudinal axis (Fig. 4.8a). This determines the flexion of the plate directed anteriorly and towards the right side (Fig. 4.9). The maximum Von Mises stresses within the plate are located in different areas as the elastic modulus of the fracture varies (Table 4.3). For the module lower than 363.2 MPa, mainly the right posterior side of the plate between the holes 12 and 13 is stressed, subject to traction (Fig. 4.8c). For the module equal to 1816 MPa, the left area of the plate included between the holes 11 and 12 is stressed, subjected to compression. For elastic modules greater than 3632 MPa, the most stressed area moves downwards and on the right side, which is subject to compression. The maximum stress within the plate is reduced as the fracture healing level increases. With the same variation of the elastic modulus of the fracture, for small values of this there is a big difference of the peak stresses in the plate, for great values of this this difference is reduced (Fig. 4.10b). When the elastic modulus changes within the chosen range, the peak stress undergoes variations of about 200 MPa. When the fracture is less reduced the influence of the inclination angle on the Von Mises stress peak value is greater (Fig. 4.10c). In the model in which the fracture is more yielding we observe the growth of the maximum stresses in the plate as the angle of inclination of the fracture increases. In this model the peak stress undergoes variations of about 80 MPa. For more reduced femur models the influence of the fracture inclination becomes negligible. Summarizing, the zones of maximum stress within the plaque assume increasing values, and move downwards, as the level of bone healing decreases, for the reasons already explained during the analysis on the same loading phase of the real fracture. The reduction of the inclination of the fracture determines the slight decrease of the maximum stress, negligible in case of greater bone reduction. The maximum stresses obtained inside the plate applied to oblique fracture, just before the toe-off walking phase, vary between 209.4 and 573.6 MPa.

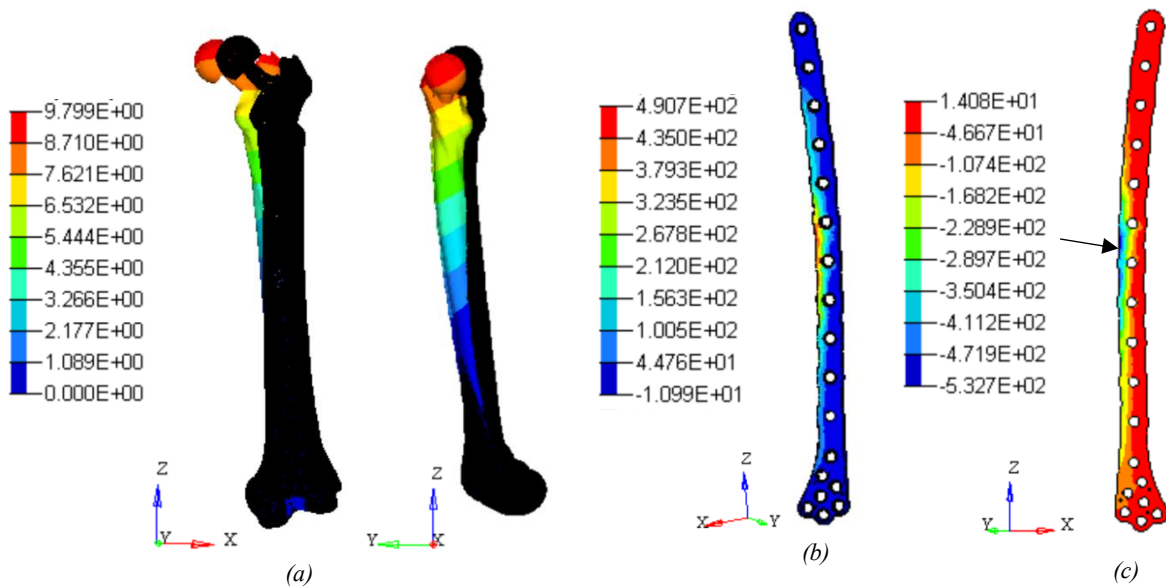


Figure 4.8: Nodal displacements [mm] of the model with non-deformed shape of the model with fracture elastic modulus of 181.6 MPa and fracture inclination of 30° (a). The displacements are amplified by a factor of 3. Maximum principal stress (b) and minimum principal stress (c) distributions within the plate of the model with fracture elastic modulus of 181.6 MPa and fracture inclination of 30°. The arrow indicates the point with maximum stress.

Fracture elastic modulus [MPa] / Fracture inclination [°]					
	181,6	363,2	1816	3632	9080
15	491,2	413,0	258,4	221,3	209,7
22,5	497,6	414,3	259,1	220,7	209,7
30	522,4	418,5	260,5	220,3	209,6
37,5	545,5	437,4	261,1	219,3	209,6
45	566,7	455,9	261,3	217,6	209,5
52,5	573,6	465,0	258,6	214,4	209,4
Peak area	12 - 13 r	12 - 13 r	11 - 12 l	10 - 11 r	9 - 10 r

Table 4.3: Von Mises maximum stress in the plate varying the fracture elastic modulus and inclination. The “peak area” field indicate the number of the holes near the peak zone and the side of it (left, right) respect to the plate.

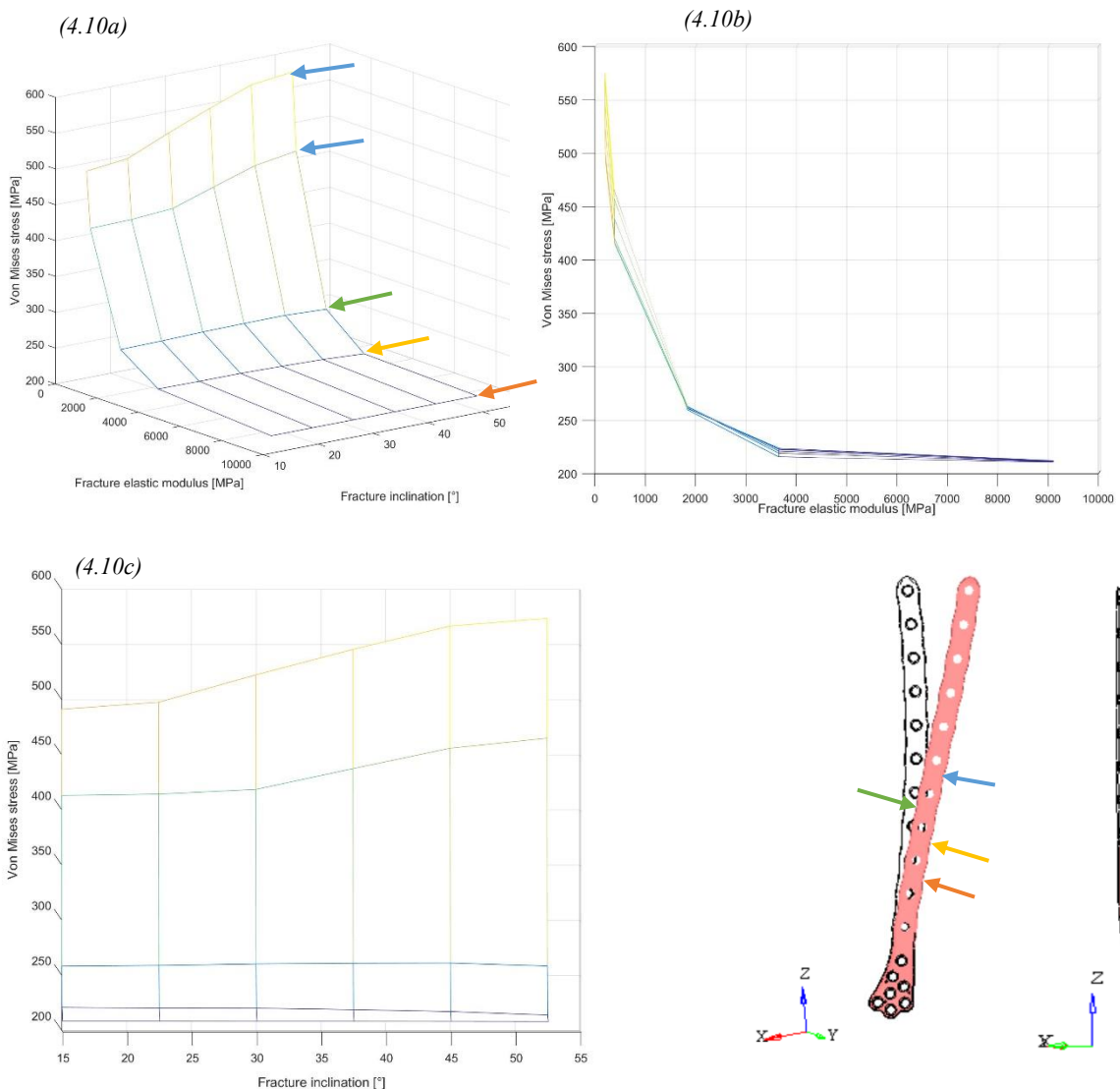


Figure 4.10: Von Mises maximum stresses in the plate varying the fracture inclination and elastic module. Tridimensional (a), xy plane (b) and yz plane (c) views. The arrows represents the stressed areas with reference to figure 4.9.

Figure 4.9: Plate deformed and non-deformed shapes, with amplified nodal displacements. The arrows represent the areas of maximum Von Mises stress, varying the fracture elastic modulus.

4.2.2 Walking - B configuration

During the heel strike walking phase, in which the maximum force on the prosthetic head is applied, the model deformation is similar to those obtained during the instant at the 10% of the walking phase. The femoral body is bended towards the negative y semi-axis and undergoes a torsion around its longitudinal axis. The body is, instead, bended towards the negative x semi-axis (Fig. 4.11a). This determines the bending of the plate directed posteriorly and towards the left side (Fig. 4.12). The maximum Von Mises stresses within the plate are located in different areas depending on the fracture elastic modulus (Table 4.4). In every model the higher stressed area is located on the left side, and represents a compression (Fig. 4.11b). For module values lower than 1816 MPa, the left area of the plate between the holes 12 and 13 is the most stressed. For module values greater than 3632 MPa, zone between the holes 10 and 11 is more stressed. The maximum stress within the plate is reduced as the fracture healing level increases. With the same variation of the elastic modulus of the fracture, for small values of this there is a big difference of the peak tensions in the plate, for great values of this this difference is reduced (Fig. 4.13b). When the modulus of elasticity varies within the chosen range, the peak stress undergoes variations greater than 180 MPa. When the fracture is less reduced, the influence of its inclination angle on the Von Mises stress peak value is greater. In the model in which the fracture is more yielding we observe the growth of the maximum stresses in the plate with the increase of the fracture inclination, for angles inferior to 45° . Instead, the maximum stresses are reduced for angles increasing above 45° (Fig. 4.13c). The maximum peak stress variation in the case of more yielding bone is approximately 20 MPa. For more reduced femur models the influence of the inclination of the fracture becomes negligible. Summarizing, the zones of maximum stress within the plaque assume increasing values, and move downwards, as the level of bone healing decreases, for the reasons already explained during the analysis of real fracture. The inclination of the fracture determines the increase of the maximum stress for angles close to 45° , negligible in case of greater bone reduction. The maximum stresses obtained inside the plate applied to an oblique fracture, during the heel strike walking instant, vary between 98.4 and 314.7 MPa.

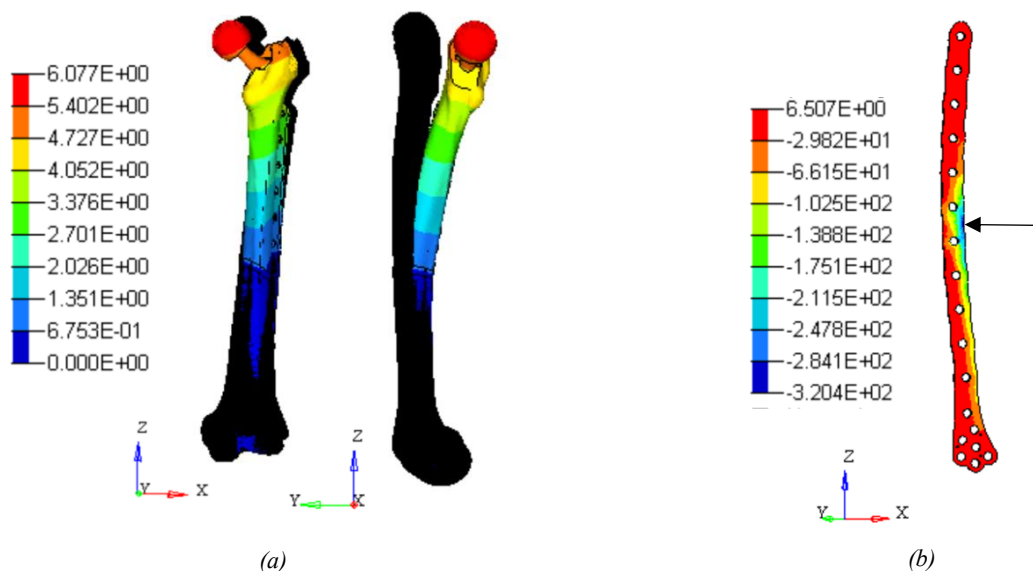


Figure 4.11: Nodal displacements [mm] of the model with non-deformed shape of the model with fracture elastic modulus of 181.6 MPa and fracture inclination of 30° (a). The displacements are amplified by a factor of 10. Minimum principal stress (b) distribution within the plate of the model with fracture elastic modulus of 181.6 MPa and fracture inclination of 30° . The arrow indicate the point with minimum value.

Fracture elastic modulus [MPa] / Fracture inclination [°]	181,6	363,2	1816	3632	9080
15	283,1	217,5	119,8	107,6	100,0
22,5	293,6	224,4	122,5	107,3	100,9
30	303,9	231,2	125,5	107,0	99,8
37,5	311,2	235,8	127,7	106,6	99,5
45	314,7	238,0	129,6	105,1	99,0
52,5	305,7	231,6	129,4	105,6	98,4
Peak area	12- 13 l	12- 13 l	12- 13 l	10- 11 l	10- 11 l

Table 4.4: Von Mises maximum stress in the plate varying the fracture elastic modulus and inclination. The “peak area” field indicate the number of the holes near the peak zone and the side of it (left, right) respect to the plate.

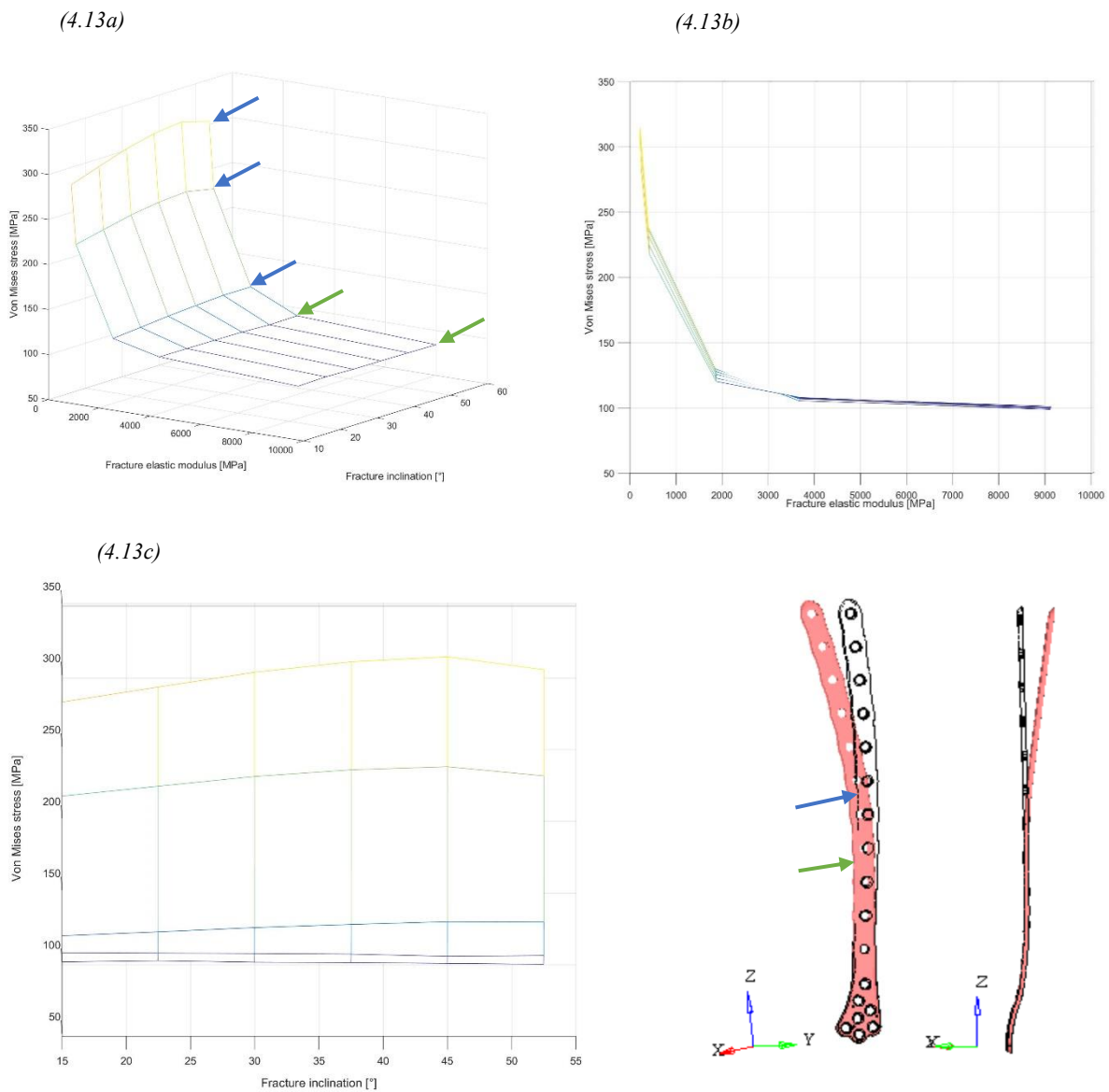


Figure 4.13: Von Mises maximum stresses in the plate varying the fracture inclination and elastic module. Tridimensional (a), xy plane (b) and yz plane (c) views. The arrows represents the stressed areas with reference to figure 4.12.

Figure 4.12: Plate deformed and non-deformed shapes, with amplified nodal displacements. The arrows represent the areas of maximum Von Mises stress, varying the fracture elastic modulus.

4.2.3 Stumbling

During stumbling from standing position, the direction of the contact force is the same as the one applied during walking analysed B configuration. The femoral body is bended towards the negative x semi-axis and towards the negative y semi-axis of the ordinates (Fig. 4.14). This determines the flexion of the plate directed posteriorly and towards its left side (Fig. 4.15). The maximum Von Mises stresses within the plate are located in different areas depending on the fracture elastic modulus (Table 4.5). For values of the module lower than 363.2 MPa, the right side of the plate between the holes 12 and 13 is mainly stressed, subject to traction (Fig. 4.14b). For the module equal to 1816 MPa, the left area of the plate included between the holes 12 and 13 is mainly stressed, subjected to compression. For elastic modules greater than 3632 MPa, the most stressed area moves downwards and on the left side, subjected to compression (Fig. 4.14c). The maximum stress within the plate is reduced as the fracture healing level increases. With the same variation of the elastic modulus of the fracture, for small values of this there is a big difference of the peak stresses in the plate, for great values of this this difference is reduced (Fig. 4.16b). When the modulus of elasticity varies within the chosen range, the peak stress undergoes variations greater than 1500 MPa. When the fracture is less reduced the influence of its inclination angle on the Von Mises stress peak value is greater (Fig. 4.16c). In the model in which the fracture is more yielding we observe the growth in the maximum stresses in the plate as the angle of inclination increases, when this is less than 37.5° . For greater angles the peak stress in the plate decreases as the inclination increases. In this model the peak stress undergoes variations of about 400 MPa. For more reduced femur models the influence of the inclination of the fracture becomes negligible. Summarizing, the zones of maximum stress within the plaque assume increasing values, and move downwards, as the level of bone healing decreases, for the reasons already explained during the analysis of real fracture. The inclination of the fracture determines a peak tension of the plaque around 37.5° , negligible in case of greater bone reduction. The maximum stresses obtained inside the plate applied to an oblique fracture, during stumbling from standing height position, vary between 209.4 and 573.6 MPa.

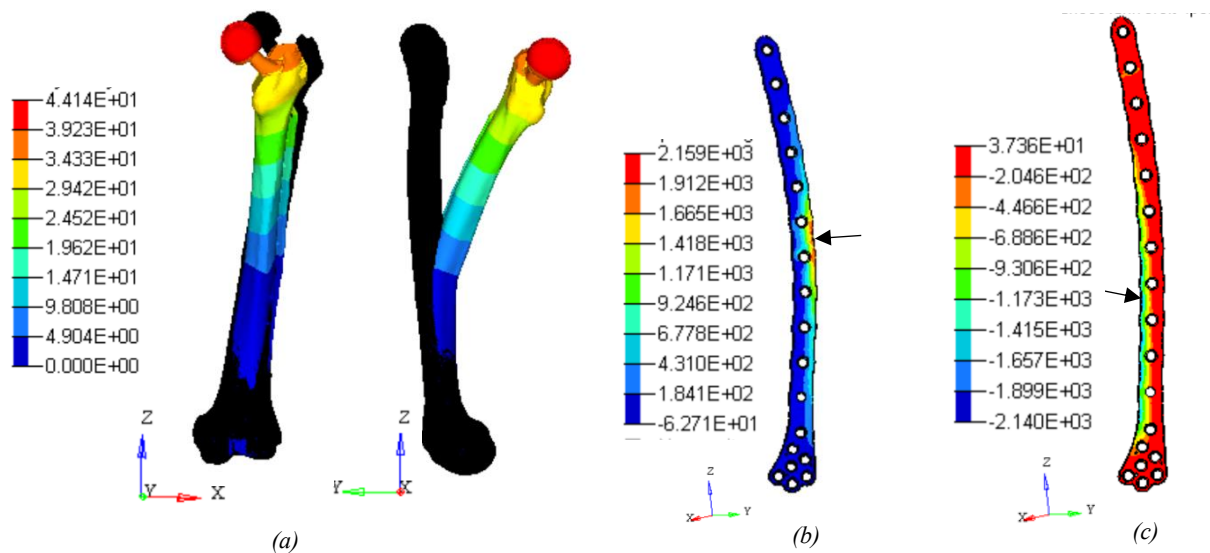


Figure 4.14: Nodal displacements [mm] of the model with non-deformed shape of the model with fracture elastic modulus of 181.6 MPa and fracture inclination of 30° (a). The displacements are amplified by a factor of 10. Maximum principal stresses distribution within the plate of the model with fracture elastic modulus of 181.6 MPa and fracture inclination of 30° (b). Minimum principal stresses distribution within the plate of the model with fracture elastic modulus of 9080 MPa and fracture inclination of 30° (c). The arrows indicate the point with maximum stress.

Fracture elastic modulus [MPa] / Fracture inclination [°]	181,6	363,2	1816	3632	9080
15	1970,6	1236,6	514,6	435,0	390,2
22,5	2084,4	1290,2	528,2	434,4	389,9
30	2181,3	1335,6	542,5	433,6	389,6
37,5	2206,2	1349,5	552,1	430,4	388,4
45	2148,5	1331,4	558,4	424,7	386,6
52,5	1819,6	1217,3	551,9	414,7	383,7
Peak area	12-13 r	12-13 r	12-13 l	10-11 l	10-11 l

Table 4.5: Von Mises maximum stress in the plate varying the fracture elastic modulus and inclination. The “peak area” field indicate the number of the holes near the peak zone and the side of it (left, right) respect to the plate.

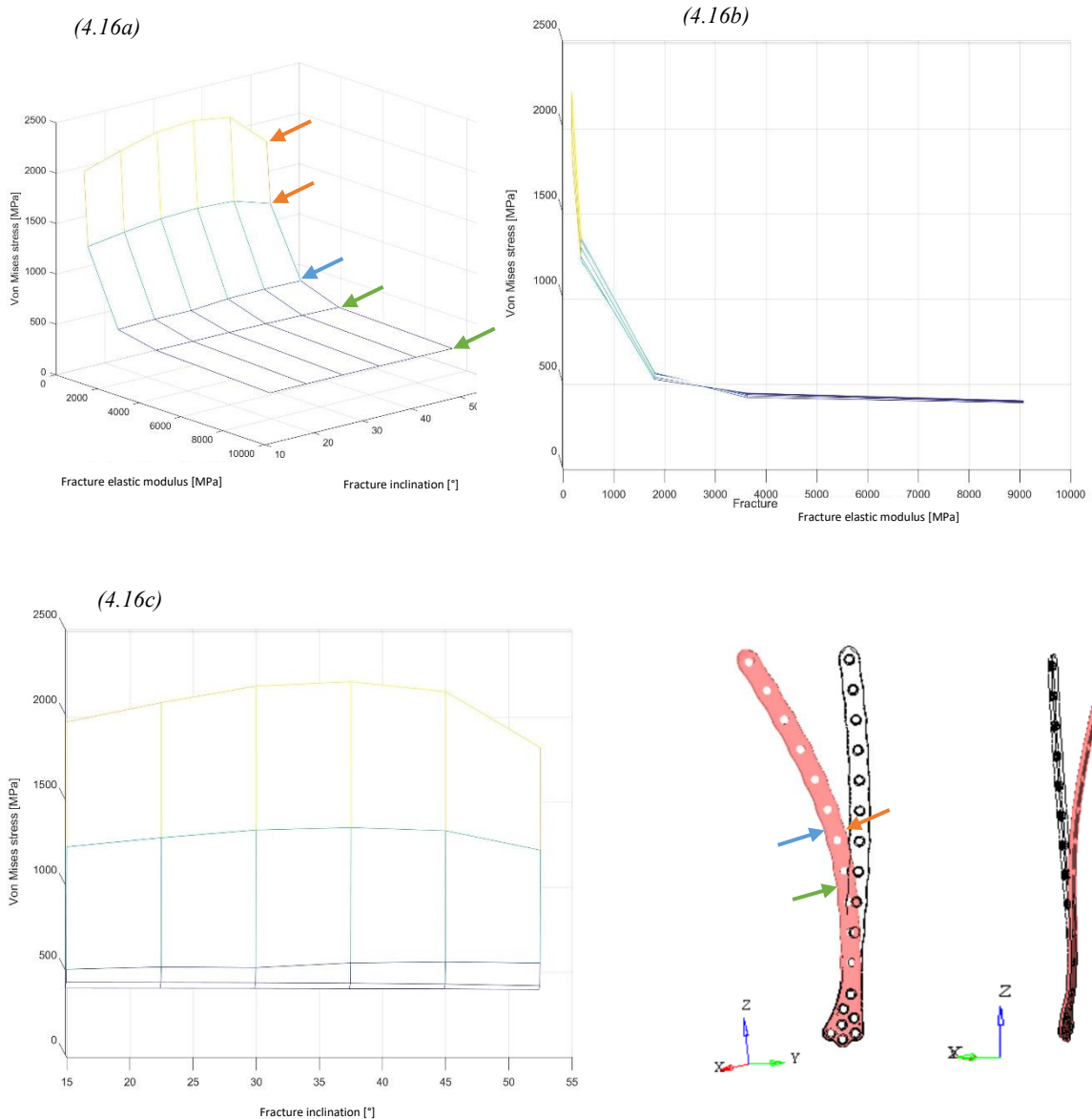


Figure 4.16: Von Mises maximum stresses in the plate varying the fracture inclination and elastic module. Tridimensional (a), xy plane (b) and yz plane (c) views. The arrows represents the stressed areas with reference to figure 4.15.

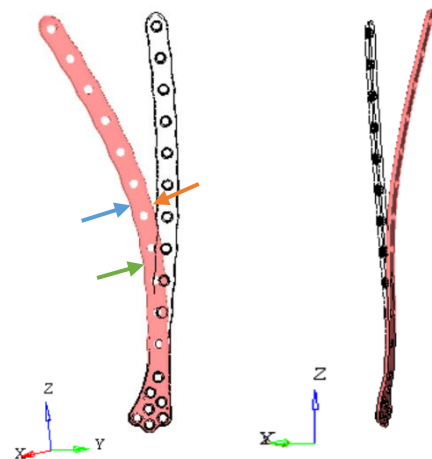


Figure 4.15: Plate deformed and non-deformed shapes, with amplified nodal displacements. The arrows represent the areas of maximum Von Mises stress, varying the fracture elastic modulus.

4.2.4 Falling

Falling A configuration

The model of fall whose distal zone is constrained along all the degrees of freedom, shows the bending of the central femoral body towards the negative x semi-axis. The femoral head is subjected to a horizontal displacement towards the negative y semi-axis, for this reason the bone undergoes a torsion around its longitudinal axis (Fig. 4.20). This determines the bending of the plate directed posteriorly and towards the right side, and its partial torsion around the z axis (Fig. 4.24). The maximum stresses within the plate are located in different areas as the elastic modulus of the fracture varies (Table 4.7). For module values greater than 1816 MPa, the left area between the holes 7 and 8 is subjected to the highest stresses, of traction type. For the module values equal to 363.2 MPa the area of the plate to the left side of the hole number 11, mainly to traction, is more stressed. For elastic modulus equal to 181.6 the greater stresses are concentrated around the hole number 12, and the peak of these is found in the lower part of its internal surface (Fig. 4.21). The bending of the model near the constraint generates an oblique band of tensile stresses in the lower left volume of the plate. The higher left volume is instead stressed in compression, and within there are two areas subjected to traction stress, close to the hole number 12 and diametrically opposed with respect to it (Fig. 4.22). The maximum stress within the plate is reduced as the fracture healing level increases. With the same variation of the elastic modulus of the fracture, for small values of this there is a big difference of the peak stresses in the plate, for great values of this, the difference is reduced (Fig. 4.23b). When the modulus of elasticity varies within the chosen range, the peak stress undergoes variations of less than 150 MPa. For each value of elastic modulus the stress in the plate shows a peak for inclinations equal to 22.5° with respect to the horizontal. Beyond this angle the stress decreases as the fracture inclination increases (Fig. 4.23c). In summary, the areas of maximum stress within the plate assume increasing values, and move downwards, as the level of bone healing decreases, for the reasons already explained during the analysis of real fracture. The reduction of the inclination of the fracture determines the growth of the maximum stress in the plate up to an angle of 22.5° . The maximum stresses obtained inside the plate applied to oblique fracture, during the lateral fall with beat on the greater trochanter, simulated assuming the knee foothold fixed, vary between 169.1 and 326.8 MPa.

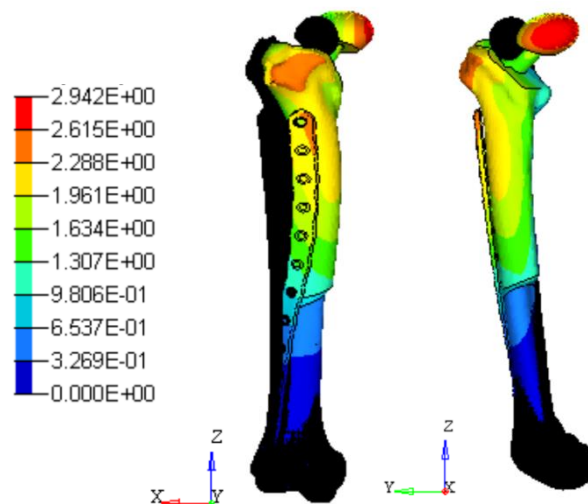


Figure 4.20: Nodal displacements [mm] of the model with non-deformed shape of the model with fracture elastic modulus of 181.6 MPa and fracture inclination of 30° . The displacements are amplified by a factor of 20.

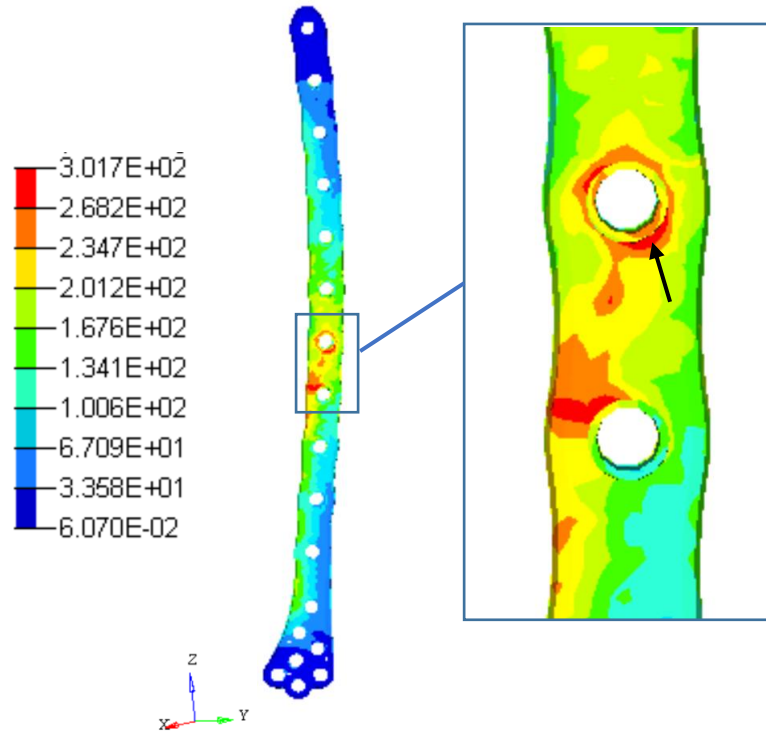


Figure 4.21: Von Mises stresses distribution of the model with fracture elastic modulus of 181.6 MPa and fracture inclination of 30°. The arrow indicate the most stressed point.

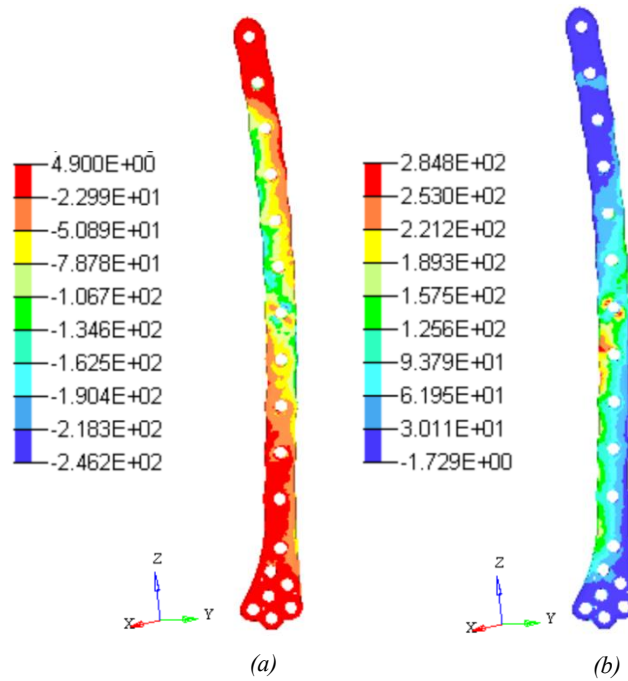


Figure 4.22: Minimum (a) and maximum (b) principal stresses of the model with fracture elastic modulus of 181.6 MPa and fracture inclination of 30°.

Fracture elastic modulus [MPa] / Fracture inclination [°]	181,6	363,2	1816	3632	9080
15	325	225	169,2	169,1	169,4
22,5	326,8	229,7	181,1	180,9	181,0
30	301,7	211,1	173,1	172,8	172,7
37,5	280,1	205	173,3	173	172,9
45	254,5	196,3	170,3	170,2	170,0
52,5	250,4	196	170,6	170,6	170,3
Peak area	12	111	7 - 81	7 - 81	7 - 81

Table 4.7: Von Mises maximum stress in the plate varying the fracture elastic modulus and inclination. The “peak area” field indicate the number of the holes near the peak zone and the side of it (left, right) respect to the plate.

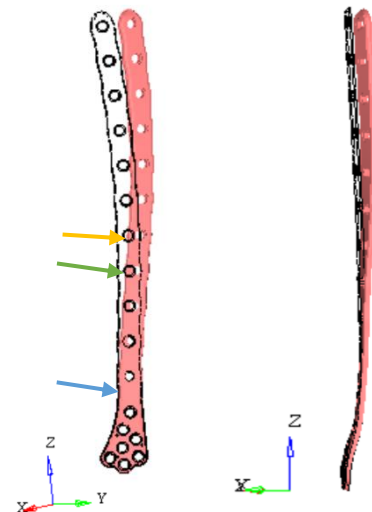
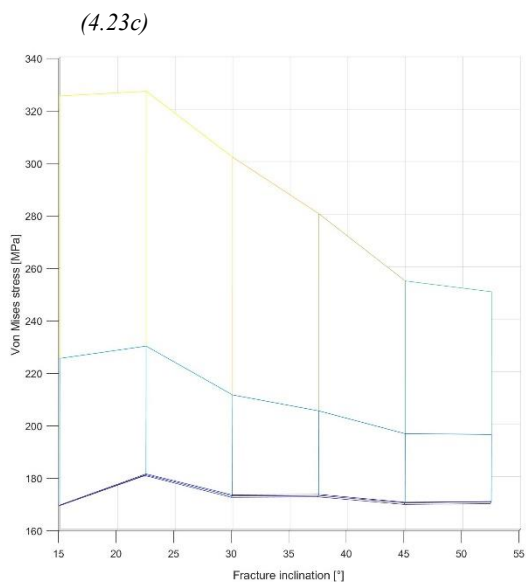
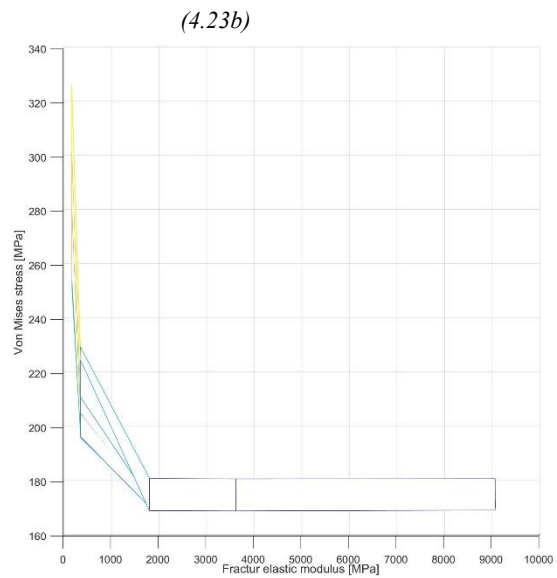
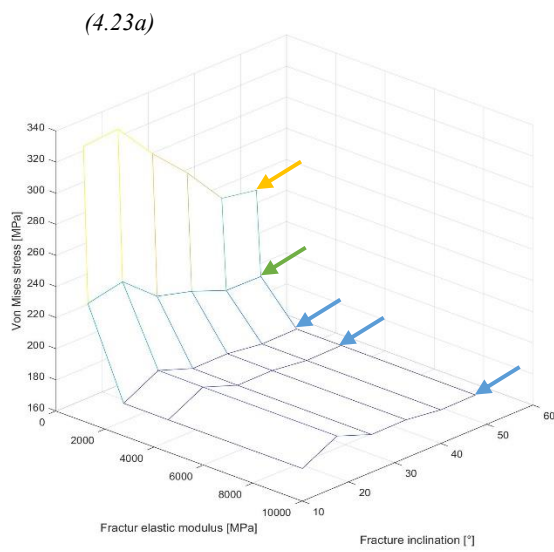


Figure 4.22: Von Mises maximum stresses in the plate varying the fracture inclination and elastic module. Tridimensional (a), xy plane (b) and yz plane (c) views. The arrows represents the stressed areas with reference to figure 4.24.

Figure 4.24: Plate deformed and non-deformed shapes, with amplified nodal displacements. The arrows represent the areas of maximum Von Mises stress, varying the fracture elastic modulus.

Falling B configuration

The model of fall whose distal zone is constrained through a hinge constraint, shows the bending of the central femoral body towards the negative x semi-axis. This deformation causes a slight torsion of the prosthetic head around the trochanteric area (Fig. 4.17a). This determines the bending of the plate directed anteriorly and towards the right side, and its partial torsion around the z axis (Fig. 4.18). The maximum stresses within the plate are located in different areas as the elastic modulus of the fracture varies (Table 4.6). For each level of bone healing considered, the most stressed area within the plate is subjected to compression, and is situated on the left side. For module values greater than 3632 MPa, the left area between the holes 14 and 15 is subjected to the highest stresses. For the module values equal to 1816 MPa the area of the plate between the holes 13 and 14 is more stressed. For elastic modulus values lower than 181.6 MPa the greater stresses are located between the holes 12 and 13 (Fig. 4.17b). The maximum stress within the plate is reduced as the fracture healing level increases. With the same variation of the elastic modulus of the fracture, for small values of this there is a big difference of the peak stresses in the plate, for great values of this, the difference is reduced (Fig. 4.19b). When the modulus of elasticity varies within the chosen range, the peak stress undergoes variations of less than 500 MPa. For each value of elastic modulus the stress in the plate shows a slight peak for inclination angles equal to 22.5 °, with respect to the horizontal. Beyond this angle the stress decreases as the fracture inclination increases (Fig. 4.19c). In summary, the areas of maximum stress within the plate assume increasing values, and move upwards, as the level of bone healing decreases, for the reasons already explained during the analysis of real fracture. The reduction of the fracture inclination determines the growth of the maximum stress in the plate up to an angle of 22.5 °. The maximum stresses obtained inside the plate applied to oblique fracture, during the lateral fall with beat on the greater trochanter, simulated assuming the possibility of knee rotation around the y axis, vary between 276.5 and 785.8 MPa.

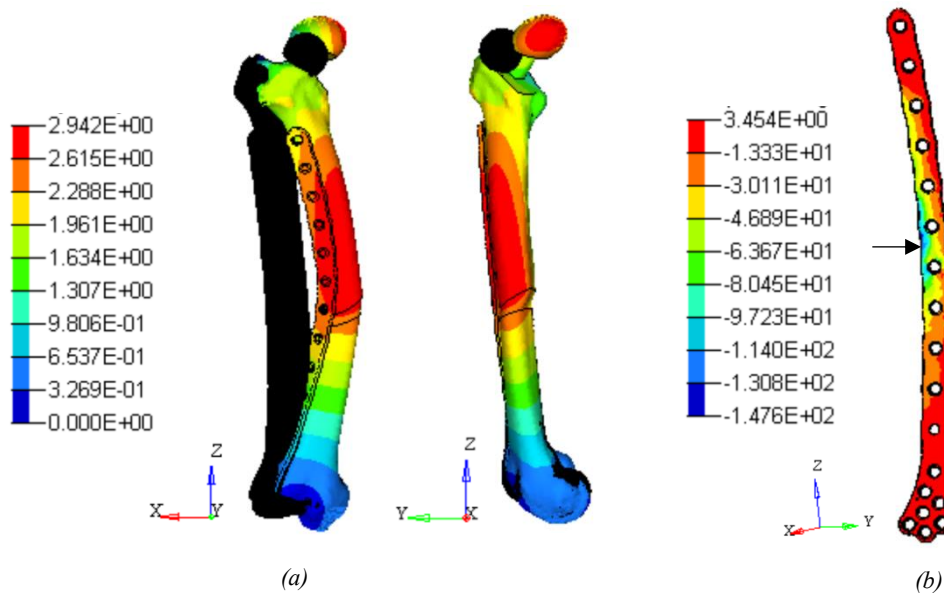


Figure 4.17: Nodal displacements [mm] of the model with non-deformed shape of the model with fracture elastic modulus of 181.6 MPa and fracture inclination of 30° (a). The displacements are amplified by a factor of 10. Minimum principal stresses distribution within the plate of the model with fracture elastic modulus of 181.6 MPa and fracture inclination of 30° (b). The arrow indicate the point with minimum value.

Fracture elastic modulus [MPa] / Fracture inclination [°]	181,6	363,2	1816	3632	1860
15	753,6	525,0	306,6	284,4	276,5
22,5	785,8	568,5	334,6	307,2	298,4
30	722,8	538,9	332,8	292,1	283,3
37,5	687,2	527,6	327,4	292,8	283,8
45	650,2	512,3	326,3	287,7	278,5
53	622,3	498,5	331,7	291,1	280,3
Peak area	12 e 13 l	12 e 13 l	13 e 14 l	14 e 15 l	14 e 15 l

Table 4.6: Von Mises maximum stress in the plate varying the fracture elastic modulus and inclination. The “peak area” field indicate the number of the holes near the peak zone and the side of it (left, right) respect to the plate.

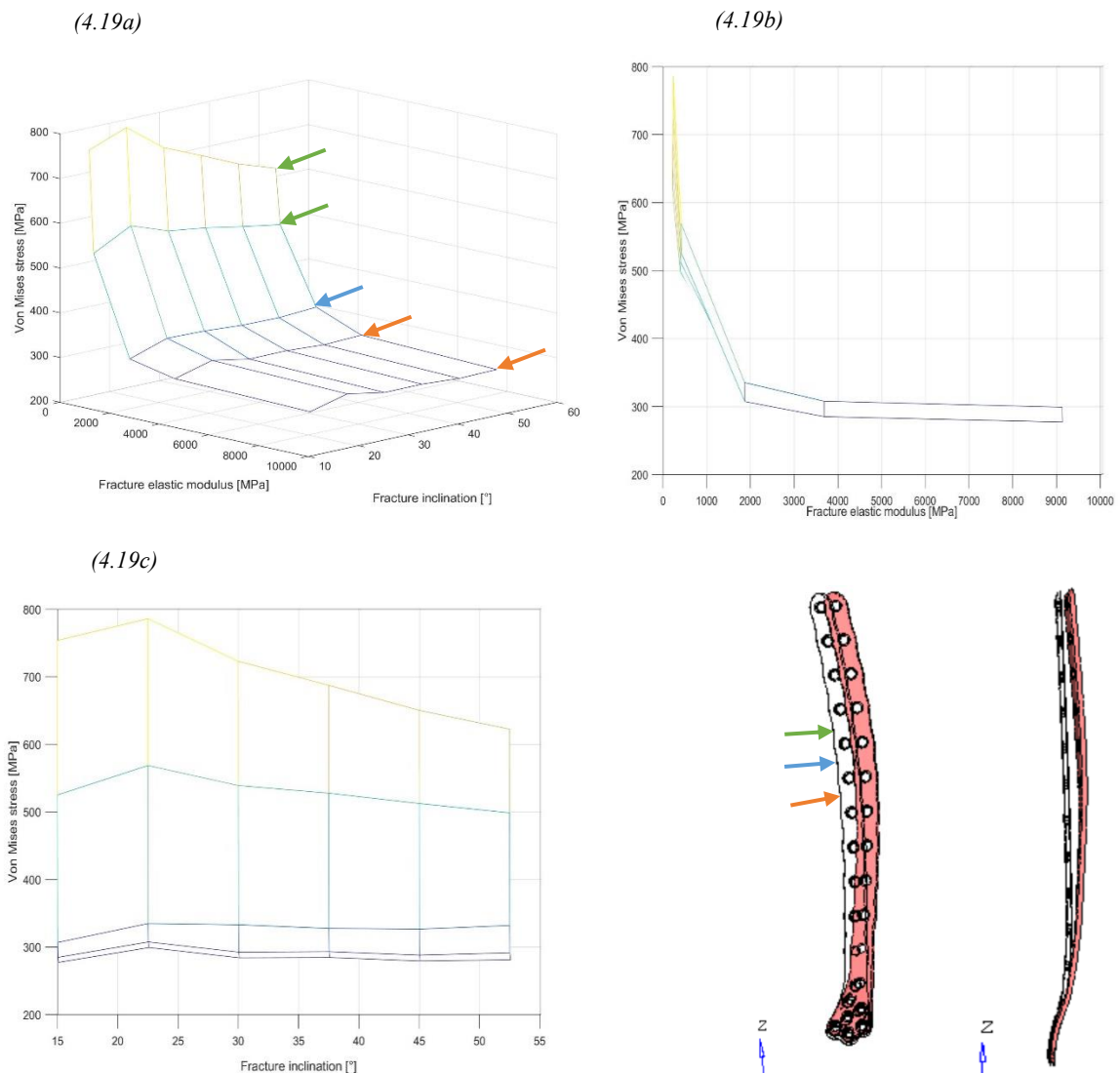


Figure 4.19: Von Mises maximum stresses in the plate varying the fracture inclination and elastic module. Tridimensional (a), xy plane (b) and yz plane (c) views. The arrows represents the stressed areas with reference to figure 4.18.

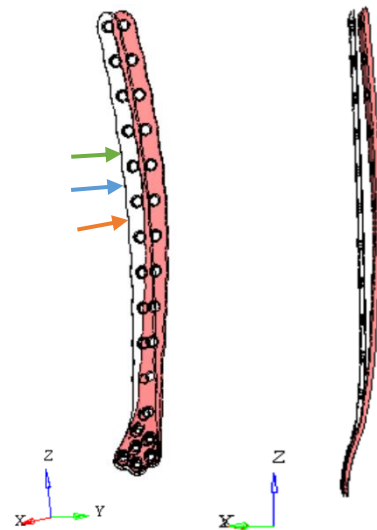


Figure 4.18: Plate deformed and non-deformed shapes, with amplified nodal displacements. The arrows represent the areas of maximum Von Mises stress, varying the fracture elastic modulus.

4.3 Conclusions

In each of the implemented models, the elastic modulus of the fracture has great influence on the stress inside the plate, which vary inversely with respect to the level of bone healing.

The fracture inclination has different influence on the peak stress in the plate, based on the type of acting load configuration. With the same elastic modulus of the fracture, stress peaks were found for different angles when varying the load condition. In almost all cases, however, the fracture inclination has negligible influence on the possibility of failure of the plate. The variation of the stress peak inside it, in fact, is of the order of tens of MPa in cases in which the fracture elastic modulus is equal to 181.6 MPa, except for the stumbling. Here the variation of the stress peak reaches orders of hundreds of MPa. For the more reasonable value of the fracture elastic modulus, equal to 9080.0 MPa, the stress peak variation, in dependence on the angle of inclination of the fracture, assume orders of MPa, except for the case of stumbling where it reach tens of MPa. These values are too low to consider the influence of the inclination angle of the fracture, relevant on the probability of plate failure. It can be affirmed that the angle of inclination of a hypothetical oblique periprosthetic fracture, treated with the internal plate fixator O'Nil, does not significantly affect the maximum stress within it, and therefore the possibility of failure of fixation.

Also in this case, as indicated in the previous chapter, the nominal values obtained regarding the maximum stresses inside the plate are not representative. It is instead useful to quantify their orders of magnitude. The assumptions made are manifold, including bone homogeneity and isotropy, absence of cortical component, linear elastic materials behaviour. It is assumed that these simplifications do not bring substantial and unrealistic changes to the obtained results, and that the considered stress distributions and the orders of magnitude that these assume are representative of the analysed situation.

Bibliography

- [1] Ran Schwarzkopf, Julius K. Oni, Scott E. Marwin, - *Total Hip Arthroplasty Periprosthetic Femoral Fractures, A Review of Classification and Current Treatment* - Bulletin of the Hospital for Joint Diseases, 2013.
- [2] Antonio Capone, Stefano Congia, Roberto Civinini, Giuseppe Marongiu - *Periprosthetic fractures: epidemiology and current treatment* - Clinical Cases in Mineral and Bone Metabolism, 2017.
- [3] Rebecca F. Lyons, Robert P. Piggott, William Curtin, Colin G. Murphy - *Periprosthetic hip fractures: A review of the economic burden based on length of stay* - Journal of Orthopaedics, 2018.
- [4] Stephan Frenzel, Vilmos Vécsei, Lukas Negrin - *Periprosthetic femoral fractures—incidence, classification problems and the proposal of a modified classification scheme* - International Orthopaedics, 2015.
- [5] Jeffrey N Katzl, Elizabeth A Wright, Julian JZ Polaris, Mitchel B Harris, Elena Losina - *Prevalence and risk factors for periprosthetic fracture in older recipients of total hip replacement: a cohort study* - BMC Musculoskeletal Disorders, 2014.
- [6] Daniel Marsland, Simon C. Mears - *A Review of Periprosthetic Femoral Fractures Associated With Total Hip Arthroplasty* - Geriatric Orthopaedic Surgery and Rehabilitation, 2012.
- [7] Jamie T. Griffiths, Arash Taheri, Robert E. Day, Piers J. Yates – *Better Axial Stiffness of a Bicortical Screw Construct for Comminuted Vancouver B1 Proximal Femoral Fractures* - The Journal of Arthroplasty, 2015.
- [8] G. Calvosa, E. Bonicoli, M. Tenucci, G. Morescalchi, F. Po - *Le fratture periprotetiche di femore dopo una protesi totale d'anca* – Giornale italiano di ortopedia e traumatologia, 2004.
- [9] Jordi Tomàs Hernández, Kim Holck – *Periprosthetic femoral fractures: When I use strut grafts and why?* – Injury, 2015.
- [10] Michael G. Dennis, Jordan A. Simon, Frederick J. Kummer, Kenneth J. Koval, and Paul E. DiCesare - *Fixation of Periprosthetic Femoral Shaft Fractures Occurring at the Tip of the Stem* - The Journal of Arthroplasty, 2000.
- [11] Gavin C.A, Doug R. Naudie, James McAuley, Richard W. McCalden - *Locking Compression Plates for the Treatment of Periprosthetic Femoral Fractures Around Well-Fixed Total Hip and Knee Implants* - The Journal of Arthroplasty, 2011.
- [12] Huaming Xue, Yihui Tu, Minwei Cai , and Anli Yang - *Locking Compression Plate and Cerclage Band for Type B1 Periprosthetic Femoral Fractures* - The Journal of Arthroplasty, 2011.
- [13] Ulf Schmid, Rainer Penzkofer, Samuel Bachmaier, Peter Augat - *Implant Material and Design Alter Construct Stiffness in Distal Femur Locking Plate Fixation: A Pilot Study* - Clinical Orthopaedics and Related Research, 2013.
- [14] Daniel J. Berry - *Treatment of Vancouver B3 Periprosthetic Femur Fractures With a Fluted Tapered Stem* - Clinical Orthopaedics and Related Research, 2003.
- [15] Bernd Füchtmeier, Michael Galler, Franz Müller - *Mid-Term Results of 121 Periprosthetic Femoral Fractures: Increased Failure and Mortality Within but not After One Postoperative Year* – The Journal of Arthroplasty, 2015.
- [16] *O'Nil Serie 5 for distal femur* – Intrauma – [brochure]
- [17] *NCB Distal Femur System* – Zimmer – [brochure]

- [18] *Less Invasive Stabilisation System – Synthes* - [brochure]
- [19] Byung-Woo Min, Chul-Hyun Cho, Eun-Suck Son, Kyung-Jae Lee, Si-Wook Lee, Kyung-Keun Min – *Minimally invasive plate osteosynthesis with locking compression plate in patients with Vancouver type B1 periprosthetic femoral fractures* – Injury, 2018.
- [20] Ulf Schmidt, Rainer Penzkofer, Samuel Bachmaier, Peter Augat - *Implant Material and Design Alter Construct Stiffness in Distal Femur Locking Plate Fixation: A Pilot Study* - Clinical Orthopaedics and Related Research, 2013.
- [21] Ni Putu Mira Sumarta, Coen Pramono Danudiningrat, Ester Arijani Rachmat, Pratiwi Soesilawati - *Cytotoxicity difference of 316L stainless steel and titanium reconstruction plate* – Dental Journal, 2011.
- [22] Qizhi Chen, George A. Thouas – *Metallic implant biomaterials* – Materials Science and Engineering, 2015.
- [23] Anupam Srivastav – *An Overview of Metallic Biomaterials for Bone Support and Replacement* - Biomedical Engineering, Trends in Materials Science, 2011.
- [24] *LCP locking compression plate* – Depuy-Synthes – [brochure]
- [25] *PDF-LP Periarticular Distal Femoral Locking Plate* – Zimmer – [brochure]
- [26] *Polyax distal femoral Locking Plate* – Depuy – [brochure]
- [27] *LAP Locking attachment plate* – Depuy-Synthes – [brochure]
- [28] *NCB-PPS Non contact bridging periprosthetic plate system* – Zimmer – [brochure]
- [29] *Cable Ready system* – Zimmer – [brochure]
- [30] Nino Cartabellotta – *La formulazione dei quesiti di ricerca, Da un'idea generica alla formulazione strutturata con EPICOT+* - Gimbe News.
- [31] S. De Riu, M.L. Casagrande, A. Da Porto, I. Gaeta, A. Maffettone¹, S. Gentile - *Come pianificare uno studio clinico* - Il Giornale di AMD 2013.
- [32] John S. Cox, Thomas D. Kowalik, Hanne A. Gehling, Matthew L. DeHart, Paul J. Duwelius, Amer J. Mirza - *Frequency and Treatment Trends for Periprosthetic Fractures About Total Hip Arthroplasty in the United States* - The Journal of Arthroplasty, 2016.
- [33] Byung-Woo Min, Chul-Hyun Cho, Eun-Suck Son, Kyung-Jae Lee, Si-Wook Lee, Kyung-Keun Min – *Minimally invasive plate osteosynthesis with locking compression plate in periprosthetic femoral fractures* – Injury, 2018.
- [34] J. B. Erhardt, K. Grob, G. Roderer, A. HoVmann, T. N. Forster, M. S. Kuster - *Treatment of periprosthetic femur fractures with the non-contact bridging plate: a new angular stable implant* – Trauma surgery, 2007.
- [35] Steffen Ruchholt, Bilal El-Zayat, Dimitri Kreslo, Benjamin Bucking, Ulrike Lewan, Antonio Kruger, Ralph Zetti - *Less invasive polyaxial locking plate fixation in periprosthetic and peri-implant fractures of the femur: a prospective study of 41 patients* – Injury, 2013.
- [36] Christopher E. Henderson, Trevor J. Lujan, Lori L. Kuhl, Michael Bottlang, Daniel C. Fitzpatrick, John L. Marsh - *2010 Mid-America Orthopaedic Association Physician in Training Award: Healing Complications Are Common After Locked Plating for Distal Femur Fractures* – Clinical Orthopaedics and Related Research, 2011.

- [37] R. Pascarella, C. Bettuzzi, G. Bosco, D. Leonetti, S. Dessi, P. Forte, L. Amendola - *Results in treatment of distal femur fractures using polyaxial locking plate* - Strategies in Trauma and Limb Reconstruction, 2014.
- [38] William H. Harvin, Lasun O. Oladeji, Gregory J. Della Rocca, Yvonne M. Murtha, David A. Volgas, James P. Stannard, Brett D. Crist – *Working length and proximal screw constructs in plate osteosynthesis of distal femur fractures* – Injury, 2017.
- [39] M. F. Hoffmann, S. Lotzien, T. A. Schildhauer - *Outcome of periprosthetic femoral fractures following total hip replacement treated with polyaxial locking plate* - The European Journal of Orthopaedic Surgery & Traumatology, 2017.
- [40] H. Lindahl, H. Malchau, A. Odén, G. Garellick - *Risk factors for failure after treatment of a periprosthetic fracture of the femur* – The journal of bone and joint surgery, 2005.
- [41] Lonnie Froberg, Anders Troelsen, and Michael Brix - *Periprosthetic Vancouver type B1 and C fractures treated by locking-plate osteosynthesis* - Acta Orthopaedica, 2012.
- [42] M. Papini, R. Zdero, E.H. Schemitsch, P. Zalzal – *The biomechanics of human femurs in axial and torsional loading: comparaisou of finite element analysis, human cadaveric femurs, and synthetic femurs* – Journal of biomechanical engineering, 2007.
- [43] Marco Viceconti, Luisella Bellingeri, Luca Cristofolini, Aldo Toni - *A comparative study on different methods of automatic mesh generation of human femurs* – Medical engineering and physics, 1998.
- [44] A. Ramos, J.A. Simoes – *Tetrahedral versus hexahedral finite elements in numerical modelling of the proximal femur* - Medical engineering and physics, 2006.
- [45] K Polgar, M Viceconti, J J O'Connor - *A comparison between automatically generated linear and parabolic tetrahedra when used to mesh a human femur* - Proceedings of the Institution of Mechanical Engineers, 2001.
- [46] R.K. Nalla, J.J. Kruzic, .H. Kinney, R.O.Ritchie – *Effect of aging on the toughness of human cortical bone: evaluation by R-curves* – Bone, 2004.
- [47] Elise F. Morgan, Ginu U. Unnikrisnan, Amira I. Hussein - *Bone Mechanical Properties in Healthy and Diseased States* - Annual Review of Biomedical Engineering, 2018.
- [48] Wei Sheng, Aimin Ji, Changsheng Chen - *Biomechanical research of the femur finite element model combined with different material assignment methods* - MATEC Web of Conferences, 2017.
- [49] Fuvia Taddei, Luca Cristofolini, Saulo Martelli, H.S. Gill, Marco Viceconti – *Subject-specific finite element models of long bones: An in vitro evaluation of the overall accuracy* – Juournal of Biomechanics, 2006.
- [50] Haisheng Yang, Xin Ma, Tongtong Guo - *Some factors that affect the comparison between isotropic and orthotropic inhomogeneous finite element material models of femur* - Medical engineering and physics, 2010.
- [51] T. San Antonio, M. Ciaccia, C. Muller-Karger, E. Casanova – *Orientation of orthotropic material properties in a femur FE model: A method based on the principal stresses directions* - Medical engineering and physics, 2012.
- [52] W.S. Enns-Bray, O.Ariza, S.Gilchrist, R.P.Widmer Soyoka, P.J. Vogt, H. Palsson, S.K. Boyd, P. Guy, P.A.Cripton, S.J. Ferguson, B. Helgason – *Morphology based anisotropic finite element models of the proximal femur validated with experimental data* - Medical engineering and physics, 2016.

- [53] Dieter Christian Wirtz, Norbert Schiffers, Thomas Pandorf, Klaus Radermacher, Dieter Weichert, Raimund Forst - *Critical evaluation of known bone material properties to realize anisotropic FE-simulation of the proximal femur* – Journal of biomechanics, 2000.
- [54] I. Manjubala, Y. Liu, D.R. Epari, P. Roschger, H. Schell, P. Fratzl a, G.N. Duda - *Spatial and temporal variations of mechanical properties and mineral content of the external callus during bone healing* – Bone, 2009.
- [55] Christopher L Vaughan, Brian L Davis, Jeremy C O'Connor – *Dynamics of human gait*, 1999 [book].
- [56] G. Bergmann, G. Deuretzbacher, M. Heller, F. Graichen, A. Rohlmann, J. Strauss, G.N. Duda - *Hip contact forces and gait patterns from routine activities* - Journal of Biomechanics, 2001.
- [57] Tomas A. Correa, Kay M. Crossley, Hyung J. Kim, Marcus G. Pandy - *Contributions of individual muscles to hip joint contact force in normal walking* - Journal of biomechanics, 2010.
- [58] M. Ehlinger, P. Adam, A. Di Marco, Y. Arlettaz, B.-K. Moor, F. Bonnomet - *Periprosthetic femoral fractures treated by locked plating: Feasibility assessment of the mini-invasive surgical option. A prospective series of 36 fractures* - Orthopaedics and Traumatology: Surgery and Research, 2011.
- [59] Dirk Wahnert, Niklas Gruneweller, Dominic Gehweiler, Benjamin Brunn, Michael J. Raschke, Richard Stange - *Double Plating in Vancouver Type B1 Periprosthetic Proximal Femur Fractures: A Biomechanical Study* – Jpurnal of orthopaedic research, 2017.
- [60] J. Stolk, N. Verdonschot, R. Huiskes - *Hip-joint and abductor-muscle forces adequately represent in vivo loading of a cemented total hip reconstruction* - Journal of Biomechanics, 2001.
- [61] Charalampos Bitsakos, Jan Kerner, Ian Fisher, Andrew A. Amis - *The effect of muscle loading on the simulation of bone remodelling in the proximal femur* - Journal of Biomechanics, 2005.
- [62] G. Bergmann, F. Graichen, A. Rohlmann - *Hip joint contact forces during stumbling* - Langenbecks Arch Surg, 2004.
- [63] Alessandra Aldieri, Mara Terzini, Giangiacomo Osella, Adriano M. Priola, Alberto Angeli, Andrea Veltri, Alberto L. Audenino, Cristina Bignardi - *Osteoporotic Hip Fracture Prediction: Is T-Score-Based Criterion Enough? A Hip Structural Analysis-Based Model* - Journal of Biomechanical Engineering, 2018.
- [64] Stephen Robinovitch, Wilson C Hayes - *Prediction of Femoral Impact Forces in Falls on the Hip* - Journal of Biomechanical Engineering, 1991.
- [65] H. Kheirollahi, Y. Luo - *Identification of High Stress and Strain Regions in Proximal Femur during Single-Leg Stance and Sideways Fall Using QCT-Based Finite Element Model* - Journal of Biomedical and Biological Engineering, 2015.
- [66] Masoud Nasiri Sarvi, Yunhua Luo - *A two-level subject-specific biomechanical model for improving prediction of hip fracture risk* – ClinicalBiomechanics, 2015.
- [67] A. J. van den Kroonenberg, W. C. Hayes, T. A. McMahon - *Dynamic Models for Sideways Falls From Standing Height* - Journal of Biomechanical Engineering, 1995.